AN INTEGRATED FINITE ELEMENT AND FINITE VOLUME CODE TO SOLVE THERMO-HYDRO-MECHANICAL PROBLEMS IN POROUS MEDIA

by

SHEKHAR VISHWANATH GOSAVI

B.S., University of Pune, India, 1995
M.S., Kansas State University, 2000

AN ABSTRACT OF A DISSERTATION

Submitted in partial fulfillment of the requirements for the degree

DOCTOR OF PHILOSOPHY

Department of Mechanical Engineering
College of Engineering

KANSAS STATE UNIVERSITY
Manhattan, Kansas
2006

ABSTRACT

The objective of the thesis is to provide a fully coupled thermo-hydro-mechanical (THM) tool, T2STR, which enables quantitative understanding and prediction of thermal as well as mechanical effects on flow in the porous media under multiphase conditions. This is achieved by incorporating a finite element based hydro-thermo-mechanical stress capability into the well-established IFDM (Integrated Finite Difference Method) based flow simulation code TOUGH2. TOUGH2 is a program for calculation of multi-phase, multi-component, non-isothermal flow in porous media. It implements several equation-of-state modules to represent different fluid mixtures.

The dual mesh technique is natural for combining both discretization methods and is used innovatively and effectively. A generalized approach is developed to accommodate the switching of variables implemented in TOUGH2 to adapt the phase changes. The forward coupling is achieved by using the thermal, hydrostatic, and poroelastic effects in the stress calculations. The backward coupling includes the effect of strain on the fluid flow. T2STR also allows the user to study the variation in porosity, permeability and capillary pressure as function of mean effective stress in the porous media. Multiple materials can be used to model the reservoir in T2STR, parallel to the implementation in TOUGH2.

T2STR is implemented to carry out as a fully coupled, one way coupled (only deformation as function of hydro-thermal effects), or original TOUGH2 implementation. It provides the ability to switch on and off the thermal and/or poroelastic effects.

T2STR is developed to model the fractured porous media using discrete fractures. The modeling of fractured porous media is limited to a staggered coupling approach. The

fluid parameters like permeability, porosity are modified based on the stresses and/or aperture changes due to deformation.

A set of verification problems, used to validate the code and display the capabilities of the code, are discussed. A graphical user interface is designed to pre process the necessary data. Macros are developed for excel and Tecplot to post-process the results for easy visualization.

AN INTEGRATED FINITE ELEMENT AND FINITE VOLUME CODE TO SOLVE THERMO-HYDRO-MECHANICAL PROBLEMS IN POROUS MEDIA

by

SHEKHAR VISHWANATH GOSAVI

B.S., University of Pune, India, 1995
M.S., Kansas State University, 2000

A DISSERTATION

Submitted in partial fulfillment of the requirements for the degree

DOCTOR OF PHILOSOPHY

Department of Mechanical and Nuclear Engineering
College of Engineering

KANSAS STATE UNIVERSITY
Manhattan, Kansas
2006

Approved by:

Major Professor
Dr. Daniel V. Swenson
Department of Mechanical Engineering

ABSTRACT

The objective of the thesis is to provide a fully coupled thermo-hydro-mechanical (THM) tool, T2STR, which enables quantitative understanding and prediction of thermal as well as mechanical effects on flow in the porous media under multiphase conditions. This is achieved by incorporating a finite element based hydro-thermo-mechanical stress capability into the well-established IFDM (Integrated Finite Difference Method) based flow simulation code TOUGH2. TOUGH2 is a program for calculation of multi-phase, multi-component, non-isothermal flow in porous media. It implements several equation-of-state modules to represent different fluid mixtures.

The dual mesh technique is natural for combining both discretization methods and is used innovatively and effectively. A generalized approach is developed to accommodate the switching of variables implemented in TOUGH2 to adapt the phase changes. The forward coupling is achieved by using the thermal, hydrostatic, and poroelastic effects in the stress calculations. The backward coupling includes the effect of strain on the fluid flow. T2STR also allows the user to study the variation in porosity, permeability and capillary pressure as function of mean effective stress in the porous media. Multiple materials can be used to model the reservoir in T2STR, parallel to the implementation in TOUGH2.

T2STR is implemented to carry out as a fully coupled, one way coupled (only deformation as function of hydro-thermal effects), or original TOUGH2 implementation. It provides the ability to switch on and off the thermal and/or poroelastic effects.

T2STR is developed to model the fractured porous media using discrete fractures. The modeling of fractured porous media is limited to a staggered coupling approach. The

fluid parameters like permeability, porosity are modified based on the stresses and/or aperture changes due to deformation.

A set of verification problems, used to validate the code and display the capabilities of the code, are discussed. A graphical user interface is designed to pre process the necessary data. Macros are developed for excel and Tecplot to post-process the results for easy visualization.

ACKNOWLEDGEMENTS

This dissertation is result of more than four years of work.

Dr. Daniel Swenson, my advisor, has been, to say the least, very patient and encouraging. He helped me learn how to learn and educated me on education of life by teaching through his actions. The wealth of these philosophies will be constructive in my future life. It is a privilege to work with him and I would like to thank him for everything he has done.

My thanks also go to my committee members, Dr. Eckels, Dr. Steward, Dr. Xin, and Dr. Moore for serving on my committee and taking interest in my work. I would also like to thank Brian Hardeman who gave the initial impetus by helping to decipher the TOUGH2 code.

Dr. Karsten Pruess and Dr. Jonny Rutqvist at LBNL have been very kind to take interest in the project and share insights related to the coupling.

I must thank the faculty, staff, and colleagues of the Department of Mechanical and Nuclear Engineering for their years of support and friendship.

Kansas State University and Manhattan have become my second home through these years. As part of life, I have seen lot of good and tough times. If it would not have been for the friends I have, I cannot say with certainty that overcoming the challenges of life would have been possible. We all might have taken different paths in life but I have learnt at least a little from every one of them. I am very grateful to each and every friend who shared a word of wisdom and support during the time when our paths intersected.

Some will stay forever the friends we are, and my sincere gratitude to them for their kindness and tolerance.

My family has been source of inspiration since childhood. My grandfather, Late P. T. Gosavi, emphasized the value of education. My parents, Mr. V. P. Gosavi (Ph.D., Mechanical Engineering) and Mrs. S. V. Gosavi (Master in Arts), built the roads to travel on the successful journey of life for me. Their love and immense support is highly instrumental in my achievements. This is an opportunity for me to express my love and appreciation for them. My brothers, Sachin and Sarang, have always helped me to stay on track through their unique brotherly ways. Bhagyashree and Piyush have brought bountiful of joys to me. I am thankful to have their unending love and support.

Finally I would like to thank plentiful to the authors of all the books I have read and will read; for their efforts to share their knowledge and understanding about scientific and/or spiritual aspects of the human life.

This work is supported by the U.S. Department of Energy, under DOE Financial Assistance Award DE-FC07-01ID14186.

TABLE OF CONTENTS

LIST OF FIGURES ..... **v**
LIST OF TABLES ..... **viii**
NOMENCLATURE ..... **ix**
1 Introduction **1**
1.1 Problem Statement 1
1.2 Field Cases 2
1.2.1 Enhanced Geothermal Systems (http://egs.egi.utah.edu/) 2
1.2.2 Phlegrean Fields, Italy (Todesco et al., 2003) 3
1.3 Literature Survey 4
1.3.1 Poroelasticity 4
1.3.2 Multiphase Analysis 5
1.3.3 Coupling Methods 5
1.3.4 Discretization Methods 7
1.3.5 Fracture modeling 9
1.4 Outline of Thesis 10
2 Conservation Equations for Porous Media **11**
2.1 Conservation of Mass of Solid 11
2.2 Conservation of Mass of Fluid Phase 13
2.3 Conservation of Energy (Internal Energy Balance) 17
2.3.1 Energy Balance using Enthalpy 18
2.3.2 Energy Balance Equation (without K.E. term) 19
2.4 Conservation of Momentum 20
3 Constitutive Equations for Porous Media **22**
3.1 Hydraulic 22
3.1.1 Advective Flux (Darcy's law) 22
3.1.2 Diffusive Flux (Fick's law) 22
3.2 Thermal 23
3.2.1 Heat Conduction (Fourier's law) 23
3.3 Mechanical 23
3.3.1 Strains 23
3.3.2 Terzaghi's effective stress law 24
3.3.3 Biot's (Modified) effective stress law 26
4 Changes in Hydraulic Properties for Porous Media **28**
4.1 Porous rock 28
4.1.1 Porosity 28
4.1.2 Permeability 28
4.1.3 Capillary Pressure 29
5 Modeling of Fractures **30**
5.1 Calculation and Modification of Fracture properties 30
5.1.1 Permeability 31
5.1.2 Porosity 31

6 Discretization 32
6.1 Dual Mesh Concept 32
6.2 Mass and Energy Balance using IFDM (Pruess et al., 1999) 34
6.2.1 Original TOUGH2 Methodology 34
6.2.2 IFDM representation of volumetric strain 35
6.2.3 Mass balance 37
6.2.4 Implementation Procedure 39
6.2.5 Mass balance [Incompressible Solid Phase] 39
6.2.6 Energy balance 40
6.3 Momentum Conservation using Finite Element Formulation 41
6.3.1 Terzaghi's Effective Stress Law 41
6.3.2 Biot's (Modified) Effective Stress Law 43
6.3.3 Implementation details 45
6.4 Fracture Behavior (Finite Element Implementation) 47
7 Solution Technique 49
7.1 Original TOUGH2 implementation 49
7.2 One way coupling 49
7.2.1 Formulation for Newton-Raphson solution (Unmodified stress law) 49
7.3 Fully coupled formulation 52
7.4 Fully coupled formulation for TOUGH2 primary variables 55
7.4.1 Single phase formulation 56
7.4.2 Two phase formulation 56
7.5 Generalized fully coupled formulation for TOUGH2 Variables 61
7.6 Other Changes required for implementation in TOUGH2 for Fully Coupled formulation 62
7.7 Staggered Coupling for Fractured media 63
7.7.1 Fluid flow equations 63
7.7.2 Newton-Raphson formulation (Modified stress law) for Porous Media 63
7.7.3 Newton-Raphson formulation for Fracture Behavior 64
8 Evaluation of Jacobian Terms 69
8.1 Conservation of Mass 69
8.1.1 General Method for derivatives 69
8.1.2 Derivative with respect to displacements $(\mathbf{J}_{\mathbf{FS}})$ 69
8.1.3 Derivative of additional terms with respect to TOUGH2 variables $(\mathbf{J}_{\mathbf{FF}})$ 70
8.2 Conservation of Energy 70
8.2.1 Derivatives with respect to displacements $(\mathbf{J}_{\mathbf{FS}})$ 71
8.2.2 Derivatives with respect to TOUGH2 variables $(\mathbf{J}_{\mathbf{FF}})$ 71
8.3 Conservation of Momentum 72
8.4 Derivative common to multiple terms 72
8.5 Conservation of Mass (Re-look) 74
8.6 Conservation of Energy (Re-look) 74
8.7 Conservation of Momentum (Re-look) 75
8.8 Non-diagonal blocks (Connection Terms) 75
9 Verification Problem 1 (Terzaghi's Problem) 76

9.1 Mathematical Model for flow problem 76
9.1.1 Conservation of Mass 76
9.1.2 Darcy's Law and Permeability 78
9.1.3 Conservation of Mass using Darcy's law 80
9.2 Mathematical Model for displacement problem 81
9.2.1 Effective Stress Law 81
9.2.2 Force Equilibrium Equation 82
9.2.3 Constitutive Equations 82
9.3 Mathematical Model for Fluid (re-evaluated) 84
9.4 Mathematical Model for Incompressible Fluid and Solid 85
9.5 Analytical Solution 86
9.5.1 Parameter Definitions 87
9.5.2 Initial and Boundary conditions 88
9.5.3 Pore Pressure 88
9.5.4 Displacement 89
9.6 Simulations 90
9.7 Results and Comparison (Set 1 [$\alpha = 1$]) 90
9.7.1 Pressure 90
9.7.2 Displacements 92
9.8 Results and Comparison (Set 2 [$\alpha = 0.778$]) 92
9.8.1 Pressure 93
9.8.2 Displacements 95
9.9 Results and Comparison (Set 3 [$\alpha = 1$, Kf $=\infty$]) 95
9.9.1 Pressure 95
9.9.2 Displacements 95
9.10 Conclusion 97
10 Verification Problem 2 (Gibson's 2D problem) 98
10.1 Mathematical Model for flow problem 98
10.2 Mathematical Model for displacement problem 99
10.3 Analytical Solution 100
10.3.1 Initial and Boundary conditions 100
10.3.2 Displacement 101
10.4 Simulations 102
10.5 Results and Comparison (Set 1 [h/b = 1,$\nu = 0$]) 102
10.6 Results and Comparison (Set 2 [h/b = 1,$\nu = 0.2$]) 104
10.7 Conclusion 105
11 Verification Problem 3 (1D THM problem, Lewis-Schrefler) 106
11.1 Governing Equations 107
11.2 Simulation 109
11.3 Results and Comparison 110
12 Verification Problem 4 (Well Test Analysis) 111
12.1 Analytic Solution 111
12.2 Simulation 111
12.3 Results and Conclusion 113
13 Demonstration Problem 1 (1D THM problem, Two-Phase) 115

13.1 Governing Equations 116
13.2 Simulation 116
13.3 Results and Comparison 116
14 Verification Problem 6 (Fracture Behavior) 124
14.1 Verification Problem A (Contact Stresses) 124
14.1.1 Simulation 124
14.1.2 Analytical Solution 124
14.2 Verification Problem B (Pressure Forces) 126
14.3 Demonstration examples 126
15 Demonstration Problem 2 (5 Spot Example – One Way) 129
15.1 Simulation 129
15.2 Results and conclusion 130
16 Conclusions and Recommendations 134
16.1 Summary and Conclusions 134
16.2 Recommendations 135
References 136
APPENDIX A Material Derivative 150
APPENDIX B Solid velocity and Volumetric Strain 151
APPENDIX C Pre-processor and Post-processors 153
C.1 Java based GUI for Pre-processor 153
C.2 Post-processor 154
APPENDIX D Jacobian Analysis 155
D.1 Conservation of Mass (Term by term) 155
D.1.1 Derivative with respect to displacements 155
D.1.2 Derivative with respect to TOUGH2 primary variables 156
D.1.3 Non-diagonal derivatives 157
D.1.3.1 Derivative with respect to displacements 157
D.1.3.2 Derivative with respect to primary variables 158
D.2 Conservation of Energy (Term by term) 158
D.2.1 Derivative with respect to displacements 158
D.2.2 Derivative with respect to TOUGH2 primary variables 158
D.2.3 Non-diagonal derivatives 159
D.2.3.1 Derivative with respect to displacements 159
D.2.3.2 Derivative with respect to primary variables 159

LIST OF FIGURES

Figure 1.1 Enhanced Geothermal System (http://egs.egi.utah.edu/). 2

Figure 1.2 Phlegrean Fields, Italy (Todesco et al., 2003). 3

Figure 2.1 Causes of variation in solid density. 12

Figure 2.2 Differential Soil Element (Bear, 1988). 13

Figure 5.1 Mesh for fracture model (Purple color represents the fracture in both meshes). 30

Figure 6.1 An example of dual meshes, a Delaunay mesh and a Voronoi mesh (Cosmi and Marino, 2000). 32

Figure 6.2 Duals for different meshes (Tonti, 2001). 33

Figure 6.3 Space discretization and geometry data in the IFDM (Pruess et al., 1999). 34

Figure 6.4 IFDM representation of volumetric strain. 37

Figure 6.5 Node numbering for mesh of 8-noded Brick Element. 46

Figure 6.6 Node numbering and representative forces in fracture behavior. 47

Figure 9.1 Schematic of uniaxially constrained soil consolidation (Wang, 2000). 76

Figure 9.2 Differential Soil Element (Terzaghi's Problem). 77

Figure 9.3 Comparison of pressures in column for times following the step load (Set 1). 91

Figure 9.4 Comparison of drainage displacements (Set 1). 92

Figure 9.5 Comparison of pressured in column for times following the step load (Set 2). 94

Figure 9.6 Comparison of drainage displacements (Set 2). 94

Figure 9.7 Comparison of pressured in column for times following the step load (Set 3). 96

Figure 9.8 Comparison of drainage displacements (Set 3). 96

Figure 10.1 Schematic of plain strain consolidation on a smooth impervious boundary. 98

Figure 10.2 Comparison of Corner Node displacement (dimensionless) for $\nu = 0$ 103

Figure 10.3 Comparison of $\mathrm{U}\left[\left(w - w_0\right)/\left(w_\infty - w_0\right)\right]$ at corner node for $\nu = 0$ 104

Figure 10.4 Comparison of Corner Node displacement (dimensionless) for $\nu = 0.2$ 105

Figure 11.1 One dimensional model of thermo-elastic consolidation problem. 106

Figure 11.2 Comparison of displacements at the top. 110

Figure 12.1 Comparison of pressures at the well during withdrawal test. 113

Figure 13.1 One dimensional thermo-elastic consolidation problem (Two-phase). 115

Figure 13.2 Comparison of pressures and deformation of the column (Two Phase). 118

Figure 13.3 Comparison of temperature and deformation of the column (Two Phase). 119

Figure 13.4 Comparison of saturation of gas in the column (Two Phase). 119

Figure 13.5 Comparison of displacements for analysis of two phase problem. 120

Figure 13.6 Pressure and Temperature comparisons between 1500 to 3000 secs. 121

Figure 13.7 Pressure and Gas Saturation comparisons between 1500 to 3000 secs. 121

Figure 13.8 Saturation comparison between 1500 and 3000 seconds. 123

Figure 14.1 Schematic representation to obtain analytical solution. 125

Figure 14.2 3D fracture implementation demonstration problem with planar fracture.. 127

Figure 14.3 Material assignment for multiple fracture problem. 128

Figure 14.4 Deformed mesh with pressure contours at 10secs and temperature contours at 5e5 secs. 128

Figure 15.1 Five-spot geothermal well pattern model. 129

Figure 15.2 Gas phase saturation at the end of steady state simulation run. 131

Figure 15.3 Pressure and deformation at equilibrium condition..... 131

Figure 15.4 Gas phase saturation at the end of 36.5 years..... 132

Figure 15.5 Stress in Z direction and deformation of the reservoir after 36.5 years. 132

Figure: C.1 Example GUI of the Java based pre-processor. 153

LIST OF TABLES

Table 9.1 Simulation Parameters (Terzaghi's Problem Set 1). 91

Table 9.2 Simulation Parameters (Terzaghi's Problem - Set 2). 93

Table 10.1 Simulation Parameters (Gibson's Problem - Set 1). 103

Table 10.2 Simulation Parameters (Gibson's Problem - Set 2). 104

Table 11.1 Simulation Parameters (Thermo-elastic consolidation). 109

Table 12.1 Simulation Parameters (Well test analysis). 112

Table 13.1 Simulation Parameters (Two Phase). 117

Table 14.1 Simulation Parameters (Fracture). 125

Table 15.1 Simulation Parameters (Five-Spot Example). 130

NOMENCLATURE

a_d current aperture in the principal direction d (m)

a_{id} initial aperture in the principal direction d (m)

b body forces (N)

$\mathbf{B}$ matrix containing derivative of shape functions

$\mathbf{C}^{\mathbf{p}}_{\mathbf{S_g}}$ phase co-efficient matrix between solid phase pressure and gas phase saturation

$\mathbf{C}^{\mathbf{T}}_{\mathbf{p_g}}$ phase co-efficient matrix between temperature and gas phase pressure

$\mathbf{C}^{\mathbf{T}}_{\mathbf{S_g}}$ phase co-efficient matrix between temperature and gas phase saturation

D_v effective molecular diffusion of water vapor (m^2/s)

$\mathbf{F}$ force vector (N)

g acceleration due to gravity (m/s^2)

h_ψ specific enthalpy per unit mass of phase ψ (J/kg)

$\mathbf{I}^\kappa_\psi$ advective mass flux of component κ in phase ψ ($kg/(m^2s)$)

$\mathbf{J}$ Jacobian matrix in Newton-Raphson formulation

$\mathbf{J}^H_{C\psi}$ conductive heat flux density for energy in phase ψ ($J/(m^2s)$)

$\mathbf{J}^H_{D\psi}$ combined diffusive and dispersive heat flux density for energy in phase ψ ($J/(m^2s)$)

$\mathbf{J}^H_S$ conductive heat flux density for energy in solid ($J/(m^2s)$)

$\mathbf{k}$ hydraulic or intrinsic permeability tensor (m^2)

$k_{r\psi}$ relative permeability for flow of phase ψ

K bulk modulus of the material (Pa)

K_f compressibility of the fluid (Pa)

K_S bulk modulus of the solid grains (Pa)

$\mathbf{K_e}$ stiffness matrix or coefficient matrix for displacement variable (part of Jacobian)

M^κ_ψ mass of component κ in phase ψ (kg/m^3)

$\mathbf{N}$ shape functions for the finite element

p_c capillary pressure (Pa)

p_ψ fluid pressure in phase ψ (Pa)

p_S fluid pressure acting in the solid phase(Pa)

$\mathbf{q}_\psi^\kappa$ total mass flux of component κ in phase ψ (kg/m^3)

$\mathbf{q}_{r\psi}^\kappa$ total mass flux of component κ in phase ψ with respect to moving solid (kg/m^3)

Q_ψ^κ rate of production of component κ in phase ψ (kg/m^{3}s)

$Q_\psi^{\kappa e}$ evaporation-condensation term

$\mathbf{Q}_\mathbf{v}$ coefficient matrix for fluid flow variable v, (part of the Jacobian)

R residual in the Newton-Raphson formulation

S_ψ saturation of phase ψ

T temperature (C)

$\mathbf{t}$ surface traction (Pa)

u_ψ^E specific internal energy of phase ψ (J/kg)

u_S^E specific internal energy of solid (J/kg)

$\mathbf{u}_a$ unknown displacement vector (m)

$\mathbf{u}_u$ known displacement vector (m)

$\mathbf{u}$ displacement vector (m)

$\mathbf{v}_\psi$ velocity of phase ψ with respect to fixed system (m/s)

$\mathbf{v}_{r\psi}$ velocity of phase ψ with respect to moving solid particles (m/s)

$\mathbf{v}_S$ solid velocity with respect to fixed system (m/s)

α Biot-Willis coefficient

α_T thermal expansion coefficient of the medium (1/K)

$\boldsymbol{\varepsilon}$ total strain tensor

ε_V volumetric strain

κ component like air, water in any phase

λ_ψ thermal conductivity of fluid phase ψ (W/mK)

λ_S thermal conductivity of solid (W/mK)

μ_ψ viscosity of fluid phase ψ (Pa s)

ϕ porosity

ψ fluid phase, l = liquid and g = gas

ρ_ψ^κ mass of component κ per unit volume of phase ψ (kg/m^3)

ρ_S solid mass density (kg/m^3)

$\boldsymbol{\sigma}$ total stress tensor (Pa)

$\boldsymbol{\sigma}'$ Terzaghi's effective stress (Pa)

$\boldsymbol{\sigma}''$ Biot's modified effective stress (Pa)

$\boldsymbol{\sigma}_0$ insitu stress (Pa)

$\boldsymbol{\sigma}_{ct}$ contact stress in fractures (Pa)

$\boldsymbol{\sigma}'_M$ mean effective stress (Pa)

1 INTRODUCTION

1.1 Problem Statement

Geologic media, like soils and rocks, contain pores and fractures that can be filled with fluid and are deformable. A porous medium containing multiphase fluid is called partially saturated, while a porous medium containing only a single-phase fluid is called saturated. Deformation of a porous medium or fractured rock can occur as a result of either a change in external load or change in the internal pore pressure. In general, a hydro-mechanical coupling can occur through deformation of the porous material and the pore-fluid interaction. The two basic couplings occurring are:

(i) a solid-to-fluid coupling occurs when a change in the applied stress produces a change in the fluid pressure or fluid mass;

(ii) a fluid-to-solid coupling occurs when a change in the fluid pressure produces a change in the volume of the porous medium.

This thesis describes the development of a computer code (T2STR) that combines TOUGH2 and a newly developed finite element code to fulfill this requirement. The TOUGH2 code solves coupled problems of non-isothermal, multiphase, multi-component fluid flow problems in complex geological systems using the integrated finite difference method. The developed finite element code is designed to extend the application to incorporate stress analysis and include poro-thermo-elastic effects in the analysis. The T2STR code is fully coupled for porous media applications to solve the equation system simultaneously without any phase lag. It is extended to fractured porous media using staggered approach for discrete fracture networks.

1.2 Field Cases

Coupled thermal-hydro-mechanical (THM) processes under multiphase flow conditions are prevalent in a number of geo-scientific applications (Rutqvist and Stephansson, 2003, Rutqvist et al., 2002, Stephansson et al., 1996, Tsang, 1999). Some of the most important include nuclear waste disposal in geological media, construction of underground openings, deep underground extraction of hazardous waste, geothermal energy extraction, micro-earthquake induced by fluid injection, enhanced recovery from oil and gas extraction, and underground storage of natural gas.

1.2.1 Enhanced Geothermal Systems (http://egs.egi.utah.edu/)

In conventional geothermal-electricity generation, wells are drilled deep into fractured, high-temperature rock. Naturally occurring hot, pressurized water and steam are allowed to flow through the wells to the surface to turn steam turbines and produce electricity. Naturally occurring geothermal reservoirs are, however, limited in size, extent and duration. One mechanism of extending the resource is through the design and construction of Enhanced Geothermal Systems (EGS).

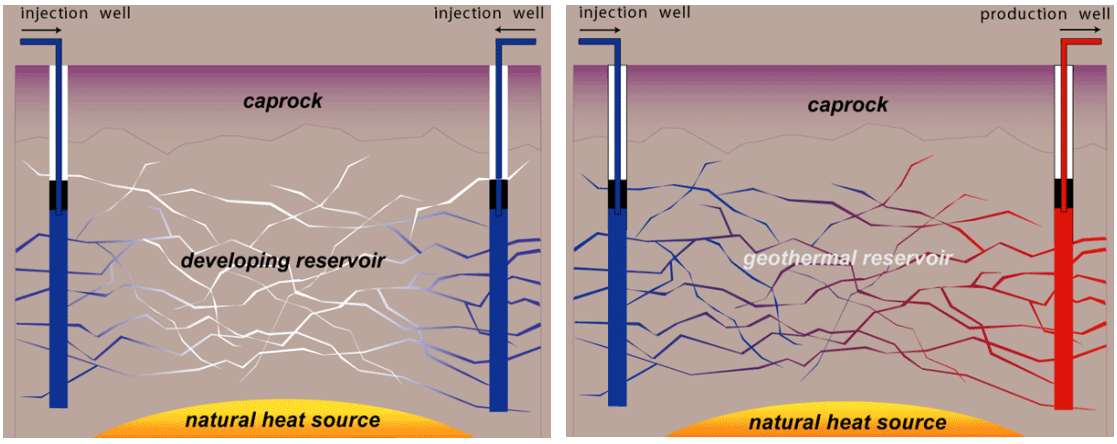

Figure 1.1 Enhanced Geothermal System (http://egs.egi.utah.edu/).

A hot, tectonically stressed region in the subsurface is identified and targeted for the process called stimulation. In such a system, the rock cannot support fluid production at commercially viable rates. Wells are drilled and cold water is injected under high pressure. The increase in pore pressure and thermal stresses, allow the tectonically stressed rock to fail in friction or shear, thus opening, extending and connecting fractures and creating an artificial geothermal reservoir. By circulating water heat is extracted from the rock for use in producing geothermal electric power.

1.2.2 Phlegrean Fields, Italy (Todesco et al., 2003)

The Phlegrean Fields is an active and densely populated caldera structure. Due to period of intense magmatic degassing, there was severe subsidence causing structural damage and loss of human life. The relation between different rates at which deep fluids are injected into the shallow hydrothermal system leading to important changes in composition of the reservoir was evident from the studies conducted. The gas composition appeared to be controlled by the complex multi-phase and multi-component nature of this system.

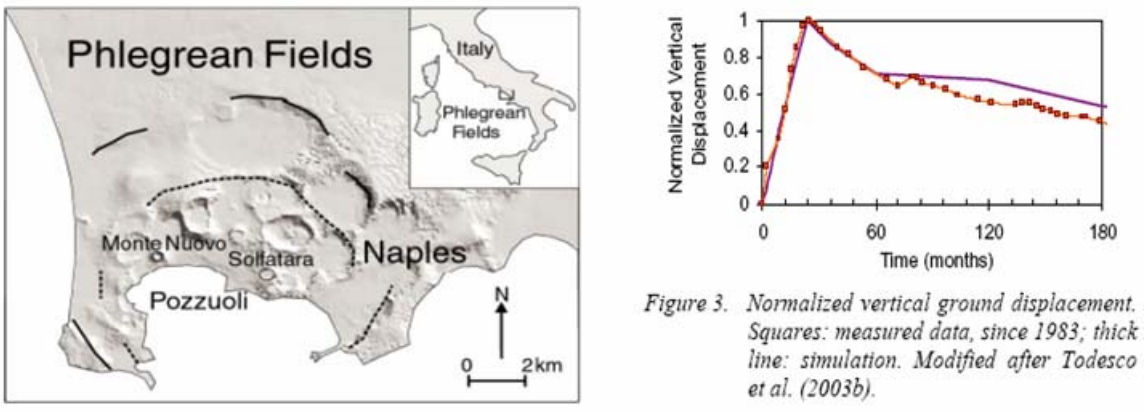

Figure 3. Normalized vertical ground displacement. Squares: measured data, since 1983; thick line: simulation. Modified after Todesco et al. (2003b).

Figure 1.2 Phlegrean Fields, Italy (Todesco et al., 2003).

Coupled THM simulations were successfully used to understand the relation between the ground deformation and hydrothermal fluid circulation. The fast uplift phase followed by slower subsidence as observed in the field was matched in the simulation. It was also observed that maximum deformation was attained at the end of periods of intense degassing. Such an analysis would serve an effective step toward hazard assessment, especially in densely populated areas such as Phlegrean Fields.

1.3 Literature Survey

Various aspects are involved in the development of a numerical simulator for a coupled thermo-hydro-mechanical problem in porous media. The governing equations and their development, multiphase and multicomponent analysis, different coupling methods, different discretization techniques, and further application of all these to fractured porous media need careful consideration during the development of numerical code. We will look at the evolution of these aspects in the geomechanics literature.

1.3.1 Poroelasticity

Terzaghi (1943) introduced the first consolidation theory for 1-D systems, by introducing the principle of effective stresses. According to the law of the effective stress, total stress and pore pressure are related as:

$$\boldsymbol{\sigma}' = \boldsymbol{\sigma} - \mathbf{m}p \tag{1.1}$$

Biot (1941) extended the Terzaghi's concept of 1-D consolidation to a general theory of three-dimensional consolidation. Biot based his theory on a linear stress-strain constitutive relationship and a linear form of Darcy's law. Biot and Willis (1957) characterized the compressibility of the real solid material and that of the solid skeleton.

The analytical theory of poroelasticity was further developed by the work of Pratt and Johnson, Geertsma, Verruijt, Rice and Cleary (Lewis and Schrefler, 1987).

The earlier work in development of numerical modeling was done by Sandhu and Wilson (1969). Ghaboussi and Wilson (1973) introduced compressibility of fluid and Zienkiewicz et al. introduced the compressibility of the solid grains (Lewis and Schrefler, 1987) in numerical modeling. Small et al. (1976) introduced plasticity in the consolidation analysis, using the Mohr-Coulomb model. Non-isothermal consolidation was studied by Bear and Corapcioglu (1982) and Aboustit et al. (1982). Lewis et al. (1976) considered the permeability changes during consolidation.

1.3.2 Multiphase Analysis

Traditionally, the theory of consolidation deals with single-phase problems. The consolidation of partly saturated soil masses was first proposed by Bishop. Narasimhan and Witherspoon (1976) utilized Bishop's effective stress factor to develop a numerical model for three dimensional water flow and one dimensional consolidation of an unsaturated soil. Safai et al. and Chang and Duncan studied the consolidation of a saturated-unsaturated porous medium (Lewis and Schrefler, 1987). Lewis and Schrefler (1998) carried out multiphase analysis based on the single phase 1D thermal consolidation problem solved by Aboustit et al. (1982, 1985).

1.3.3 Coupling Methods

The formulations of modeling the problem of poroelasticity and multiphase flow have been categorized into three basic algorithms: One-way coupling, loose/iterative coupling, and full coupling. In one-way coupling, two separate sets of equations are solved independently and output from one simulator is passed as input to the other at certain

time intervals. The information is passed only in one direction. Under specific conditions, one-way coupling can be used effectively to obtain the correct solution (Wang, 2000). Also, one can gain valuable insight into the physical situation, especially for fluid flow dominated problems. The one-way coupling approach has been successfully used by Fedrich et al., Boade et al., Sulak et al., and Cook et al. (Chen et al., 2000).

In iterative coupling, the two sets of equations are solved independently, but the information is passed in both directions between the two simulators. The iterative coupling has advantages like flexibility and modularity, relative ease of implementation, and better computational efficiency. The iterative coupling is basically equivalent to the modified Newton-Raphson version of the fully coupled method (Wan, 2002). When the iterative process converges, the iterative analysis yields the true solution of the coupled problem. Settari and Walters (1999) discussed the different methods of coupling and gave iterative coupling the advantage of flexibility and reliability over other methods (Wan 2002). The iterative scheme has been used effectively by Settari and Mourtis (1998), Minkoff et al. (1999), Rutqvist et al. (2003), and Bodvarsson et al. (2003). Chin et al (2002) developed and implemented a parallel computing method in an iterative scheme and indicated a increase in speed of geo-mechanical computations by an order of magnitude.

Gutierrez and Lewis (1998) emphasized the importance of fully coupled models over reservoir simulators using only pore compressibility parameter. Minkoff et al. (2003) explain the convergence issues in iterative schemes if the mechanical deformation is not linear-elastic. The main drawback to iteratively coupled approach is that the calculations may display a first order of convergence and may require large number of iterations for

difficult problems. Dean et al. (2003) compared these three techniques and concluded that no technique works best for all kinds of problems. They showed that for the problems involving geo-mechanical effects, the fully coupled approach gives faster convergence while preserving the second order convergence of nonlinear iterations. Wan (2002) compared the fully coupled and iteratively coupled models and prefers the fully coupled models for internal consistency and avoiding of phase lags. She also suggests a stabilized finite element implementation to avoid pressure oscillation situations in certain kind of problems. But as in most cases of fully coupled analysis found in the literature, she also considers simplified and small problems for the fully coupled analysis restricting it to the single phase problems.

1.3.4 Discretization Methods

Several numerical codes have been developed for this purpose. Most of these codes adopt a specialized simplified approach catering to the primary application for which they are developed. There are several underlying assumptions in the modeling phase as well as the development phase in the numerical codes developed for modeling and simulating the coupled THM processes. A need for single numerical code that handles the general coupled THM processes, including multiphase and multi-component fluid flow, has been expressed (Rutqvist and Tsang, 2003). Different models predicting the complex effects like of capillary pressure, relative permeability, complex rock and fluid properties and multiphase behavior have been developed. The selection of a suitable combination of these for a given application demands a single computer code that makes these models available as user selected options.

One of the early attempts was ROCMAS (Noorishad et al., 1996) which is a coupled THM formulation and finite element scheme for fractured rock. It is continuously developed and applied to many problems in rock mechanics and related fields. Some of the other codes developed based on finite element method are THAMES (Ohnishi and Kobayashi, 1996), FRACON (Nguyen, 1996), ABAQUS (Borgesson, 1996), FRACture (Kohl and Hopkirk, 1995). ABAQUS is a commercially available code to study these phenomena. Other commercial codes are FLAC (Israelsson, 1996) which is based on finite difference scheme and UDEC (Israelsson, 1996), a discrete element code. Lewis and Schrefler (1998) describe a finite element based formulation used for solving problems in geomechanics. An excellent overview of four of the existing finite element coupled codes is given by Rutqvist et al. (2001a). Chen and Teufel (1997), and Stone et al. (2000), extended Biot's theory and developed their models using the finite difference method.

Gray (1982) has compared the application of finite element and finite difference approaches. Diersch and Koditz (2002) have discussed the concerns over local conservation errors and local accuracy in both methods. Pyrah (1991) pointed out the deficiency of finite difference methods in plasticity calculations (Gray, 1982). The finite element technique has been widely used in mechanics, and the fluid flow modeling has been widely done using the finite volume approach. A practical approach to couple poroelasticity and multiphase flow would be to develop a hybrid finite element and finite volume scheme. The hybrid finite element and finite volume scheme has been iteratively coupled by Settari and Mourits (1998), Chin et al. (2002), Dean et al. (2003). The only attempt of fully coupled hybrid approach known to the author is Wan (2002). She

developed a combined formulation with stabilized finite element formulation to solve force balance and pressure equations and a control-volume finite difference method to solve the remaining component mass balance equations. But her approach is limited by lack of local mass conservation and she advocates use of the CVFE type (dual mesh type) grids. The CVFE type grid has been discussed by Eymard and Sonier (1994) and by Verma and Aziz (1997) but was restricted by applications to reservoir simulations and not applied to geomechanics.

1.3.5 Fracture modeling

The simplest way to incorporate fractures and fracture behavior is to assume that the fractured rock is a homogeneous, isotropic, and elastic medium having elastic properties that can be calculated from measured properties of intact rock and from ubiquitous fractures with known properties and abundance (Berryman, 96). Goodman (1976) developed an equivalent anisotropic medium concept to represent behavior of fractures in the rock masses. The rock joint model adopts the non-linear behavior of a discontinuous, homogeneous and anisotropic body of rock containing up to three orthogonal joint sets developed by Amadei et al. (1981).

An isotropic, elastic, but inhomogeneous model can be used by assuming the domain is homogeneous except for a few fractures that can be represented in the computer model as interfaces where displacement is allowed, for example, FLAC (Rutqvist and Tsang, 2003), ABAQUS (Borgesson, 1996), Geocrack2D(Swenson, 1997) allow such interfaces.

1.4 Outline of Thesis

We will first derive the fully coupled conservation equations of mass and energy for the porous media. Then we will list the hydraulic, thermal, and mechanical constitutive equations. The variable permeability and porosity model will be discussed.

Once we look at the current implementation in TOUGH2, the approach for inclusion of the stress effects i.e. implementation of the fully coupled equations will be discussed.

The interface fracture behavior developed to model the fractured rock will be discussed later.

Then we will look at all the specific implementation details like formulation of the poroelastic equilibrium equations for solution by Newton-Raphson solution technique currently implemented in TOUGH2 and the derivations of the additional derivatives required for Jacobian formulation due to fully coupled set of equations. The formulation for the one-way as well as staggered coupling used for fractured rock implementation also will be discussed.

Finally the details of the verification problems used to validate the code will be discussed with their results and comparison.

2 CONSERVATION EQUATIONS FOR POROUS MEDIA

The conservation equations for the porous medium as a whole are derived using the continuum approach. These derivations are consistent with those of Lewis and Schrefler (1998), and Rutqvist et al.(2002a). We will first write the mass balance for the solid mass and use the evaluated terms in the fluid mass balance.

In general, the reservoir deformation occurs very slow compared to the multiphase flow (Wan, 2002). Hence, the small strain theory assumption is common in geomechanical models. In this, the fluid velocity is significantly larger than the solid velocity.

2.1 Conservation of Mass of Solid

The mass balance for the solid phase of the porous medium in Eulerian form can be written as follows

$$\frac{\partial\left((1-\phi)\rho_S\right)}{\partial t}+\nabla\bullet\left((1-\phi)\rho_S\mathbf{v}_S\right)=0 \tag{2.1}$$

Using chain rule we can write (2.1) as

$$\left[(1-\phi)\frac{\partial\rho_S}{\partial t}-\rho_S\frac{\partial\phi}{\partial t}\right]+\left[(1-\phi)\rho_S\nabla\bullet\mathbf{v}_S-\rho_S\mathbf{v}_S\bullet\nabla\phi+(1-\phi)\mathbf{v}_S\bullet\nabla\rho_S\right]=0 \tag{2.2}$$

Solving for $\mathbf{v}_S\bullet\nabla\phi$, to be utilized in the fluid mass balance,

$$\mathbf{v}_S\bullet\nabla\phi=\frac{(1-\phi)}{\rho_S}\frac{\partial\rho_S}{\partial t}-\frac{\partial\phi}{\partial t}+(1-\phi)\nabla\bullet\mathbf{v}_S+\frac{(1-\phi)}{\rho_S}\mathbf{v}_S\bullet\nabla\rho_S \tag{2.3}$$

Since generally $\left(\left|\mathbf{v}_S\bullet\nabla\rho_S\right|<<\left|\frac{\partial\rho_S}{\partial t}\right|\right)$ is true, we can neglect the term $\frac{(1-\phi)}{\rho_S}\mathbf{v}_S\bullet\nabla\rho_S$, then we get

$$\mathbf{v}_S \bullet \nabla\phi = \frac{(1-\phi)}{\rho_S}\frac{\partial \rho_S}{\partial t} - \frac{\partial \phi}{\partial t} + (1-\phi)\nabla \bullet \mathbf{v}_S \tag{2.4}$$

We know (APPENDIX B) that

$$\nabla \bullet \mathbf{v}_S \approx \frac{\partial \varepsilon_V}{\partial t} \tag{2.5}$$

Using (2.5), we can write equation (2.4) as

$$\mathbf{v}_S \bullet \nabla\phi = \frac{(1-\phi)}{\rho_S}\frac{\partial \rho_S}{\partial t} - \frac{\partial \phi}{\partial t} + (1-\phi)\frac{\partial \varepsilon_V}{\partial t} \tag{2.6}$$

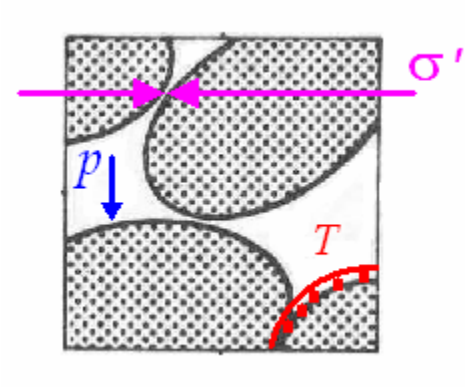

Figure 2.1 Causes of variation in solid density.

Assuming the solid density to be function of pressure, temperature and volumetric strain, we can derive (Lewis and Schrefler, 1998)

$$\frac{1}{\rho_S}\frac{\partial \rho_S}{\partial t} = \frac{1}{(1-\phi)}\left[\frac{(\alpha-\phi)}{K_S}\frac{\partial p_S}{\partial t} - (\alpha-\phi)\alpha_T\frac{\partial T}{\partial t} - (1-\alpha)\frac{\partial \varepsilon_V}{\partial t}\right] \tag{2.7}$$

where, α is the Biot-Willis factor, α_T is the thermal expansion coefficient, and the fluid pressure in the solid phase is given as

$$p_S = p_l S_l + p_g S_g = \sum_{\psi} p_\psi S_\psi \tag{2.8}$$

2.2 Conservation of Mass of Fluid Phase

The macroscopic balance equation for mass for the fluid flow in the differential element of the porous media shown in Figure 2.2 can be written as follows,

$$\frac{\partial}{\partial t}\left(M_{\psi}^{\kappa}\right)+\nabla\bullet\mathbf{I}_{\psi}^{\kappa}+\nabla\bullet\mathbf{J}_{\psi}^{\kappa}-Q_{\psi}^{\kappa}=0 \tag{2.9}$$

where M_{ψ}^{κ}, $\mathbf{I}_{\psi}^{\kappa}$, and $\mathbf{J}_{\psi}^{\kappa}$ respectively denote, the mass per unit volume of the porous medium and the advective and the diffusive/dispersive mass flux respectively, of a component κ in a phase ψ. Q_{ψ}^{κ} is the rate of production of component κ per unit volume.

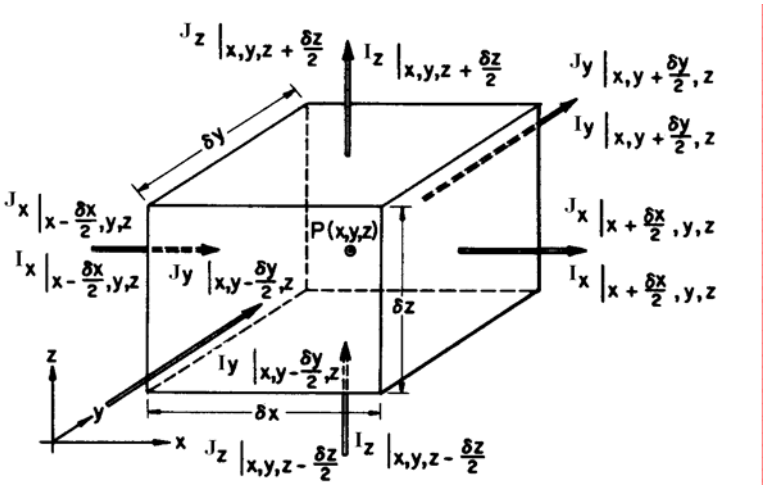

Figure 2.2 Differential Soil Element (Bear, 1988).

The total mass flux $\mathbf{q}_{\psi}^{\kappa}$ (mass per unit area per unit time) is composed of the advective mass flux $\mathbf{I}_{\psi}^{\kappa}$, representing the transport of mass by the bulk motion of the fluid and the diffusive (and/or dispersive) flux $\mathbf{J}_{\psi}^{\kappa}$, representing the transport of mass by molecular motion, i.e.,

$$\mathbf{q}_{\psi}^{\kappa} = \mathbf{I}_{\psi}^{\kappa} + \mathbf{J}_{\psi}^{\kappa} \tag{2.10}$$

then (2.9) can be written as

$$\frac{\partial}{\partial t}\left(M_{\psi}^{\kappa}\right) + \nabla \bullet \mathbf{q}_{\psi}^{\kappa} - Q_{\psi}^{\kappa} = 0 \tag{2.11}$$

For a unit volume of the porous medium, the mass of a component κ in a phase ψ can be written as

$$M_{\psi}^{\kappa} = \phi S_{\psi} \rho_{\psi}^{\kappa} \tag{2.12}$$

where ϕ is porosity, S_{ψ} is phase saturation, and ρ_{ψ}^{κ} denotes the density of respective component (mass of the component κ per unit volume of phase ψ).

The ratio of area of pores through which the phase ψ flows to the total area (i.e. the areal porosity) is assumed to be on average equal to the volumetric porosity (Bear, 1988). Hence the specific (vol.) discharge (i.e. the volumetric flux per unit area per unit time) of the fluid is given as $\phi \mathbf{v}_{\psi}$, where $\mathbf{v}_{\psi}$ denotes the velocity of the fluid with respect to a fixed reference system. For phase ψ, since the saturation is S_{ψ}, term $\phi S_{\psi} \mathbf{v}_{\psi}$ gives the specific (vol.) discharge. Then the advective mass flux $\mathbf{I}_{\psi}^{\kappa}$ of the component κ in phase ψ is given as

$$\mathbf{I}_{\psi}^{\kappa} = \left(\phi S_{\psi} \mathbf{v}_{\psi}\right)\rho_{\psi}^{\kappa} \tag{2.13}$$

The problem can be considered with an extra solid phase for the case of deformable porous media and the fluxes can be written relative to the solid, denoted by subscript r. The fluid velocity can be written as

$$\mathbf{v}_{\psi} = \mathbf{v}_{r\psi} + \mathbf{v}_{S} \tag{2.14}$$

where $\mathbf{v}_S$ denotes the velocity of the solid. Then the advective mass flux $\mathbf{I}_{\psi}^{\kappa}$ can be written as the advective mass flux of the solid and the advective flux with respect to the moving solid particles, $\mathbf{I}_{r\psi}^{\kappa}$, as follows

$$\mathbf{I}_{\psi}^{\kappa} = \mathbf{I}_{r\psi}^{\kappa} + \mathbf{I}_{S\psi}^{\kappa} \tag{2.15}$$

where

$$\mathbf{I}_{r\psi}^{\kappa} = \phi\, S_{\psi}\, \rho_{\psi}^{\kappa}\, \mathbf{v}_{r\psi} \quad \textit{and} \quad \mathbf{I}_{S\psi}^{\kappa} = \phi\, S_{\psi}\, \rho_{\psi}^{\kappa}\, \mathbf{v}_{S\psi} \tag{2.16}$$

Combining the diffusive/dispersive and advective flux with respect to the moving solids, we can write the total mass flux of each component κ within each fluid phase ψ as

$$\mathbf{q}_{r\psi}^{\kappa} = \mathbf{I}_{r\psi}^{\kappa} + \mathbf{J}_{\psi}^{\kappa} \tag{2.17}$$

while the total flux can be written as

$$\begin{aligned} \mathbf{q}_{\psi}^{\kappa} &= \mathbf{I}_{r\psi}^{\kappa} + \mathbf{I}_{S\psi}^{\kappa} + \mathbf{J}_{\psi}^{\kappa} \\ &= \mathbf{q}_{r\psi}^{\kappa} + \mathbf{I}_{S\psi}^{\kappa} \end{aligned} \tag{2.18}$$

Now, the mass balance of the fluid component, (2.11) can be written as

$$\left[\frac{\partial\left(\phi\, S_{\psi}\, \rho_{\psi}^{\kappa}\right)}{\partial t} + \nabla \bullet \mathbf{q}_{r\psi}^{\kappa} + Q_{\psi}^{\kappa e}\right] + \left[\nabla \bullet \left(\phi\, S_{\psi}\, \rho_{\psi}^{\kappa}\, \mathbf{v}_{S}\right)\right] = 0 \tag{2.19}$$

where $Q_{\psi}^{\kappa e}$ is an evaporation-condensation term for water mass exchange between the gas phase and the liquid phase. The external source term Q_{ψ}^{κ} is dropped from the equations just for simplicity of equation and can be added at any stage and only the $Q_{\psi}^{\kappa e}$ term is retained.

Expanding the term $\nabla \bullet \left(\phi S_\psi \rho_\psi^\kappa \mathbf{v}_S\right)$ we can write

$$\left[\frac{\partial\left(\phi S_\psi \rho_\psi^\kappa\right)}{\partial t} + \nabla \bullet \mathbf{q}_{r\psi}^\kappa + Q_\psi^{\kappa e}\right] + \left[\mathbf{v}_S \bullet \nabla\left(\phi S_\psi \rho_\psi^\kappa\right) + \left(\phi S_\psi \rho_\psi^\kappa\right)\nabla \bullet \mathbf{v}_S\right] = 0 \qquad (2.20)$$

Further breaking down the first term in the second bracket we can write

$$\begin{aligned}&\left[\frac{\partial\left(\phi S_\psi \rho_\psi^\kappa\right)}{\partial t} + \nabla \bullet \mathbf{q}_{r\psi}^\kappa + Q_\psi^{\kappa e}\right] + \\ &\left[\left\{S_\psi \rho_\psi^\kappa \mathbf{v}_S \bullet \nabla\phi + \phi \mathbf{v}_S \bullet \nabla\left(S_\psi \rho_\psi^\kappa\right)\right\} + \left(\phi S_\psi \rho_\psi^\kappa\right)\nabla \bullet \mathbf{v}_S\right] = 0\end{aligned} \qquad (2.21)$$

Neglecting the terms $\mathbf{v}_S \bullet \nabla\left(S_\psi \rho_\psi^\kappa\right)$ since $\left|\phi \mathbf{v}_S \bullet \nabla\left(S_\psi \rho_\psi^\kappa\right)\right| << \left|\frac{\partial\left(\phi S_\psi \rho_\psi^\kappa\right)}{\partial t}\right|$, we get

$$\left[\frac{\partial\left(\phi S_\psi \rho_\psi^\kappa\right)}{\partial t} + \nabla \bullet \mathbf{q}_{r\psi}^\kappa + Q_\psi^{\kappa e}\right] + \left[S_\psi \rho_\psi^\kappa\left(\mathbf{v}_S \bullet \nabla\phi\right) + \left(\phi S_\psi \rho_\psi^\kappa\right)\nabla \bullet \mathbf{v}_S\right] = 0 \qquad (2.22)$$

Using the expressions from (2.5) and (2.6), and simplifying, we can write the above equation in terms of solid density and volumetric strain as

$$\left(\frac{\partial\left(\phi S_\psi \rho_\psi^\kappa\right)}{\partial t} + \nabla \bullet \mathbf{q}_{r\psi}^\kappa + Q_\psi^{\kappa e}\right) + S_\psi \rho_\psi^\kappa\left(\frac{(1-\phi)}{\rho_S}\frac{\partial \rho_S}{\partial t} + \frac{\partial \varepsilon_V}{\partial t} - \frac{\partial \phi}{\partial t}\right) = 0 \qquad (2.23)$$

This can also be written as

$$\phi\frac{\partial\left(S_\psi \rho_\psi^\kappa\right)}{\partial t} + S_\psi \rho_\psi^\kappa \frac{(1-\phi)}{\rho_S}\frac{\partial \rho_S}{\partial t} + S_\psi \rho_\psi^\kappa \frac{\partial \varepsilon_V}{\partial t} + Q_\psi^{\kappa e} = -\nabla \bullet \mathbf{q}_{r\psi}^\kappa \qquad (2.24)$$

Substituting from (2.7) and re-inserting the source term, we can write the fluid mass balance equation as

$$\boxed{\begin{aligned}&\left[\frac{\partial\left(\phi S_\psi \rho_\psi^\kappa\right)}{\partial t}+\nabla\bullet\mathbf{q}_{r\psi}^\kappa+Q_\psi^{\kappa e}-Q^\kappa\right]+\\&\left[S_\psi \rho_\psi^\kappa\left(\frac{(\alpha-\phi)}{K_S}\frac{\partial\left(\sum S_\psi p_\psi\right)}{\partial t}-(\alpha-\phi)\alpha_T\frac{\partial T}{\partial t}+\alpha\frac{\partial\varepsilon_V}{\partial t}-\frac{\partial\phi}{\partial t}\right)\right]=0\end{aligned}} \tag{2.25}$$

The second set of terms represents the additional terms required to include the effects of deformable porous media. We will use the above equation for implementation in fully coupled model.

If we neglect the term reflecting the rate change of the water mass caused by change in the grain volume from (2.23) we get

$$\left(\frac{\partial\left(\phi S_\psi \rho_\psi^\kappa\right)}{\partial t}+\nabla\bullet\mathbf{q}_{r\psi}^\kappa+Q_\psi^{\kappa e}\right)+S_\psi \rho_\psi^\kappa\left(\frac{\partial\varepsilon_V}{\partial t}-\frac{\partial\phi}{\partial t}\right)=0 \tag{2.26}$$

2.3 Conservation of Energy (Internal Energy Balance)

The general internal energy balance equation for a porous medium can be written as follows

$$\frac{\partial(\rho U)}{\partial t}=-\nabla\bullet(\rho U\mathbf{v})-\nabla\bullet\mathbf{J}^H-\boldsymbol{\sigma}:\nabla\mathbf{v} \tag{2.27}$$

where the left hand side represents the rate of increase in internal energy per unit time. The right hand side, term by term, represents

- Net rate of addition of internal energy by convective transport (per unit volume).
- Rate of internal energy addition by heat conduction, per unit volume.
- Rate of conversion of kinetic energy into internal energy.

2.3.1 Energy Balance using Enthalpy

Using the following thermodynamic relation between internal energy, U and enthalpy, h

$$h = U + pV = U + \frac{p}{\rho} \tag{2.28}$$

the energy balance can be written in terms of enthalpy as

$$\left[\frac{\partial(\rho h)}{\partial t} - \frac{\partial(p)}{\partial t}\right] = -\nabla \bullet (\rho h \mathbf{v}) + \nabla \bullet (p\mathbf{v}) - \nabla \bullet \mathbf{J}^H - \boldsymbol{\sigma} : \nabla \mathbf{v} \tag{2.29}$$

In component form, the energy balance for a component κ of the fluid phase ψ can be written as (Faust and Mercer, 1979)

$$\begin{aligned}\frac{\partial(\phi S_\psi \rho_\psi^\kappa h_\psi)}{\partial t} - \frac{\partial(\phi S_\psi p_\psi)}{\partial t} &= -\nabla \bullet (\rho_\psi^\kappa h_\psi \phi S_\psi \mathbf{v}_\psi) + \nabla \bullet (p_\psi \phi S_\psi \mathbf{v}_\psi) \\ &\quad - \nabla \bullet \mathbf{J}_{C\psi}^H - \nabla \bullet \mathbf{J}_{D\psi}^H - \boldsymbol{\sigma}_\psi : \nabla(\phi S_\psi \mathbf{v}_\psi)\end{aligned} \tag{2.30}$$

where the subscript C denotes the conductive flux and subscript D stands for the combined diffusive and dispersive (hydrodynamic dispersion) heat flux (thermal mixing).

If we neglect the term related to the conversion of kinetic energy to internal energy, we can write the fluid balance in component form as

$$\begin{aligned}\frac{\partial(\phi S_\psi \rho_\psi^\kappa h_\psi)}{\partial t} - \frac{\partial(\phi S_\psi p_\psi)}{\partial t} &= -\nabla \bullet (\rho_\psi^\kappa h_\psi \phi S_\psi \mathbf{v}_\psi) + \nabla \bullet (p_\psi \phi S_\psi \mathbf{v}_\psi) \\ &\quad - \nabla \bullet \mathbf{J}_{C\psi}^H - \nabla \bullet \mathbf{J}_{D\psi}^H\end{aligned} \tag{2.31}$$

The energy balance equation for the solid can be written as

$$\begin{aligned}\frac{\partial((1-\phi)\rho_S u_S^E)}{\partial t} &= -\nabla \bullet (\rho_S h_S (1-\phi)\mathbf{v}_S) + \nabla \bullet (p_S (1-\phi)\mathbf{v}_S) \\ &\quad - \nabla \bullet \mathbf{J}_S^H - \boldsymbol{\sigma}_S : \nabla((1-\phi)\mathbf{v}_S)\end{aligned} \tag{2.32}$$

where u^E represents the specific internal energy. The last term, the viscous dissipation term, for solids will be neglected.

The energy transfer associated with solid velocity is negligible compared to the energy transfer by the fluid. Hence all the terms associated with the solid velocity, from the fluid as well solid energy balance, will be neglected. Then we can write the fluid and solid energy balance equations respectively as follows

$$\frac{\partial\left(\phi S_\psi \rho_\psi^\kappa h_\psi\right)}{\partial t} - \frac{\partial\left(\phi S_\psi p_\psi\right)}{\partial t} = -\nabla\bullet\left(\rho_\psi^\kappa h_\psi \phi S_\psi \mathbf{v}_{r\psi}\right) + \nabla\bullet\left(p_\psi \phi S_\psi \mathbf{v}_{r\psi}\right) - \nabla\bullet\mathbf{J}_{C\psi}^H - \nabla\bullet\mathbf{J}_{D\psi}^H - \boldsymbol{\sigma}_\psi : \nabla\left(\phi S_\psi \mathbf{v}_{r\psi}\right) \tag{2.33}$$

and

$$\frac{\partial\left((1-\phi)\rho_S u_S^E\right)}{\partial t} = -\nabla\bullet\mathbf{J}_S^H \tag{2.34}$$

2.3.2 Energy Balance Equation (without K.E. term)

Taking into account (2.28) and readjusting the fluid energy balance equation (2.33), we can write the component form with internal energy on the left hand side and the enthalpy on the right hand side as

$$\frac{\partial\left(\phi S_\psi \rho_\psi^\kappa u_\psi^E\right)}{\partial t} = -\nabla\bullet\left(\mathbf{I}_{r\psi}^\kappa h_\psi\right) - \nabla\bullet\left(\mathbf{J}_{D\psi} h_\psi\right) - \nabla\bullet\mathbf{J}_{C\psi}^H + \nabla\bullet\left(p_\psi \phi S_\psi \mathbf{v}_{r\psi}\right) + Q_\psi^E \tag{2.35}$$

where Q_ψ^E representing the inter-phase energy exchange terms.

Using the identity in (2.17) we can write

$$\frac{\partial\left(\phi S_\psi \rho_\psi^\kappa u_\psi^E\right)}{\partial t} = -\nabla\bullet\left(\mathbf{q}_{r\psi}^\kappa h_\psi\right) - \nabla\bullet\mathbf{J}_{C\psi}^H + \nabla\bullet\left(p_\psi \phi S_\psi \mathbf{v}_{r\psi}\right) + Q_\psi^E \tag{2.36}$$

and adding up the energy balance equations for three phases, the inter-phase exchange energy terms are cancelled , and we can arrive at the energy balance equation

$$\frac{\partial\left(\phi\sum S_\psi \rho_\psi^\kappa u_\psi^E + (1-\phi)\rho_S u_S^E\right)}{\partial t} = -\nabla\bullet\left(\sum \mathbf{q}_{r\psi}^\kappa h_\psi\right) - \nabla\bullet\mathbf{J}_C^H + \nabla\bullet\left(\phi\sum p_\psi S_\psi \mathbf{v}_{r\psi}\right) \quad (2.37)$$

where (Bear and Buchlin, 1991)

$$\begin{aligned}\mathbf{J}_C^H &= \sum\nolimits_\psi \mathbf{J}_{C\psi}^H + \mathbf{J}_S^H \\ &= \left(\phi\sum\nolimits_\psi \lambda_\psi + (1-\phi)\lambda_S\right)\Delta T\end{aligned} \quad (2.38)$$

The λ s represent the thermal conductivities of the solid and fluids.

Neglecting the term $\nabla\bullet\left(p_\psi\phi S_\psi \mathbf{v}_{r\psi}\right)$, since we are ignoring viscous dissipation (Garg and Pritchett, 1977) assuming either single phase liquid or two phase condition in the reservoir, we can write

$$\boxed{\frac{\partial\left(\phi\sum S_\psi \rho_\psi^\kappa u_\psi^E + (1-\phi)\rho_S u_S^E\right)}{\partial t} = -\nabla\bullet\left(\sum \mathbf{q}_{r\psi}^\kappa h_\psi\right) - \nabla\bullet\mathbf{J}_C^H} \quad (2.39)$$

This is same as the TOUGH2 energy balance equation and hence no additional changes are required in the TOUGH2 related to it.

2.4 Conservation of Momentum

The law of conservation of momentum can be written as

$$\frac{\partial(\rho\mathbf{v})}{\partial t} = -\nabla\bullet(\rho\mathbf{v}\mathbf{v} - \boldsymbol{\sigma}) + \rho\mathbf{F} \quad (2.40)$$

where the left hand side represents the rate of accumulation of momentum. The first term on the right hand side combines the rate of momentum gained by advection and diffusion,

where $\boldsymbol{\sigma}$ is the stress tensor that represents the diffusive flux of the momentum. The second term on right hand side represents the supply of momentum by the body forces.

Neglecting the inertial terms and the forces due to the interaction between the non-wetting and wetting fluid, the momentum equation becomes a static equilibrium equation as follows (Bear and Bachmat, 1991)

$$\nabla \bullet \boldsymbol{\sigma} = \rho \mathbf{F} \tag{2.41}$$

which also is written as

$$\sigma_{ij,j} + b_i = 0 \tag{2.42}$$

where b_i denotes the body forces. Considering only the gravitational forces as body forces, we can write

$$\rho \mathbf{F} = \rho_m \mathbf{g} = \left\{ \phi \left(\sum S_\psi \rho_\psi \right) + (1 - \phi) \rho_S \right\} \mathbf{g} \tag{2.43}$$

where $\mathbf{g} = -g\hat{\mathbf{z}}$ is the gravity acceleration (vector) directed downward.

3 CONSTITUTIVE EQUATIONS FOR POROUS MEDIA

The hydraulic, thermal, and mechanical constitutive equations required to complete the formulation and are discussed below.

3.1 Hydraulic

3.1.1 Advective Flux (Darcy's law)

The advective mass flux of the component κ of a fluid phase ψ is given by the generalized Darcy law as follows

$$\mathbf{I}_{r\psi}^{\kappa} = -\rho_{\psi}^{\kappa} \frac{\mathbf{k} k_{r\psi}}{\mu_{\psi}} \left(\nabla p_{\psi} + \rho_{\psi} g \nabla z \right) = -\rho_{\psi}^{\kappa} \frac{\mathbf{k} k_{r\psi}}{\mu_{\psi}} \left(\nabla p_{\psi} - \rho_{\psi} \mathbf{g} \right) \tag{3.1}$$

where the $\mathbf{k} = \mathbf{k}(\phi)$ is the hydraulic permeability tensor which is a function of porosity and is a property of the solid, while $k_{r\psi}$ is the relative permeability function of the fluid phases. The permeability of the porous medium as a whole can be defined as

$$\mathbf{k}_{\psi} = \mathbf{k}\, k_{r\psi} \tag{3.2}$$

3.1.2 Diffusive Flux (Fick's law)

The diffusive flux can been computed using the Fick's law,

$$J_{\psi} = -\rho_{\psi} D_{v} \mathbf{m} \nabla X_{\psi}^{\kappa} = -\rho_{\psi} D_{v} \mathbf{m} \nabla \left(\frac{\rho_{\psi}^{\kappa}}{\rho_{\psi}} \right) \tag{3.3}$$

where D_v is the effective molecular diffusion coefficient in a porous media.

The density and viscosity for fluid phases, which are functions of pressure and temperature, can be obtained from steam tables.

3.2 Thermal

3.2.1 Heat Conduction (Fourier's law)

Heat conduction is governed by Fourier's law and is given by

$$\mathbf{J}_C^H = -\lambda_m \mathbf{m} \nabla T \tag{3.4}$$

where λ_m is the thermal conductivity over all phases and vector $\mathbf{m}$ is $[1 \;\; 1 \;\; 1 \;\; 0 \;\; 0 \;\; 0]^T$.

3.3 Mechanical

3.3.1 Strains

The total strain tensor, $\boldsymbol{\varepsilon}$, and the volumetric strain, ε_V, assuming the small strain condition, are defined as,

$$\boldsymbol{\varepsilon} = \frac{1}{2}\left(\nabla \mathbf{u} + (\nabla \mathbf{u})^{tr}\right) \tag{3.5}$$

and

$$\varepsilon_V = \nabla \bullet \mathbf{u} \tag{3.6}$$

where $\mathbf{u}$ is the displacement vector.

The thermal strain is given by

$$\Delta \boldsymbol{\varepsilon}_T = \mathbf{m} \alpha_T \Delta T \tag{3.7}$$

where α_T is the linear thermal expansion coefficient.

The strain due to the poroelastic effect, $\Delta \varepsilon_p$, caused by the uniform compression of the particles by the pore pressure is given by (Lewis and Schrefler, 1998)

$$\Delta\boldsymbol{\varepsilon}_p = \left(\frac{-1}{3K_s}\right)\mathbf{m}\Delta p \tag{3.8}$$

where K_s represents the bulk modulus of the solid phase and Δp represents the change in pore pressure.

3.3.2 Terzaghi's effective stress law

The basic "unmodified" effective stress law for a partially saturated medium gives the total stress as (Lewis and Schrefler, 1998)

$$\boldsymbol{\sigma} = \boldsymbol{\sigma}' - \mathbf{m}p \tag{3.9}$$

where $\boldsymbol{\sigma}'$ represents the effective stress.

When only effective stress law is mentioned it indicates the "unmodified" effective stress law (3.9).

The effective stress causes all relevant deformation of the solid skeleton (excluding grain compressibility) and the constitutive equation relating the effective stress to strain, in incremental form, is

$$\boldsymbol{\sigma}' = \mathbf{D}(\Delta\boldsymbol{\varepsilon} - \Delta\boldsymbol{\varepsilon}_P - \Delta\boldsymbol{\varepsilon}_T) + \boldsymbol{\sigma}'_0 \tag{3.10}$$

where: $\mathbf{D}$ is the elastic material matrix, $\Delta\boldsymbol{\varepsilon}$ is the total strain, $\Delta\boldsymbol{\varepsilon}_P$ is the volumetric strain caused by uniform compression of the solid particles of the skeleton by the change of pressure of the pore fluid, $\Delta\boldsymbol{\varepsilon}_T$ is the thermal strain, and $\boldsymbol{\sigma}'_0$ is the initial effective stress.

The elastic material matrix $\mathbf{D}$ is

$$\mathbf{D} = \frac{E}{(1+\upsilon)(1-2\upsilon)} \begin{bmatrix} (1-\upsilon) & \upsilon & \upsilon & 0 & 0 & 0 \\ \upsilon & (1-\upsilon) & \upsilon & 0 & 0 & 0 \\ \upsilon & \upsilon & (1-\upsilon) & 0 & 0 & 0 \\ 0 & 0 & 0 & \frac{1-2\upsilon}{2} & 0 & 0 \\ 0 & 0 & 0 & 0 & \frac{1-2\upsilon}{2} & 0 \\ 0 & 0 & 0 & 0 & 0 & \frac{1-2\upsilon}{2} \end{bmatrix} \tag{3.11}$$

Then, using the effective stress law (3.9), the total stress can be written as

$$\begin{aligned} \boldsymbol{\sigma} &= \left(\mathbf{D}\left(\Delta\boldsymbol{\varepsilon} - \Delta\boldsymbol{\varepsilon}_P - \Delta\boldsymbol{\varepsilon}_T\right) + \boldsymbol{\sigma}'_0\right) - \mathbf{m}p \\ &= \mathbf{D}\left(\left[\Delta\boldsymbol{\varepsilon}\right] - \left[-\mathbf{m}\left(\frac{1}{3K_s}\right)\Delta p\right] - \left[\mathbf{m}\alpha_T \Delta T\right]\right) + \boldsymbol{\sigma}'_0 - \mathbf{m}p \\ &= \mathbf{D}\Delta\boldsymbol{\varepsilon} + \mathbf{D}\mathbf{m}\left(\frac{1}{3K_s}\right)\Delta p - \mathbf{D}\mathbf{m}\alpha_T \Delta T + \boldsymbol{\sigma}'_0 - \mathbf{m}p \end{aligned} \tag{3.12}$$

Using the identities,

$$\frac{E}{1-2\upsilon} = 3K \tag{3.13}$$

and

$$\frac{K}{K_s} = 1-\alpha \quad or \quad \alpha = 1-\frac{K}{K_s} \tag{3.14}$$

we can do the following simplification,

$$\mathbf{D}\mathbf{m}\frac{1}{3K_s} = \begin{bmatrix} 3K \\ 3K \\ 3K \\ 0 \\ 0 \\ 0 \end{bmatrix}\frac{1}{3K_s} = \begin{bmatrix} 1-\alpha \\ 1-\alpha \\ 1-\alpha \\ 0 \\ 0 \\ 0 \end{bmatrix} = (1-\alpha)\,\mathbf{m} \tag{3.15}$$

where α is the Biot-Willis coefficient (Wang, 2000).

Now, the total stress can be written as

$$\boldsymbol{\sigma} = \left(\mathbf{D}\Delta\boldsymbol{\varepsilon} + (1-\alpha)\mathbf{m}\,\Delta p - (3K\,\alpha_T)\mathbf{m}\,\Delta T + \boldsymbol{\sigma}'_0\right) - \mathbf{m}\,p \tag{3.16}$$

Substituting for $p = p_0 + \Delta p$, we can represent the stress as

$$\boldsymbol{\sigma} = \left(\mathbf{D}\,\Delta\boldsymbol{\varepsilon} + (1-\alpha)\mathbf{m}\,\Delta p - 3K\,\alpha_T\,\mathbf{m}\,\Delta T + \boldsymbol{\sigma}'_0\right) - \mathbf{m}\,(p_0 + \Delta p) \tag{3.17}$$

which can be simplified as

$$\boldsymbol{\sigma} = \mathbf{D}\,\Delta\boldsymbol{\varepsilon} - \alpha\,\mathbf{m}\,\Delta p - 3K\,\alpha_T\,\mathbf{m}\,\Delta T + \boldsymbol{\sigma}'_0 - \mathbf{m}\,p_0 \tag{3.18}$$

3.3.3 Biot's (Modified) effective stress law

The "modified" effective stress law accounting for grain compression is given by

$$\boldsymbol{\sigma} = \boldsymbol{\sigma}'' - \alpha\,\mathbf{m}\,p \tag{3.19}$$

where α is the Biot-Willis factor and the effective stress in this case is given as

$$\Delta\boldsymbol{\sigma}'' = \mathbf{D}\left(\Delta\varepsilon - \Delta\varepsilon_T\right) \tag{3.20}$$

The modified effective stress causes all relevant deformation of the solid skeleton and the constitutive equation relating the modified effective stress to strain, in incremental form, is

$$\boldsymbol{\sigma}'' = \Delta\boldsymbol{\sigma}'' + \boldsymbol{\sigma}''_0 \tag{3.21}$$

$$\boldsymbol{\sigma}'' = \mathbf{D}\,(\Delta\boldsymbol{\varepsilon} - \Delta\boldsymbol{\varepsilon}_T) + \boldsymbol{\sigma}''_0 \tag{3.22}$$

where: $\mathbf{D}$ is the elastic material matrix, $\Delta\boldsymbol{\varepsilon}$ is the total strain, $\Delta\boldsymbol{\varepsilon}_T$ is the thermal strain, and $\boldsymbol{\sigma}''_0$ is the initial effective stress.

Then, using the modified effective stress law (3.19), the total stress can be written as

$$\begin{aligned}\boldsymbol{\sigma} &= \left(\mathbf{D}\,(\Delta\boldsymbol{\varepsilon} - \Delta\boldsymbol{\varepsilon}_T) + \boldsymbol{\sigma}''_0\right) - \alpha\,\mathbf{m}p \\ &= \mathbf{D}\left(\left[\Delta\boldsymbol{\varepsilon}\right] - \left[\mathbf{m}\,\alpha_T\,\Delta T\right]\right) + \boldsymbol{\sigma}''_0 - \alpha\,\mathbf{m}\,p \\ &= \mathbf{D}\Delta\boldsymbol{\varepsilon} - \mathbf{D}\mathbf{m}\,\alpha_T\,\Delta T + \boldsymbol{\sigma}''_0 - \alpha\,\mathbf{m}\,p\end{aligned} \tag{3.23}$$

Hence the total stress can be written as

$$\boldsymbol{\sigma} = \left(\mathbf{D}\Delta\boldsymbol{\varepsilon} - \left(3K\,\alpha_T\right)\mathbf{m}\,\Delta T + \boldsymbol{\sigma}''_0\right) - \alpha\,\mathbf{m}\,p \tag{3.24}$$

Substituting for $p = p_0 + \Delta p$, we can represent the stress as

$$\boldsymbol{\sigma} = \left(\mathbf{D}\,\Delta\boldsymbol{\varepsilon} - 3K\,\alpha_T\,\mathbf{m}\,\Delta T + \boldsymbol{\sigma}''_0\right) - \alpha\,\mathbf{m}\,(p_0 + \Delta p) \tag{3.25}$$

which can be written as

$$\boldsymbol{\sigma} = \mathbf{D}\,\Delta\boldsymbol{\varepsilon} - 3K\,\alpha_T\,\mathbf{m}\,\Delta T - \alpha\,\mathbf{m}\,\Delta p + \boldsymbol{\sigma}''_0 - \alpha\,\mathbf{m}\,p_0 \tag{3.26}$$

This completes the set of constitutive equations.

4 CHANGES IN HYDRAULIC PROPERTIES FOR POROUS MEDIA

The conservation equations take into account the effects of compressibility of solid matrix i.e. the deformable porous media on the fluid flow and the effects of pore pressure and thermal expansion on the effective stress. We also need to include the effect on the hydraulic properties like permeability and porosity as function of the effective stress.

The hydraulic properties of the porous media, the porosity and the permeability are corrected using the empirical porosity-mean stress and permeability-porosity relationships given by Davies and Davies (1999), and also used by Rutqvist et al. (2002).

4.1 Porous rock

4.1.1 Porosity

A relationship between porosity and mean effective stress is (Davies and Davies, 1999),

$$\phi = \phi_r + (\phi_0 - \phi_r)\exp(a\,\sigma'_M) \tag{4.1}$$

where, ϕ_0 is porosity at zero stress, ϕ_r is the residual porosity at high stress, a is the constant to be determined experimentally (a material property), and σ'_M is the mean effective stress.

4.1.2 Permeability

We use the permeability and porosity relation given by Rutqvist et al. (2002)

$$k = k_0 e^{\left(c\left(\frac{\phi}{\phi_0}-1\right)\right)} \tag{4.2}$$

where k_0 is the permeability at zero stress and the exponent c should be determined experimentally.

4.1.3 Capillary Pressure

The capillary pressure is modified with permeability and porosity according to the Leverett function (Rutqvist et al., 2002)

$$p_c = p_{c0} \frac{\sqrt{k_0 / \phi_0}}{\sqrt{k / \phi}} \tag{4.3}$$

Thus porosity, permeability and capillary pressure are modified as function of the mean effective stress.

5 MODELING OF FRACTURES

The fractures in T2STR are implemented as discrete fractures using joint elements. These joint elements exhibit the fracture interaction with continuum elements. The fracture behavior expresses the effects of surface traction due to joint contact stress (the non-linear relationship between the joint opening and the joint stresses) and the forces due to pressure differential in the fluid pressure between the fracture and adjacent rock element.

In T2STR, the mesh is restricted to a Cartesian mesh and hence the global and local coordinate system orientation is same for any element. In the TOUGH2 (fluid flow, IFDM) mesh the fracture is represented by two sets of rows. In the finite element mesh it would be represented by a single row of the joint elements. The idea of the mesh structure is represented in Figure 5.1.

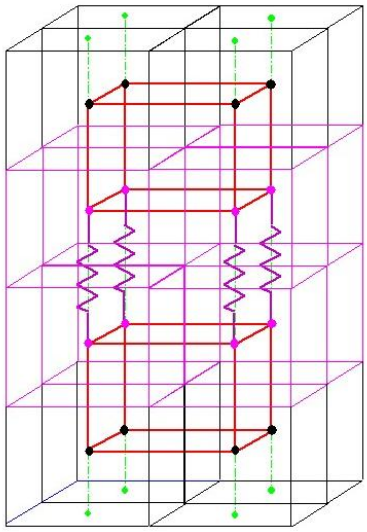

Figure 5.1 Mesh for fracture model (Purple color represents the fracture in both meshes).

5.1 Calculation and Modification of Fracture properties

The fracture porosities and permeabilities are as described below.

5.1.1 Permeability

The fracture permeability is determined using the Cubic law, which is based on the derivation for flow through fracture surfaces assuming laminar flow between parallel plates, for the relation between the fracture apertures and permeability. The permeability in principal direction i, is calculated from the apertures in the other two principal directions j and k as follows (Rutqvist et al., 2002)

$$k_i = \frac{a_j^{\,3}}{12} + \frac{a_k^{\,3}}{12} \tag{5.1}$$

As the aperture gets modified based on the displacement of the fracture walls, the permeability will automatically get modified.

5.1.2 Porosity

The initial porosity, ϕ_0 for the fracture is specified by the user. Then the fracture porosity will be modified as function of apertures as given below (Rutqvist et al., 2002)

$$\phi = \phi_0 \left(\frac{\sum_{d=1}^{3} a_d}{\sum_{d=1}^{3} a_{id}} \right) \tag{5.2}$$

where d denotes the principal directions.

The details of the behavior implementation will be discussed in the next chapter.

6 DISCRETIZATION

The conservation equations derived in Chapter 2 need to be solved numerically. The equations of conservation of mass and energy for non-isothermal, multiphase, multi-component fluid flow in complex geological systems are solved in TOUGH2 code. The aspect of deformable porous media is added through additional term and the conservation of momentum for the solid phase. The dual mesh concept will be used to implement the coupled set of equations.

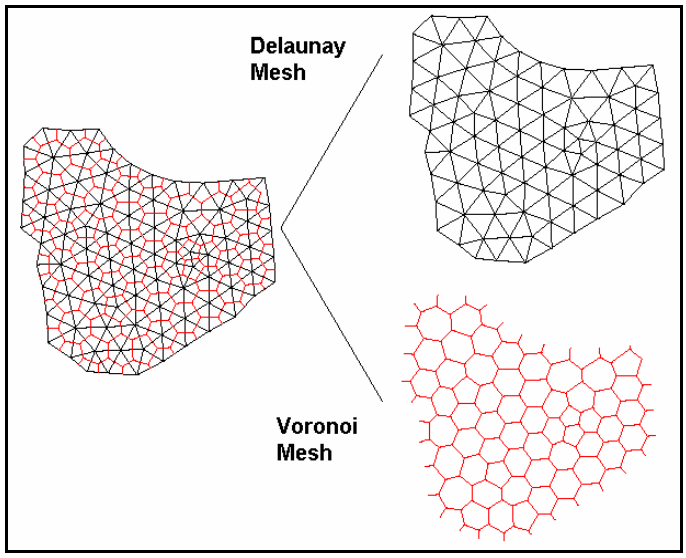

Figure 6.1 An example of dual meshes, a Delaunay mesh and a Voronoi mesh (Cosmi and Marino, 2000).

6.1 Dual Mesh Concept

The concept of a "dual mesh" is being used to implement coupled stress effects in TOUGH2. Dual meshes are alternate representations of the same geometry. An example is shown in Figure 6.1, which illustrates a Delaunay mesh and its dual, the Voronoi mesh. As can be seen in the overlapped representation, the Voronoi mesh is formed by

perpendicular bisection of the Delaunay mesh edges. This gives a volume around each node in the Delaunay mesh. The Delaunay mesh would be typical of a triangular finite element mesh, while the Voronoi mesh represents the integrated finite difference approach used in TOUGH2 for flow.

To implement the coupled stress solution in TOUGH2, the Delaunay mesh will be used for the stress calculations. By using the dual mesh, all the variables, pressure, temperature, displacement, and saturation, will be placed at the same location in the finite element and the finite volume grids. This avoids the need of averaging techniques. The details of the dual mesh concept are elaborated in Cosmi and Marino (2000). Delaunay and Voronoi are not the only approaches to dual meshes. The simplest mesh with a dual is a rectangular mesh, whose dual is a shifted rectangle, Figure 6.2(a). The current implementation is restricted to the Cartesian dual.

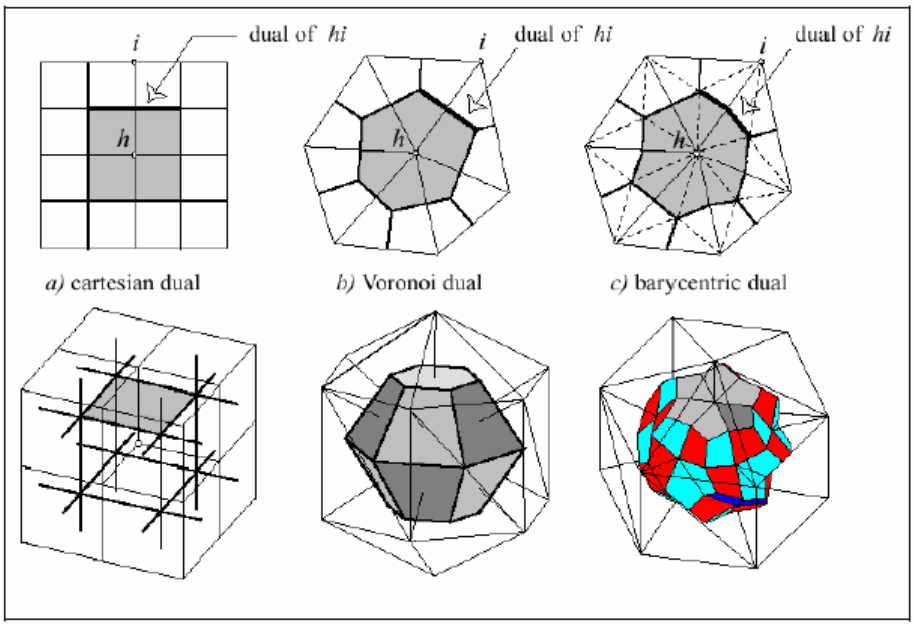

Figure 6.2 Duals for different meshes (Tonti, 2001).

Verma and Aziz (1997) have discussed in detail the application of dual mesh concept to the flow reservoir simulations. The dual mesh methods give locally mass conservative discretization, can handle the discontinuous coefficients the way the control volume methods can and have the flexibility of finite element methods (Wang, 2002).

6.2 Mass and Energy Balance using IFDM (Pruess et al., 1999)

The continuum equations (2.25) and (2.39) will be discretized in space using the Integral Finite Difference Method (IFDM) (Narasimhan and Witherspoon, 1976).

6.2.1 Original TOUGH2 Methodology

"Using the appropriate volume averages for volume-normalized extensive quantities and approximating the surface integral as a discrete sum of averages over surface segments A_{nm} (between the volume elements V_n and V_m), the general balance equation, (2.11), can be converted to a set of first-order ordinary differential equations in time as

$$\frac{\mathrm{d}M_n^\kappa}{\mathrm{dt}} = \frac{1}{V_n}\sum_m A_{nm} q_{nm}^\kappa + Q_{nm}^\kappa \tag{6.1}$$

where the nomenclature is as shown in Figure 6.3."

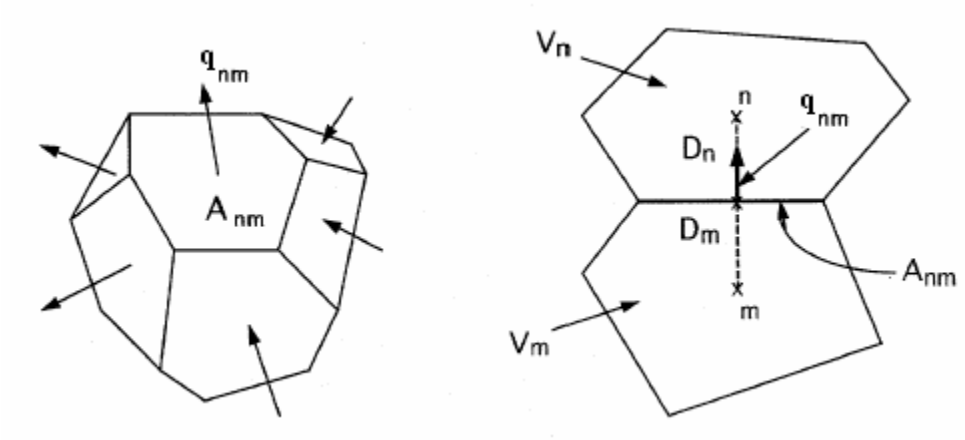

Figure 6.3 Space discretization and geometry data in the IFDM (Pruess et al., 1999).

"Time is discretized as a first-order finite difference, and a fully implicit scheme is adopted where the fluxes are expressed in the terms of the unknown thermodynamic parameters at time level $t^{i+1} = t^i + \Delta t$, leading to the following nonlinear algebraic equations.

$$R_n^{\kappa,i+1} = M_n^{\kappa,i+1} - M_n^{\kappa,i} - \frac{\Delta t}{V_n}\left\{\sum_m A_{nm} q_{nm}^{\kappa,i+1} + V_n Q_{nm}^{\kappa,i+1}\right\} \tag{6.2}$$

where, R is the residual." The TOUGH2 code performs a complete simultaneous solution of these discretized mass and energy balance equations.

6.2.2 IFDM representation of volumetric strain

The source term due to volumetric strain in the mass conservation equation needs to be discretized using either FEM or IFDM. Jacobian calculations and residual evaluation would simplify if the representation is done using IFDM. A simple but effective representation can be done if the mesh is restricted to Cartesian mesh. Hence we will assume henceforth that the mesh is Cartesian and derive the expression for the volumetric strain.

The volumetric strain is expressed as ratio of summation of displacements of the m confining areas, and the original volume,

$$\varepsilon_{V_n} = \frac{1}{V_n}\sum_m A_{nm}\left(\hat{u}_{nm} - u_n\right) \tag{6.3}$$

where displacement $\hat{u}_{nm}$ is the absolute displacement of area A_{nm}. Hence $\left(\hat{u}_{nm} - u_n\right)$ represents the relative displacement of the confining area A_{nm} with respect to the center

of the volume element V_n. The displacement $\hat{u}_{nm}$ of area A_{nm} is calculated by linear interpolation from the displacements u_n and u_m using the connection data.

$$\hat{u}_{nm} = u_n + \left[\frac{u_m - u_n}{D_m + D_n}\right] D_n \tag{6.4}$$

Hence we can write the expression for volumetric strain as

$$\begin{aligned} \varepsilon_{V_n} &= \frac{1}{V_n}\sum_m A_{nm}\left\{u_n + \left[\frac{u_m - u_n}{D_m + D_n}\right] D_n - u_n\right\} \\ &= \frac{1}{V_n}\sum_m A_{nm}\left(\frac{D_n}{D_m + D_n}\right)\left(u_m - u_n\right) \\ &= \frac{1}{V_n}\sum_m A_{nm}\, D_{nm}\left(u_m - u_n\right) \end{aligned} \tag{6.5}$$

where the quantity $D_{nm}\left\{u_m - u_n\right\}$ is the relative displacement of the confining area A_{nm} with respect to the center of the volume element, which we will denote by u_{nm}. Hence we can write

$$\varepsilon_{V_n} = \frac{1}{V_n}\sum_m A_{nm}\, u_{nm} \tag{6.6}$$

The concept is shown in Figure 6.4.

It is important to check the direction of the connection to determine if the change in volume is positive (expansion) or the negative (contraction). If the direction of connection is in the negative direction of the axis then the above expression needs to be multiplied by -1 to obtain the correct effect on the volumetric strain.

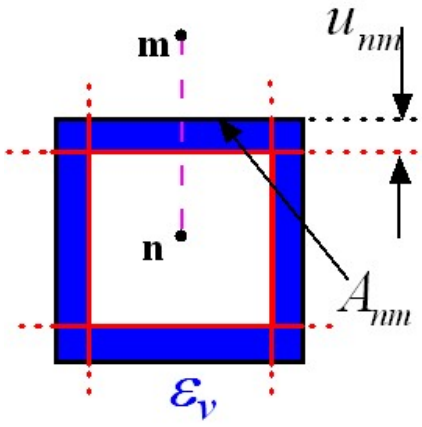

Figure 6.4 IFDM representation of volumetric strain.

6.2.3 Mass balance

Using the similar approach (IFDM) as TOUGH2 we will discretize the mass conservation equation, (2.25) as follows.

$$\left[\frac{d\left(M_n^\kappa\right)}{dt}\right]+\left[\theta_n^\kappa\left(\frac{(\alpha-\phi_n)}{K_S}\frac{d\left(\sum S_n^\psi p_n^\psi\right)}{dt}-(\alpha-\phi_n)\alpha_T\frac{dT_n}{dt}-\frac{d\phi_n}{dt}\right)\right]$$
$$+\theta_n^\kappa\frac{\alpha}{V_n}\frac{d\left(\sum_m A_{nm}u_{nm}\right)}{dt}=\frac{1}{V_n}\sum_m A_{nm}q_{nm}^\kappa-Q_{nm}^\kappa+Q_{nm}^{\kappa e} \tag{6.7}$$

where

$$M_n^\kappa=\phi_n\sum_\psi S_\psi\rho_\psi^\kappa X_\psi^\kappa$$
$$\theta_n^\kappa=\sum_\psi S_\psi\rho_\psi^\kappa X_\psi^\kappa \tag{6.8}$$
$$q_{nm}^\kappa=\sum_\psi X_\psi^\kappa q_{\psi,nm}$$

where the basic Darcy flux for each phase is given as

$$q_{\psi,nm} = -k_{nm}\left[\frac{k_{r\psi}\rho_{\psi}}{\mu_{\psi}}\right]_{nm}\left[\frac{p_{\psi,n}-p_{\psi,m}}{D_{nm}}-\rho_{\psi,nm}g_{nm}\right] \tag{6.9}$$

Again discretizing time as the first order finite difference and adopting the fully implicit method we get

$$\begin{aligned} &M_n^{\kappa,i+1}-M_n^{\kappa,i}+\left[\theta_n^{\kappa,i+1}\begin{pmatrix}\frac{\left(\alpha-\phi_n^{i+1}\right)}{K_S}\left(\sum_{\psi}S_n^{\psi}\left\{p_n^{\psi,i+1}-p_n^{\psi,i}\right\}\right)\\ -\left(\alpha-\phi_n^{i+1}\right)\alpha_T\left(T_n^{i+1}-T_n^{i}\right)-\left(\phi_n^{i+1}-\phi_n^{i}\right)\end{pmatrix}\right] \\ &+\theta_n^{\kappa,i+1}\frac{\alpha}{V_n}\left(\sum_m A_{nm}\left\{u_{nm}^{i+1}-u_{nm}^{i}\right\}\right)=\frac{\Delta t}{V_n}\left[\sum_m A_{nm}q_{nm}^{\kappa,i+1}-V_nQ_{nm}^{\kappa}+V_nQ_{nm}^{\kappa e}\right] \end{aligned} \tag{6.10}$$

Rearranging and omitting the phase energy exchange term since we will be writing a combined equation for each component, we get

$$\begin{aligned} &\left[\theta_n^{\kappa,i+1}\begin{pmatrix}\frac{\left(\alpha-\phi_n^{i+1}\right)}{K_S}\left(\sum_{\psi}S_n^{\psi}\left\{p_n^{\psi,i+1}-p_n^{\psi,i}\right\}\right)-\left(\alpha-\phi_n^{i+1}\right)\alpha_T\left(T_n^{i+1}-T_n^{i}\right)\\ -\left(\phi_n^{i+1}-\phi_n^{i}\right)+\frac{\alpha}{V_n}\left(\sum_m A_{nm}\left\{u_{nm}^{i+1}-u_{nm}^{i}\right\}\right)\end{pmatrix}\right] \\ &+M_n^{\kappa,i+1}-M_n^{\kappa,i}=\frac{\Delta t}{V_n}\left[\sum_m A_{nm}q_{nm}^{\kappa,i+1}-V_nQ_{nm}^{\kappa}\right] \end{aligned} \tag{6.11}$$

Hence the residual becomes

$$\begin{aligned} R_n^{\kappa,i+1} &= M_n^{\kappa,i+1}-M_n^{\kappa,i}-\frac{\Delta t}{V_n}\left[\sum_m A_{nm}q_{nm}^{\kappa,i+1}-V_nQ_{nm}^{\kappa}\right] \\ &+\left[\theta_n^{\kappa,i+1}\begin{pmatrix}\frac{\left(\alpha-\phi_n^{i+1}\right)}{K_S}\left(\sum_{\psi}S_n^{\psi}\left\{p_n^{\psi,i+1}-p_n^{\psi,i}\right\}\right)-\left(\alpha-\phi_n^{i+1}\right)\alpha_T\left(T_n^{i+1}-T_n^{i}\right)\\ -\left(\phi_n^{i+1}-\phi_n^{i}\right)+\frac{\alpha}{V_n}\left(\sum_m A_{nm}\left\{u_{nm}^{i+1}-u_{nm}^{i}\right\}\right)\end{pmatrix}\right] \end{aligned} \tag{6.12}$$

and we can see that the last bracket on right hand side represents the additional terms occurring due to deformable porous media.

6.2.4 Implementation Procedure

To be consistent with the implementation, we can write it as

$$
\begin{aligned}
R_n^{\kappa,i+1} = & \left[M_n^{\kappa,i+1} - M_n^{\kappa,i}\right] - \frac{\Delta t}{V_n}\left[\sum_m A_{nm} q_{nm}^{\kappa,i+1} - V_n Q_{nm}^{\kappa}\right] \\
& + \left[\begin{array}{l}
\left\{\theta_n^{\kappa,i+1}\dfrac{\left(\alpha-\phi_n^{i+1}\right)}{K_S}\left(\sum_\psi S_n^\psi p_n^{\psi,i+1}\right) - \theta_n^{\kappa,i+1}\left(\alpha-\phi_n^{i+1}\right)\alpha_T T_n^{i+1} - \theta_n^{\kappa,i+1}\phi_n^{i+1}\right\} \\
-\left\{\theta_n^{\kappa,i+1}\dfrac{\left(\alpha-\phi_n^{i+1}\right)}{K_S}\left(\sum_\psi S_n^\psi p_n^{\psi,i}\right) - \theta_n^{\kappa,i+1}\left(\alpha-\phi_n^{i+1}\right)\alpha_T T_n^{i} - \theta_n^{\kappa,i+1}\phi_n^{i}\right\} \\
+\left\{\theta_n^{\kappa,i+1}\dfrac{\alpha}{V_n}\left(\sum_m A_{nm} u_{nm}^{i+1}\right)\right\} \\
-\left\{\theta_n^{\kappa,i+1}\dfrac{\alpha}{V_n}\left(\sum_m A_{nm} u_{nm}^{i}\right)\right\}
\end{array}\right]
\end{aligned}
\tag{6.13}
$$

6.2.5 Mass balance [Incompressible Solid Phase]

We will derive the residual formulation for incompressible solid phase since it will be used in some of the verification problems. Using the similar approach (IFDM) as TOUGH2 we will discretize the mass conservation equation, (2.26), as follows.

$$
\begin{aligned}
\left[\frac{d\left(M_n^{\kappa}\right)}{dt}\right] + \theta_n^{\kappa}\left[\left(\frac{1}{V_n}\frac{d\left(\sum_m A_{nm} u_{nm}\right)}{dt}\right) - \left(\frac{d\phi_n}{dt}\right)\right] \\
= \frac{1}{V_n}\sum_m A_{nm} q_{nm}^{\kappa} - Q_{nm}^{\kappa}
\end{aligned}
\tag{6.14}
$$

Following the similar procedure as above, the residual formulation becomes

$$R_n^{\kappa,i+1} = M_n^{\kappa,i+1} - M_n^{\kappa,i} - \frac{\Delta t}{V_n}\left[\sum_m A_{nm} q_{nm}^{\kappa,i+1} - V_n Q_{nm}^{\kappa}\right] + \left[\theta_n^{\kappa,i+1}\left(\frac{1}{V_n}\left(\sum_m A_{nm}\left\{u_{nm}^{i+1} - u_{nm}^{i}\right\}\right) - \left(\phi_n^{i+1} - \phi_n^{i}\right)\right)\right] \tag{6.15}$$

6.2.6 Energy balance

The energy balance equation (2.39) is unchanged and is given by

$$\boxed{\frac{\partial\left(\phi\sum S_\psi \rho_\psi^\kappa u_\psi^E + (1-\phi)\rho_S u_S^E\right)}{\partial t} = -\nabla\bullet\left(\sum \mathbf{q}_{r\psi}^\kappa h_\psi\right) - \nabla\bullet\mathbf{J}_C^H} \tag{6.16}$$

The IFDM representation remains the same as (6.1) i.e.

$$\frac{\mathrm{d}M_n^\kappa}{\mathrm{dt}} = \frac{1}{V_n}\sum_m A_{nm} q_{nm}^\kappa + Q_{nm}^\kappa \tag{6.17}$$

where

$$\begin{aligned} M_n^\kappa &= (1-\phi_n)\rho_S C_S T + \phi_n \sum_\psi S_\psi \rho_\psi u_\psi^E \\ q_{nm}^\kappa &= -\lambda\left(\frac{T_n - T_m}{D_{nm}}\right) + \sum_\psi h_\psi q_{\psi,nm} \end{aligned} \tag{6.18}$$

and the basic Darcy flux is given as

$$q_{\psi,nm} = -k_{nm}\left[\frac{k_{r\psi}\rho_\psi}{\mu_\psi}\right]_{nm}\left[\frac{P_{\psi,n} - P_{\psi,m}}{D_{nm}} - \rho_{\psi,nm} g_{nm}\right] \tag{6.19}$$

Hence, the general residual form for energy balance equation is as follows,

$$R_n^{(\kappa)k+1} = M_n^{(\kappa)k+1} - M_n^{(\kappa)k} - \frac{\Delta t}{V_n}\left\{\sum_m A_{nm} q_{nm}^{(\kappa)k+1} + V_n Q_{nm}^{(\kappa)k+1}\right\} \tag{6.20}$$

6.3 Momentum Conservation using Finite Element Formulation

The conservation of momentum equation (2.40) is discretized using the Finite Element method. Since the momentum equation becomes the static equilibrium equations with the assumptions made, no time discretization is required.

Based on the principal of virtual work, the weak formulation of (2.40) is given as (Bathe, 1997)

$$\int_V \sigma_{ij}\,\delta\varepsilon_{ij}\,dV - \int_V b_i\,\delta u_i\,dV - \int_S t_i\,\delta u_i\,dS = 0 \tag{6.21}$$

or

$$\int_V \delta\boldsymbol{\varepsilon}^{\mathrm{T}}\,\boldsymbol{\sigma}\,dV - \int_V \delta\mathbf{u}^{\mathrm{T}}\,\mathbf{b}\,dV - \int_S \delta\mathbf{u}^{\mathrm{T}}\,\mathbf{t}\,dS = 0 \tag{6.22}$$

6.3.1 Terzaghi's Effective Stress Law

Substituting the definition of stress using the effective stress law, (3.9), in the above equation gives

$$\int_V \delta\boldsymbol{\varepsilon}^{\mathrm{T}}\,\boldsymbol{\sigma}'\,dV - \int_V \delta\boldsymbol{\varepsilon}^{\mathrm{T}}\,\mathbf{m}\,p\,dV - \int_V \delta\mathbf{u}^{\mathrm{T}}\,\mathbf{b}\,dV - \int_S \delta\mathbf{u}^{\mathrm{T}}\,\mathbf{t}\,dS = 0 \tag{6.23}$$

Using the standard finite element interpolations and same interpolation functions for displacement, pressure and temperature, we can write

$$\delta\mathbf{u} = \mathbf{N}\,\delta\mathbf{u}_a \tag{6.24}$$

and

$$\delta\boldsymbol{\varepsilon} = \mathbf{B}\,\delta\mathbf{u}_a \tag{6.25}$$

results in

$$\int_V \delta \mathbf{u}_a{}^{\mathrm{T}} \mathbf{B}^{\mathrm{T}} \boldsymbol{\sigma}' dV - \int_V \delta \mathbf{u}_a{}^{\mathrm{T}} \mathbf{B}^{\mathrm{T}} \mathbf{m} \mathbf{N} \mathbf{p} \, dV - \int_V \delta \mathbf{u}_a{}^{\mathrm{T}} \mathbf{N}^{\mathrm{T}} \mathbf{b} \, dV - \int_S \delta \mathbf{u}_a{}^{\mathrm{T}} \mathbf{N}^{\mathrm{T}} \mathbf{t} \, dS = 0 \quad (6.26)$$

We also note that

$$\int_V \mathbf{B}^{\mathrm{T}} \boldsymbol{\sigma} \, dV = \int_V \mathbf{B}^{\mathrm{T}} \boldsymbol{\sigma}' dV - \int_V \mathbf{B}^{\mathrm{T}} \mathbf{m} \mathbf{N} \mathbf{p} \, dV \quad (6.27)$$

Also, recognizing the fact that the nodal displacements associated with the weighting function are constant with respect to integration and that (6.26) must hold true for all values of the weighting function constants, gives

$$\int_V \mathbf{B}^{\mathrm{T}} \boldsymbol{\sigma}' dV - \int_V \mathbf{B}^{\mathrm{T}} \mathbf{m} \mathbf{N} \mathbf{p} \, dV = \int_V \mathbf{N}^{\mathrm{T}} \mathbf{b} \, dV + \int_S \mathbf{N}^{\mathrm{T}} \mathbf{t} \, dS \quad (6.28)$$

The displacements are interpolated using shape functions as

$$\boldsymbol{\Delta u} = \mathbf{N}_u \, \boldsymbol{\Delta u}_u + \mathbf{N} \boldsymbol{\Delta u}_a \quad (6.29)$$

and the strains by

$$\boldsymbol{\Delta \varepsilon} = \mathbf{B}_u \, \boldsymbol{\Delta u}_u + \mathbf{B} \boldsymbol{\Delta u}_a \quad (6.30)$$

where the subscript *u* refers to the known essential boundary conditions.

Using (3.16) in (6.28) we get

$$\begin{aligned} \left(\int_V \mathbf{B}^{\mathrm{T}} \mathbf{D} \mathbf{B} \, dV \right) \boldsymbol{\Delta u}_a = & \int_V \mathbf{N}^{\mathrm{T}} \mathbf{b} \, dV + \int_S \mathbf{N}^{\mathrm{T}} \mathbf{t} \, dS - \left(\int_V \mathbf{B}^{\mathrm{T}} \mathbf{D} \mathbf{B}_u \, dV \right) \boldsymbol{\Delta u}_u \\ & + \left(-(1-\alpha) \int_V \mathbf{B}^{\mathrm{T}} \mathbf{m} \mathbf{N} \boldsymbol{\Delta p} \, dV \right) + \left((3K\alpha_T) \int_V \mathbf{B}^{\mathrm{T}} \mathbf{m} \mathbf{N} \boldsymbol{\Delta T} \, dV \right) \\ & + \int_V \mathbf{B}^{\mathrm{T}} \boldsymbol{\sigma}'_{\mathbf{0}} \, dV + \int_V \mathbf{B}^{\mathrm{T}} \mathbf{m} \mathbf{N} \mathbf{p}_{\mathbf{0}} \, dV \end{aligned} \quad (6.31)$$

Equation (6.31) is used in implementation of the poroelastic behavior. For the sake of completeness, we will write the residual term in this finite element implementation, the details of which will be explained in the next section.

$$\mathbf{R} = \left(\alpha \int_V \mathbf{B}^{\mathrm{T}} \mathbf{m} \mathbf{N} \Delta \mathbf{p} \, dV \right) + \left((3K\alpha_T) \int_V \mathbf{B}^{\mathrm{T}} \mathbf{m} \mathbf{N} \Delta \mathbf{T} \, dV \right) + \int_V \mathbf{B}^{\mathrm{T}} \mathbf{m} \mathbf{N} \Delta \mathbf{p_0} \, dV$$
$$+ \int_V \mathbf{B}^{\mathrm{T}} \boldsymbol{\sigma}'_0 \, dV - \left(\int_V \mathbf{B}^{\mathrm{T}} \mathbf{D} \mathbf{B}_u \, dV \right) \Delta \mathbf{u}_u - \left(\int_V \mathbf{B}^{\mathrm{T}} \mathbf{D} \mathbf{B} \, dV \right) \Delta \mathbf{u}_a + \int_V \mathbf{N}^{\mathrm{T}} \mathbf{b} \, dV + \int_S \mathbf{N}^{\mathrm{T}} \mathbf{t} \, dS \tag{6.32}$$

6.3.2 Biot's (Modified) Effective Stress Law

Substituting the definition of stress using the modified effective stress law, (3.19), in the equation (6.22) we get

$$\int_V \delta \boldsymbol{\varepsilon}^{\mathrm{T}} \boldsymbol{\sigma}'' \, dV - \int_V \delta \boldsymbol{\varepsilon}^{\mathrm{T}} \alpha \mathbf{m} \, p \, dV - \int_V \delta \mathbf{u}^{\mathrm{T}} \mathbf{b} \, dV - \int_S \delta \mathbf{u}^{\mathrm{T}} \mathbf{t} \, dS = 0 \tag{6.33}$$

Using the standard finite element interpolations and same interpolation functions for displacement, pressure and temperature, we can write

$$\delta \mathbf{u} = \mathbf{N} \delta \mathbf{u}_a \tag{6.34}$$

and

$$\delta \boldsymbol{\varepsilon} = \mathbf{B} \delta \mathbf{u}_a \tag{6.35}$$

which results in

$$\int_V \delta \mathbf{u}_a{}^{\mathrm{T}} \mathbf{B}^{\mathrm{T}} \boldsymbol{\sigma}'' \, dV - \int_V \delta \mathbf{u}_a{}^{\mathrm{T}} \mathbf{B}^{\mathrm{T}} \alpha \mathbf{m} \mathbf{N} \mathbf{p} \, dV - \int_V \delta \mathbf{u}_a{}^{\mathrm{T}} \mathbf{N}^{\mathrm{T}} \mathbf{b} \, dV - \int_S \delta \mathbf{u}_a{}^{\mathrm{T}} \mathbf{N}^{\mathrm{T}} \mathbf{t} \, dS = 0 \tag{6.36}$$

We also note that

$$\int_V \mathbf{B}^{\mathrm{T}} \boldsymbol{\sigma} \, dV = \int_V \mathbf{B}^{\mathrm{T}} \boldsymbol{\sigma}'' \, dV - \int_V \mathbf{B}^{\mathrm{T}} \alpha \mathbf{m} \mathbf{N} \mathbf{p} \, dV \tag{6.37}$$

Also, recognizing the fact that the nodal displacements associated with the weighting function are constant with respect to integration and that (6.36) must hold true for all values of the weighting function constants, gives

$$\int_V \mathbf{B}^{\mathrm{T}}\,\boldsymbol{\sigma}\,dV = \int_V \mathbf{N}^{\mathrm{T}}\,\mathbf{b}\,dV + \int_S \mathbf{N}^{\mathrm{T}}\,\mathbf{t}\,dS \tag{6.38}$$

The displacements are interpolated using shape functions as

$$\boldsymbol{\Delta u} = \mathbf{N}_u\,\boldsymbol{\Delta u}_u + \mathbf{N}\,\boldsymbol{\Delta u}_a \tag{6.39}$$

and the strains by

$$\boldsymbol{\Delta\varepsilon} = \mathbf{B}_u\,\boldsymbol{\Delta u}_u + \mathbf{B}\,\boldsymbol{\Delta u}_a \tag{6.40}$$

where the subscript *u* refers to the known essential boundary conditions.

Using (3.24) in (6.38) we get

$$\left(\int_V \mathbf{B}^{\mathrm{T}}\left\{\left(\mathbf{D}\boldsymbol{\Delta\varepsilon} - \left(3K\,\alpha_T\right)\mathbf{m}\,\Delta T + \boldsymbol{\sigma}''_0\right) - \alpha\,\mathbf{m}\,p\right\}dV\right) = \int_V \mathbf{N}^{\mathrm{T}}\,\mathbf{b}\,dV + \int_S \mathbf{N}^{\mathrm{T}}\,\mathbf{t}\,dS \tag{6.41}$$

Using the interpolations, we can write

$$\begin{aligned}&\left(\int_V \mathbf{B}^{\mathrm{T}}\left\{\left(\mathbf{D}\left(\mathbf{B}_u\,\boldsymbol{\Delta u}_u + \mathbf{B}\,\boldsymbol{\Delta u}_a\right) - \left(3K\,\alpha_T\right)\mathbf{m}\,\mathbf{N}\,\boldsymbol{\Delta T} + \boldsymbol{\sigma}''_0\right) - \alpha\,\mathbf{m}\,\mathbf{N}\,\mathbf{p}\right\}dV\right)\\ &= \int_V \mathbf{N}^{\mathrm{T}}\,\mathbf{b}\,dV + \int_S \mathbf{N}^{\mathrm{T}}\,\mathbf{t}\,dS\end{aligned} \tag{6.42}$$

Rearranging, we get

$$\begin{aligned}\left(\int_V \mathbf{B}^{\mathrm{T}}\,\mathbf{D}\mathbf{B}\,dV\right)\boldsymbol{\Delta u}_a = {} & \int_V \mathbf{N}^{\mathrm{T}}\,\mathbf{b}\,dV + \int_S \mathbf{N}^{\mathrm{T}}\,\mathbf{t}\,dS - \left(\int_V \mathbf{B}^{\mathrm{T}}\,\mathbf{D}\mathbf{B}_u\,dV\right)\boldsymbol{\Delta u}_u\\ & + \left(\left(3K\alpha_T\right)\int_V \mathbf{B}^{\mathrm{T}}\,\mathbf{m}\,\mathbf{N}\,\boldsymbol{\Delta T}\,dV\right) - \int_V \mathbf{B}^{\mathrm{T}}\,\boldsymbol{\sigma}''_0\,dV + \int_V \mathbf{B}^{\mathrm{T}}\alpha\,\mathbf{m}\mathbf{N}\,\mathbf{p}\,dV\end{aligned} \tag{6.43}$$

Equation (6.43) is used in the implementation of the poroelastic behavior. Using the alternative form of (3.24), i.e. expressing current pressure as sum of incremental pressure and initial pressure, we can write the above equation as

$$\begin{aligned}\left(\int_V \mathbf{B}^{\mathrm{T}}\mathbf{D}\mathbf{B}\,dV\right)\Delta\mathbf{u}_a = &\int_V \mathbf{N}^{\mathrm{T}}\mathbf{b}\,dV + \int_S \mathbf{N}^{\mathrm{T}}\mathbf{t}\,dS - \left(\int_V \mathbf{B}^{\mathrm{T}}\mathbf{D}\mathbf{B}_u\,dV\right)\Delta\mathbf{u}_u \\ &- \int_V \mathbf{B}^{\mathrm{T}}\boldsymbol{\sigma}''_0\,dV + \left(\int_V \mathbf{B}^{\mathrm{T}}\alpha\ \mathbf{m}\mathbf{N}\mathbf{p}_0\,dV\right) \\ &+ \left\{\int_V \mathbf{B}^{\mathrm{T}}\alpha\,\mathbf{m}\mathbf{N}\Delta\mathbf{p}\,dV\right\} + \left(3K\alpha_T\right)\int_V \mathbf{B}^{\mathrm{T}}\mathbf{m}\mathbf{N}\Delta\mathbf{T}\,dV\end{aligned} \tag{6.44}$$

For the sake of completeness we will write the residual term in this finite element implementation, the details of which will be explained in the next section.

$$\begin{aligned}\mathbf{R} = &\int_V \mathbf{N}^{\mathrm{T}}\mathbf{b}\,dV + \int_S \mathbf{N}^{\mathrm{T}}\mathbf{t}\,dS - \left(\int_V \mathbf{B}^{\mathrm{T}}\mathbf{D}\mathbf{B}_u\,dV\right)\Delta\mathbf{u}_u - \left(\int_V \mathbf{B}^{\mathrm{T}}\mathbf{D}\mathbf{B}\,dV\right)\Delta\mathbf{u}_a \\ &+ \left(\int_V \mathbf{B}^{\mathrm{T}}\alpha\ \mathbf{m}\mathbf{N}\mathbf{p}_0\,dV\right) + \int_V \mathbf{B}^{\mathrm{T}}\alpha\,\mathbf{m}\mathbf{N}\Delta\mathbf{p}\,dV - \int_V \mathbf{B}^{\mathrm{T}}\boldsymbol{\sigma}''_0\,dV \\ &+ \left(\left(3K\alpha_T\right)\int_V \mathbf{B}^{\mathrm{T}}\mathbf{m}\mathbf{N}\Delta\mathbf{T}\,dV\right)\end{aligned} \tag{6.45}$$

6.3.3 Implementation details

A conscious effort has been made to keep the coupling, between the TOUGH2 and the Stress, as clean as possible. The aim has been to keep the changes in TOUGH2 to minimum. Also, the code implementation allow to carry out only the TOUGH2 (fluid flow-heat transfer) simulation, without incorporating stress as well as switching on/off the poroelastic and thermo-elastic effects.

6.3.3.1 The Volume Element

An 8-noded linear serendipity Brick element has been used for the finite element analysis. The shape function for this element are given as,

$$N_i = \frac{1}{8}(1+\xi\xi_i)(1+\eta\eta_i)(1+\zeta\zeta_i) \tag{6.46}$$

where $\xi, \eta, \text{and } \zeta$ represent the natural coordinates with the range (-1,1) in its natural coordinate space for the 8 nodes. Figure 6.5 shows the node numbering convention for the 8-noded Brick element.

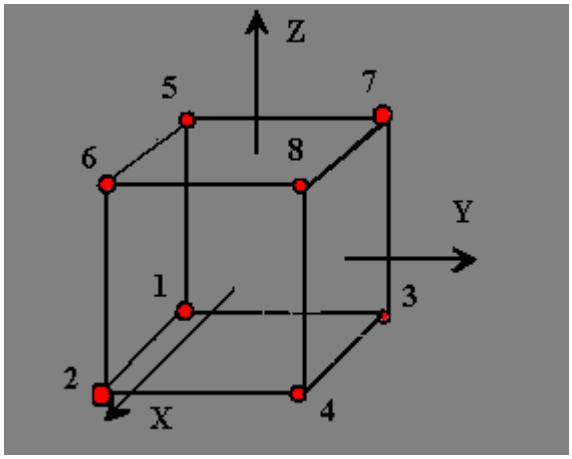

Figure 6.5 Node numbering for mesh of 8-noded Brick Element.

6.3.3.2 Numerical Integration Scheme

The volume integrals for each element in the finite element formulation are carried out using Gauss Quadrature as

$$\begin{aligned}\int_{V_e} f(x,y,z)\,dV_e &= \int_{-1}^{1}\int_{-1}^{1}\int_{-1}^{1} f(\xi,\eta,\zeta)|J|\,d\xi\,d\eta\,d\zeta \\ &= \sum_i\sum_j\sum_k W_i W_j W_k\, f(\xi_i,\eta_j,\zeta_k)|J|\end{aligned} \tag{6.47}$$

The implemented integrator uses the combined gauss weights $W_{GP} = W_i W_j W_k$, related to respective gauss point and hence can be written as

$$\int_{V_e} f(x,y,z)\,dV_e = \sum_{n=1}^{numGP} W_{GP}\left|J\right|_{GP_n} f(GP_n) \tag{6.48}$$

In the T2STR code, the higher order 8 Gauss point integration is implemented.

6.4 Fracture Behavior (Finite Element Implementation)

The finite element formulation for the fracture behavior is derived as follows. The fracture element is a volume element with the surface tractions and pressures acting on the faces of the fracture. Consider a single element with the node numbering as shown in Figure 6.6.

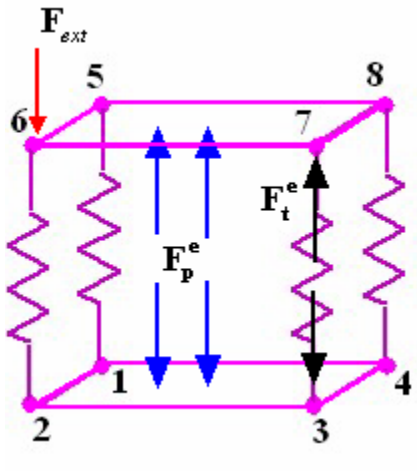

Figure 6.6 Node numbering and representative forces in fracture behavior.

The force balance for the element due to surface traction $\mathbf{t}^e$ from the contact, the fluid pressure $\mathbf{p}^e$, and external forces $\mathbf{F}_{ext}$ is given as

$$\mathbf{F}_{ext} - \int_V \mathbf{B}^T \boldsymbol{\sigma}\, dV = 0 \tag{6.49}$$

where $\boldsymbol{\sigma}$ is used for representing the stresses due to combined effect of contact stresses and fluid pressure as follows

$$\boldsymbol{\sigma} = \mathbf{t}^{\mathbf{e}} + \mathbf{p}^{\mathbf{e}} \tag{6.50}$$

The pressure forces due $\mathbf{p}^{\mathbf{e}}$ to are given by

$$\mathbf{F}_{\mathbf{p}}^{\mathbf{e}} = \left(\int_V \mathbf{B}^{\mathbf{T}} \mathbf{m} \mathbf{N} \, dV \right) \mathbf{p} \tag{6.51}$$

The forces due to surface traction $\mathbf{t}^{\mathbf{e}}$ at the joint are expressed using contact stresses $\boldsymbol{\sigma}_{\mathbf{ct}}$ as

$$\mathbf{F}_{\mathbf{t}}^{\mathbf{e}} = \int_V \mathbf{B}^{\mathbf{T}} \left(\boldsymbol{\sigma}_{\mathbf{ct}}(\mathbf{a}) \right) dV \tag{6.52}$$

The residual for the element with fracture behavior can be written as

$$\mathbf{R} = \left\{ \mathbf{F}_{ext} - \left(\int_V \mathbf{B}^{\mathbf{T}} \mathbf{m} \mathbf{N} \, dV \right) \mathbf{p} \right\} - \left(\int_V \mathbf{B}^{\mathbf{T}} \left(\boldsymbol{\sigma}_{\mathbf{ct}}(\mathbf{a}) \right) dV \right) \tag{6.53}$$

where $\boldsymbol{\sigma}_{\mathbf{ct}}$ is the contact stress vector corresponding to the current aperture vector $\mathbf{a}$.

7 SOLUTION TECHNIQUE

All the discretized equations are solved by the Newton-Raphson iteration technique already implemented in TOUGH2 to handle nonlinearity.

7.1 Original TOUGH2 implementation

Expanding the residuals (in equation (6.2)) at $p+1$ iteration step in a Taylor series and retaining only the first order terms and setting the expansion equal to zero, we obtain

$$-\sum_m \left.\frac{\partial R_n^{\kappa,i+1}}{\partial x_m}\right|_p \left(x_{m,p+1} - x_{m,p}\right) = R_n^{\kappa,i+1}\left(x_{m,p}\right) \tag{7.1}$$

Most of the terms $\frac{\partial R_n}{\partial x_m}$ in the Jacobian matrix are evaluated numerically in TOUGH2 code for the selected primary variables. The solution is achieved when the residual R becomes small.

7.2 One way coupling

The initial formulation was implemented for one way coupling. The formulation was derived to solve the FEM equations using the same solver in TOUGH2. The implementation was based on unmodified effective stress law.

7.2.1 Formulation for Newton-Raphson solution (Unmodified stress law)

To solve the finite element equations using the same solver in TOUGH2 the formulation is implemented as follows. The residual for the Newton-Raphson method for a finite element formulation in its functional form is given as

$$\mathrm{f}\left(\Delta u_a^{\,*}\right) = 0 \tag{7.2}$$

where,

$$\begin{aligned}\mathbf{R} &= {}^{t+\Delta t}\mathbf{F}_{\text{ext}}\left(\Delta u_a{}^{*}\right) - {}^{t+\Delta t}\mathbf{F}_{\text{int}}\left(\Delta u_a{}^{*}\right) \\ &= g - f\left(\Delta u_a{}^{*}\right)\end{aligned} \tag{7.3}$$

Here * is used to denote the solution. Assume that in the iterative solution we have evaluated ${}^{t+\Delta t}\Delta u_a{}^{(i-1)}$; then a Taylor series Expansion gives

$$\mathrm{f}\left(\Delta u_a{}^{*}\right) = \mathrm{f}\left({}^{t+\Delta t}\Delta u_a{}^{(i-1)}\right) + \left[\frac{d\,\mathrm{f}}{d\left(\Delta u_a\right)}\right]\Bigg|_{t+\Delta t_{\Delta ua}(i-1)} \left(\Delta u_a{}^{*} - {}^{t+\Delta t}\Delta u_a{}^{(i-1)}\right) + \cdots \tag{7.4}$$

Substituting (7.4) in (7.3) and neglecting higher order terms, we get

$$\mathbf{R}^{i} = g - \left(\mathrm{f}\left({}^{t+\Delta t}\Delta u_a{}^{(i-1)}\right) + \left[\frac{d\,\mathrm{f}}{d\left(\Delta u_a\right)}\right]\Bigg|_{t+\Delta t}^{(i-1)} \left(\Delta u_a{}^{*} - {}^{t+\Delta t}\Delta u_a{}^{(i-1)}\right) \right) \tag{7.5}$$

Assuming that the externally applied loads are independent of the deformation, the increment in the displacement can be calculated as

$$\begin{aligned}{}^{t+\Delta t}\mathbf{K}^{(i-1)}\left(\delta\left(\Delta u_a\right)^{(i)}\right) &= g - \mathrm{f}\left({}^{t+\Delta t}\Delta u_a{}^{(i-1)}\right) \\ &= {}^{t+\Delta t}\mathbf{F}_{\text{ext}} - {}^{t+\Delta t}\mathbf{F}_{\text{int}}^{(i-1)}\end{aligned} \tag{7.6}$$

where ${}^{t+\Delta t}\mathbf{K}^{(i-1)}$ is the current tangent stiffness matrix given as

$${}^{t+\Delta t}\mathbf{K}^{(i-1)} = \left[\frac{d\,\mathrm{f}}{d\left(\Delta u_a\right)}\right]\Bigg|_{t+\Delta t_{\Delta ua}(i-1)} \tag{7.7}$$

Now, rearranging the (6.28) we can write

$$\left(\int_V \mathbf{N}^{\mathrm{T}}\mathbf{b}\,dV + \int_S \mathbf{N}^{\mathrm{T}}\mathbf{t}\,dS\right) - \left(\int_V \mathbf{B}^{\mathrm{T}}\boldsymbol{\sigma}\,dV\right) = 0 \tag{7.8}$$

Here the first two terms represent the external body forces and the third term represents the internal forces (or the nodal point forces corresponding to the elemental stresses).

Using the (7.8) in (7.6) we can write

$$
\begin{aligned}
{}^{t+\Delta t}\mathbf{K}^{(i-1)}\left(\delta\left(\Delta u_a\right)^{(i)}\right) = & \ {}^{t+\Delta t}\left(\int_V \mathbf{N}^{\mathrm{T}}\mathbf{b}\, dV + \int_S \mathbf{N}^{\mathrm{T}}\mathbf{t}\, dS\right) \\
& - {}^{t+\Delta t}\left(\int_V \mathbf{B}^{\mathrm{T}}\boldsymbol{\sigma}\, dV\right)^{(i-1)}
\end{aligned}
\tag{7.9}
$$

The updated displacement solution is

$$
{}^{t+\Delta t}\Delta u_a{}^{(i)} = {}^{t+\Delta t}\Delta u_a{}^{(i-1)} + \delta\Delta u_a{}^{(i)} \tag{7.10}
$$

with the initial conditions at the start of each iteration as ${}^{t+\Delta t}\mathbf{K}^{(0)} = {}^{t}\mathbf{K}$; ${}^{t+\Delta t}\mathbf{F}^{(0)} = {}^{t}\mathbf{F}$ and ${}^{t+\Delta t}\Delta u_a{}^{(0)} = {}^{t}\Delta u_a$.

The required integrations are evaluated by summing the contribution of each element. Using the definition of stress (3.16) we can write (7.9) as

$$
\begin{aligned}
{}^{t+\Delta t}\mathbf{K}^{(i-1)}\left(\delta\left(\Delta u_a\right)^{(i)}\right) = & \ {}^{t+\Delta t}\left(\begin{array}{l}\displaystyle\sum_{e=1}^{numEl}\int_{V_e}\mathbf{N}^{\mathrm{T}}\mathbf{b}\, dV_e + \sum_{e=1}^{numEl}\int_{S_e}\mathbf{N}^{\mathrm{T}}\mathbf{t}\, dS_e \\ -\left(\displaystyle\sum_{e=1}^{numEl}\int_{V_e}\mathbf{B}^{\mathrm{T}}\,\mathbf{D}\,\mathbf{B}_u\, dV_e\right)\Delta\mathbf{u}_u\end{array}\right) \\
& - {}^{t+\Delta t}\left(\sum_{e=1}^{numEl}\int_{V_e}\mathbf{B}^{\mathrm{T}}\begin{bmatrix}\left(\mathbf{D}\,\mathbf{B}\,\Delta\mathbf{u}_a\right)+\left(\boldsymbol{\sigma}'_0\right) \\ -\left(\left(3K\alpha_T\right)\mathbf{m}\,\mathbf{N}\,\Delta\mathbf{T}\right) \\ +\left(\left(1-\alpha\right)\mathbf{m}\,\mathbf{N}\,\Delta\mathbf{p}\right)-\left(\mathbf{m}\,\mathbf{N}\,\mathbf{p}\right)\end{bmatrix} dV_e\right)^{(i-1)}
\end{aligned}
\tag{7.11}
$$

This completes the residual formulation of finite element implementation.

7.3 Fully coupled formulation

The fully coupled formulation was derived using modified effective stress law. The Newton-Raphson formulation was derived for implementation using the TOUGH2 set of solvers. Also, the FEM equations are re-written using the TOUGH2 primary variables in addition to the displacements.

The Newton-Raphson formulation for the FEM equations can be obtained by defining the residual $\mathbf{R}$ as follows

$$\mathbf{R} = g - f\left(\Delta u, \Delta p, \Delta T\right) \tag{7.12}$$

where g represents forces independent of unknown variables, i.e. pressure, temperature, and displacements, and f represents the internal forces and the hydrostatic forces. We can define the residual using (6.38) as

$$\mathbf{R} = \left(\int_V \mathbf{N}^{\mathrm{T}} \mathbf{b}\, dV + \int_S \mathbf{N}^{\mathrm{T}} \mathbf{t}\, dS \right) - \left(\int_V \mathbf{B}^{\mathrm{T}} \boldsymbol{\sigma}''\, dV - \int_V \mathbf{B}^{\mathrm{T}} \alpha\, \mathbf{m}\, \mathbf{N}\, \mathbf{p}\, dV \right) \tag{7.13}$$

or expanding the modified effective stress terms

$$\begin{aligned} \mathbf{R} = & \left(\int_V \mathbf{N}^{\mathrm{T}} \mathbf{b}\, dV + \int_S \mathbf{N}^{\mathrm{T}} \mathbf{t}\, dS - \left(\int_V \mathbf{B}^{\mathrm{T}} \mathbf{D} \mathbf{B}_u\, dV \right) \Delta \mathbf{u}_u \right) \\ & - \left(\begin{array}{l} \left(\int_V \mathbf{B}^{\mathrm{T}} \mathbf{D} \mathbf{B}\, dV \right) \Delta \mathbf{u}_a - \int_V \mathbf{B}^{\mathrm{T}} \alpha\, \mathbf{m} \mathbf{N} \Delta \mathbf{p}\, dV \\ - \left(\left(3K\alpha_T\right) \int_V \mathbf{B}^{\mathrm{T}} \mathbf{m} \mathbf{N} \Delta \mathbf{T}\, dV \right) - \left(\int_V \mathbf{B}^{\mathrm{T}} \alpha\, \mathbf{m} \mathbf{N} \mathbf{p}_0\, dV \right) + \int_V \mathbf{B}^{\mathrm{T}} \boldsymbol{\sigma}''_0\, dV \end{array} \right) \end{aligned} \tag{7.14}$$

where first parenthesis represents the independent terms g and second one represents the variable dependent terms f. The subscript a for the unknown displacements, 'u's, is dropped for brevity henceforth. Considering the implementation, the $\mathbf{p}_0$ and $\boldsymbol{\sigma}''_0$ terms

are included in f even if they are not dependent terms. Thus function f can be evaluated from the total stress.

Hence the solution of the FEM equations can be obtained if we make the residual zero. i.e., using the same denomination as above,

$$\begin{aligned} \mathbf{R} &= 0 \\ &= g - f\left(\Delta u^*, \Delta p^*, \Delta T^*\right) \end{aligned} \tag{7.15}$$

where * denotes the values of the variables when correct solution is obtained.

The residual at iteration i of time step $t+\Delta t$ we can write

$${}^{t+\Delta t}\mathbf{R}^i = {}^{t+\Delta t}g - {}^{t+\Delta t}f\left(\Delta u, \Delta p, \Delta T\right)^i \tag{7.16}$$

Using a first order approximation of a three variable Taylor series, we can write the f at iteration i as

$$\begin{aligned} {}^{t+\Delta t}f\left(\Delta u, \Delta p, \Delta T\right)^{(i)} = {}& {}^{t+\Delta t}f\left(\Delta u, \Delta p, \Delta T\right)^{(i-1)} \\ & + \left(\frac{\partial f}{\partial \Delta u}\right)^{(i-1)} \delta \Delta u^{(i)} + \left(\frac{\partial f}{\partial \Delta p}\right)^{(i-1)} \delta \Delta p^{(i)} + \left(\frac{\partial f}{\partial \Delta T}\right)^{(i-1)} \delta \Delta T^{(i)} \end{aligned} \tag{7.17}$$

To obtain the solution at iteration i we want to make residual ${}^{t+\Delta t}\mathbf{R}^i$ zero, hence

$$\begin{aligned} {}^{t+\Delta t}\mathbf{R}^i &= {}^{t+\Delta t}g - {}^{t+\Delta t}f\left(\Delta u, \Delta p, \Delta T\right)^i \\ &= {}^{t+\Delta t}g \\ &\quad - \left(\begin{array}{l} {}^{t+\Delta t}f\left(\Delta u, \Delta p, \Delta T\right)^{(i-1)} \\ + \left(\dfrac{\partial f}{\partial \Delta u}\right)^{(i-1)} \delta \Delta u^{(i)} + \left(\dfrac{\partial f}{\partial \Delta p}\right)^{(i-1)} \delta \Delta p^{(i)} + \left(\dfrac{\partial f}{\partial \Delta T}\right)^{(i-1)} \delta \Delta T^{(i)} \end{array} \right) \\ &= 0 \end{aligned} \tag{7.18}$$

which we can write as

$$\left(\frac{\partial f}{\partial \Delta u}\right)^{(i-1)} \delta\Delta u^{(i)} + \left(\frac{\partial f}{\partial \Delta p}\right)^{(i-1)} \delta\Delta p^{(i)} + \left(\frac{\partial f}{\partial \Delta T}\right)^{(i-1)} \delta\Delta T^{(i)} = {}^{t+\Delta t}g - {}^{t+\Delta t}f\left(\Delta u, \Delta p, \Delta T\right)^{(i-1)} \tag{7.19}$$

Now we have

$$f = \left(\int_V \mathbf{B}^{\mathrm{T}}\mathbf{D}\mathbf{B}\, dV\right)\Delta\mathbf{u}_a - \left(\int_V \mathbf{B}^{\mathrm{T}}\alpha\ \mathbf{m}\mathbf{N}\ dV\right)\Delta\mathbf{p} - \left(\left(3K\alpha_T\right)\int_V \mathbf{B}^{\mathrm{T}}\mathbf{m}\mathbf{N}\ dV\right)\Delta\mathbf{T} - \left(\int_V \mathbf{B}^{\mathrm{T}}\alpha\ \mathbf{m}\mathbf{N}\, dV\right)\mathbf{p_0} + \int_V \mathbf{B}^{\mathrm{T}}\boldsymbol{\sigma}''_0\, dV \tag{7.20}$$

Hence we can write the residual equation as

$$\left(-\int_V \mathbf{B}^{\mathrm{T}}\mathbf{D}\mathbf{B}\, dV\right)^{(i-1)} \delta\Delta u^{(i)} + \left(\int_V \mathbf{B}^{\mathrm{T}}\left(-\alpha\ \mathbf{m}\right)\mathbf{N}\ dV\right)^{(i-1)} \delta\Delta p^{(i)} + \left(\int_V \mathbf{B}^{\mathrm{T}}\left(-3K\alpha_T\mathbf{m}\right)\mathbf{N}\ dV\right)^{(i-1)} \delta\Delta T^{(i)} = {}^{t+\Delta t}g - {}^{t+\Delta t}f\left(\Delta u, \Delta p, \Delta T\right)^{(i-1)} \tag{7.21}$$

Defining matrices $\mathbf{K_e}, \mathbf{Q_p}$, and $\mathbf{Q_T}$ as,

$$\mathbf{Q_p} = -\int_V \mathbf{B}^{\mathrm{T}}\left[\alpha\ \mathbf{m}\mathbf{N}\right]dV \tag{7.22}$$

$$\mathbf{Q_T} = -\int_V \mathbf{B}^{\mathrm{T}}\left[\left(3K\alpha_T\right)\mathbf{m}\mathbf{N}\right]dV \tag{7.23}$$

and

$$\mathbf{K_e} = -\int_V \mathbf{B}^{\mathrm{T}}\ \mathbf{D}\,\mathbf{B}\, dV \tag{7.24}$$

we can write

$$\left(\mathbf{K_e}\right)^{(i-1)}\delta\Delta u^{(i)} + \left(\mathbf{Q_p}\right)^{(i-1)}\delta\Delta p^{(i)} + \left(\mathbf{Q_T}\right)^{(i-1)}\delta\Delta T^{(i)} = {}^{t+\Delta t}g - {}^{t+\Delta t}f\left(\Delta u, \Delta p, \Delta T\right)^{(i-1)} \tag{7.25}$$

Hence the Newton-Raphson formulation to be implemented can be written as

$$
\begin{aligned}
{}^{t+\Delta t}\begin{pmatrix} \left(\mathbf{K_e}\right)^{(i-1)}\boldsymbol{\delta}\Delta\mathbf{u}^{(i)} \\ +\left(\mathbf{Q_p}\right)^{(i-1)}\boldsymbol{\delta}\Delta\mathbf{p}^{(i)} \\ +\left(\mathbf{Q_T}\right)^{(i-1)}\boldsymbol{\delta}\Delta\mathbf{T}^{(i)} \end{pmatrix} &= {}^{t+\Delta t}\left(\int_V \mathbf{N}^{\mathrm{T}}\mathbf{b}\, dV + \int_S \mathbf{N}^{\mathrm{T}}\mathbf{t}\, dS - \left(\int_V \mathbf{B}^{\mathrm{T}}\mathbf{D}\mathbf{B}_u\, dV \right)\Delta\,\mathbf{u}_u \right) \\
&\quad - {}^{t+\Delta t}\begin{pmatrix} \left(\int_V \mathbf{B}^{\mathrm{T}}\mathbf{D}\mathbf{B}\, dV \right)\Delta\mathbf{u}_a - \int_V \mathbf{B}^{\mathrm{T}}\alpha\,\mathbf{m}\mathbf{N}\,\Delta\mathbf{p}\, dV \\ -\left(\int_V \mathbf{B}^{\mathrm{T}}\left(3K\alpha_T\right)\mathbf{m}\mathbf{N}\,\Delta\mathbf{T}\, dV \right) \\ -\left(\int_V \mathbf{B}^{\mathrm{T}}\alpha\ \mathbf{m}\mathbf{N}\,\mathbf{p_0}\, dV \right) + \int_V \mathbf{B}^{\mathrm{T}}\boldsymbol{\sigma}''_0\, dV \end{pmatrix}^{(i-1)}
\end{aligned}
\tag{7.26}
$$

or

$$
\begin{aligned}
{}^{t+\Delta t}\begin{pmatrix} \left(\mathbf{K_e}\right)^{(i-1)}\boldsymbol{\delta}\Delta\mathbf{u}^{(i)} \\ +\left(\mathbf{Q_p}\right)^{(i-1)}\boldsymbol{\delta}\Delta\,\mathbf{p}^{(i)} \\ +\left(\mathbf{Q_T}\right)^{(i-1)}\boldsymbol{\delta}\Delta\mathbf{T}^{(i)} \end{pmatrix} &= {}^{t+\Delta t}\left(\int_V \mathbf{N}^{\mathrm{T}}\mathbf{b}\, dV + \int_S \mathbf{N}^{\mathrm{T}}\mathbf{t}\, dS - \left(\int_V \mathbf{B}^{\mathrm{T}}\mathbf{D}\mathbf{B}_u\, dV \right)\Delta\,\mathbf{u}_u \right) \\
&\quad - {}^{t+\Delta t}\begin{pmatrix} \left(\mathbf{K_e}\right)\Delta\mathbf{u}_a + \left(\mathbf{Q_p}\right)^{(i-1)}\Delta\mathbf{p} + \left(\mathbf{Q_T}\right)^{(i-1)}\Delta\mathbf{T} \\ -\left(\int_V \mathbf{B}^{\mathrm{T}}\alpha\ \mathbf{m}\mathbf{N}\,\mathbf{p_0}\, dV \right) + \int_V \mathbf{B}^{\mathrm{T}}\boldsymbol{\sigma}''_0\, dV \end{pmatrix}^{(i-1)}
\end{aligned}
\tag{7.27}
$$

7.4 Fully coupled formulation for TOUGH2 primary variables

TOUGH2 uses phase pressure and the temperature as primary variables for single phase and gas phase pressure and gas phase saturation as primary variables for two-phase problems. The formulation for the momentum equation will have to be expressed in TOUGH2 variables to generate coherent coupled equations.

7.4.1 Single phase formulation

The single phase variable is temperature for TOUGH2 as well as for the momentum equation. But the pressure in the momentum equation is solid pressure and the corresponding primary variable in TOUGH2 is the phase pressure. For the single phase condition the solid phase pressure is actually the fluid phase pressure. Hence the formulation derived can be used as it is and can be stated as

$$\begin{aligned}{}^{t+\Delta t}\begin{pmatrix}\left(\mathbf{K_e}\right)^{(i-1)}\boldsymbol{\delta}\boldsymbol{\Delta}\mathbf{u}^{(i)}\\ +\left(\mathbf{Q_p}\right)^{(i-1)}\boldsymbol{\delta}\boldsymbol{\Delta}\mathbf{p}^{(i)}\\ +\left(\mathbf{Q_T}\right)^{(i-1)}\boldsymbol{\delta}\boldsymbol{\Delta}\mathbf{T}^{(i)}\end{pmatrix} &= {}^{t+\Delta t}\left(\int_V \mathbf{N}^{\mathrm{T}}\mathbf{b}\,dV+\int_S \mathbf{N}^{\mathrm{T}}\mathbf{t}\,dS-\left(\int_V \mathbf{B}^{\mathrm{T}}\mathbf{D}\mathbf{B}_u\,dV\right)\boldsymbol{\Delta}\,\mathbf{u}_u\right)\\ &\quad -{}^{t+\Delta t}\begin{pmatrix}\left(\mathbf{K_e}\right)\boldsymbol{\Delta}\mathbf{u}_a+\left(\mathbf{Q_p}\right)^{(i-1)}\boldsymbol{\Delta}\mathbf{p}+\left(\mathbf{Q_T}\right)^{(i-1)}\boldsymbol{\Delta}\mathbf{T}\\ -\left(\int_V \mathbf{B}^{\mathrm{T}}\alpha\ \mathbf{m}\mathbf{N}\mathbf{p_0}\,dV\right)+\int_V \mathbf{B}^{\mathrm{T}}\boldsymbol{\sigma}''_0\,dV\end{pmatrix}^{(i-1)}\end{aligned} \tag{7.28}$$

7.4.2 Two phase formulation

The primary variables in TOUGH2 for two phase situations are gas phase pressure and gas phase saturation. The momentum equations will need to be reformulated to express using those variables.

7.4.2.1 Solid phase pressure

The solid phase pressure can be written as

$$p_S = p_l S_l + p_g S_g = \sum_{\psi} p_\psi S_\psi \tag{7.29}$$

which can be written as (Pruess et al., 1999)

$$p = p_g S_g + \left(1 - S_g\right)\left(p_g + p_c\right) \qquad p_c \le 0 \tag{7.30}$$

where p_c is the capillary pressure and we will drop the subscript and use p to denote the solid phase pressure. The above expression can be simplified to

$$p = p_g + \left(1 - S_g\right) p_c \qquad p_c \le 0 \tag{7.31}$$

We can write the change in solid pressure as

$$\Delta p = \Delta p_g + \Delta\left(\left(1 - S_g\right) p_c\right) \tag{7.32}$$

Considering that the capillary pressure is function of gas phase saturation, we can write

$$\begin{aligned} \Delta p &= \Delta p_g + \left(1 - S_g\right)\Delta p_c + p_c \Delta\left(1 - S_g\right) \\ &= \Delta p_g + \left(1 - S_g\right)\frac{\partial p_c}{\partial S_g}\Delta S_g - p_c \Delta S_g \\ &= \Delta p_g + \left(\left(1 - S_g\right)\frac{\partial p_c}{\partial S_g} - p_c\right)\Delta S_g \end{aligned} \tag{7.33}$$

In vector form, it can be written as

$$\mathbf{\Delta p} = \mathbf{\Delta p_g} + \left[\mathbf{C}^{\mathbf{p}}_{\mathbf{S_g}}\right]\mathbf{\Delta S_g} \tag{7.34}$$

where $\mathbf{C}^{\mathbf{p}}_{\mathbf{S_g}}$ is the diagonal (square) matrix of size equal to number of nodes, given as

$$\left[\mathbf{C}^{\mathbf{p}}_{\mathbf{S_g}}\right] = \begin{bmatrix} \left(1 - S_g\right)\dfrac{\partial p_c}{\partial S_g} - p_c\Big|_1 & & 0 \\ & \ddots & \\ 0 & & \left(1 - S_g\right)\dfrac{\partial p_c}{\partial S_g} - p_c\Big|_{\text{numNodes}} \end{bmatrix} \tag{7.35}$$

and denominated as phase-coefficient matrix for pressure-saturation.

7.4.2.2 Temperature

The temperature for the two phase problem is expressed as function of gas phase pressure and saturation in two phase problems in TOUGH2, i.e.

$$T = T\left(p_g, S_g\right) \tag{7.36}$$

The change in temperature is calculated as

$$\Delta T = \frac{\partial T}{\partial p_g}\Delta p_g + \frac{\partial T}{\partial S_g}\Delta S_g \tag{7.37}$$

In vector form

$$\mathbf{\Delta T} = \mathbf{C}_{\mathbf{p_g}}^{\mathbf{T}}\,\mathbf{\Delta p_g} + \mathbf{C}_{\mathbf{S_g}}^{\mathbf{T}}\,\mathbf{\Delta S_g} \tag{7.38}$$

The phase coefficient matrices for temperature-pressure and for temperature-saturation are given as

$$\left[\mathbf{C}_{\mathbf{p_g}}^{\mathbf{T}}\right] = \begin{bmatrix} \left.\dfrac{\partial T}{\partial p_g}\right|_1 & & 0 \\ & \ddots & \\ 0 & & \left.\dfrac{\partial T}{\partial p_g}\right|_{\text{numNodes}} \end{bmatrix} \tag{7.39}$$

and

$$\left[\mathbf{C}_{\mathbf{S_g}}^{\mathbf{T}}\right] = \begin{bmatrix} \left.\dfrac{\partial T}{\partial S_g}\right|_1 & & 0 \\ & \ddots & \\ 0 & & \left.\dfrac{\partial T}{\partial S_g}\right|_{\text{numNodes}} \end{bmatrix} \tag{7.40}$$

respectively.

7.4.2.3 Newton-Raphson formulation for two-phase condition

Substituting (7.34) and (7.38) in (7.14) we get

$$\mathbf{R} = \left(\int_V \mathbf{N}^{\mathrm{T}} \mathbf{b}\, dV + \int_S \mathbf{N}^{\mathrm{T}} \mathbf{t}\, dS - \left(\int_V \mathbf{B}^{\mathrm{T}} \mathbf{D} \mathbf{B}_u\, dV \right) \Delta \mathbf{u}_u \right) - \left(\begin{array}{l} \left(\int_V \mathbf{B}^{\mathrm{T}} \mathbf{D} \mathbf{B}\, dV \right) \Delta \mathbf{u}_a - \int_V \mathbf{B}^{\mathrm{T}} \alpha\, \mathbf{m} \mathbf{N} \left\{ \Delta \mathbf{p}_{\mathbf{g}} + \left[\mathbf{C}_{\mathbf{S}_{\mathbf{g}}}^{\mathbf{p}} \right] \Delta \mathbf{S}_{\mathbf{g}} \right\} dV \\ - \left(\left(3K\alpha_T \right) \int_V \mathbf{B}^{\mathrm{T}} \mathbf{m} \mathbf{N} \left\{ \mathbf{C}_{\mathbf{p}_{\mathbf{g}}}^{\mathbf{T}}\, \Delta \mathbf{p}_{\mathbf{g}} + \mathbf{C}_{\mathbf{S}_{\mathbf{g}}}^{\mathbf{T}}\, \Delta \mathbf{S}_{\mathbf{g}} \right\} dV \right) \\ - \left(\int_V \mathbf{B}^{\mathrm{T}} \alpha\, \mathbf{m} \mathbf{N} \mathbf{p}_{\mathbf{0}}\, dV \right) + \int_V \mathbf{B}^{\mathrm{T}} \boldsymbol{\sigma}''_0\, dV \end{array} \right) \tag{7.41}$$

Rearranging

$$\mathbf{R} = \left(\int_V \mathbf{N}^{\mathrm{T}} \mathbf{b}\, dV + \int_S \mathbf{N}^{\mathrm{T}} \mathbf{t}\, dS - \left(\int_V \mathbf{B}^{\mathrm{T}} \mathbf{D} \mathbf{B}_u\, dV \right) \Delta \mathbf{u}_u \right) - \left(\begin{array}{l} \left(\int_V \mathbf{B}^{\mathrm{T}} \mathbf{D} \mathbf{B}\, dV \right) \Delta \mathbf{u}_a \\ - \int_V \mathbf{B}^{\mathrm{T}} \left[\left(3K\alpha_T \right) \mathbf{m} \mathbf{N} \mathbf{C}_{\mathbf{p}_{\mathbf{g}}}^{\mathbf{T}} + \alpha\, \mathbf{m} \mathbf{N} \right] \Delta \mathbf{p}_{\mathbf{g}}\, dV \\ - \int_V \mathbf{B}^{\mathrm{T}} \left[\left(3K\alpha_T \right) \mathbf{m} \mathbf{N} \mathbf{C}_{\mathbf{S}_{\mathbf{g}}}^{\mathbf{T}} + \alpha\, \mathbf{m} \mathbf{N} \mathbf{C}_{\mathbf{S}_{\mathbf{g}}}^{\mathbf{p}} \right] \Delta \mathbf{S}_{\mathbf{g}}\, dV \\ - \int_V \mathbf{B}^{\mathrm{T}} \alpha\, \mathbf{m} \mathbf{N} \mathbf{p}_{\mathbf{0}}\, dV + \int_V \mathbf{B}^{\mathrm{T}} \boldsymbol{\sigma}''_0\, dV \end{array} \right) \tag{7.42}$$

Again, here first parenthesis represents g and second represents f such that

$$\mathbf{R} = g - f\left(\Delta u, \Delta p_g, \Delta S_g \right) \tag{7.43}$$

Now we can write f as

$$
\begin{aligned}
f = & \left(\int_V \mathbf{B}^{\mathrm{T}} \mathbf{D} \mathbf{B} \, dV \right) \Delta \mathbf{u}_a \\
& - \left(\int_V \mathbf{B}^{\mathrm{T}} \left[\left(3K\alpha_T \right) \mathbf{m} \mathbf{N} \mathbf{C}_{\mathbf{p_g}}^{\mathbf{T}} + \alpha \ \mathbf{m} \mathbf{N} \right] dV \right) \Delta \mathbf{p_g} \\
& - \left(\int_V \mathbf{B}^{\mathrm{T}} \left[\left(3K\alpha_T \right) \mathbf{m} \mathbf{N} \mathbf{C}_{\mathbf{S_g}}^{\mathbf{T}} + \alpha \, \mathbf{m} \mathbf{N} \mathbf{C}_{\mathbf{S_g}}^{\mathbf{p}} \right] dV \right) \Delta \mathbf{S_g} \\
& - \int_V \mathbf{B}^{\mathrm{T}} \alpha \ \mathbf{m} \mathbf{N} \mathbf{p_0} \, dV + \int_V \mathbf{B}^{\mathrm{T}} \boldsymbol{\sigma}''_0 \, dV
\end{aligned}
\tag{7.44}
$$

The final Newton-Raphson formulation can be written as

$$
\begin{aligned}
{}^{t+\Delta t} \begin{pmatrix} \left(\mathbf{K_e} \right)^{(i-1)} \boldsymbol{\delta} \Delta \mathbf{u}^{(i)} \\ + \left(\mathbf{Q}_{\mathbf{p_g}} \right)^{(i-1)} \boldsymbol{\delta} \Delta \mathbf{p_g}^{(i)} \\ + \left(\mathbf{Q}_{\mathbf{S_g}} \right)^{(i-1)} \boldsymbol{\delta} \Delta \mathbf{S_g}^{(i)} \end{pmatrix} = & {}^{t+\Delta t} \left(\int_V \mathbf{N}^{\mathrm{T}} \mathbf{b} \, dV + \int_S \mathbf{N}^{\mathrm{T}} \mathbf{t} \, dS - \left(\int_V \mathbf{B}^{\mathrm{T}} \mathbf{D} \mathbf{B}_u \, dV \right) \Delta \mathbf{u}_u \right) \\
& - {}^{t+\Delta t} \begin{pmatrix} \left(\mathbf{K_e} \right) \Delta \mathbf{u}_a + \left(\mathbf{Q}_{\mathbf{p_g}} \right)^{(i-1)} \Delta \mathbf{p_g} + \left(\mathbf{Q}_{\mathbf{S_g}} \right)^{(i-1)} \Delta \mathbf{S_g} \\ - \left(\int_V \mathbf{B}^{\mathrm{T}} \alpha \ \mathbf{m} \mathbf{N} \mathbf{p_0} \, dV \right) + \int_V \mathbf{B}^{\mathrm{T}} \boldsymbol{\sigma}''_0 \, dV \end{pmatrix}^{(i-1)}
\end{aligned}
\tag{7.45}
$$

where the coefficient matrices are as follows,

$$
\mathbf{K_e} = \int_V \mathbf{B}^{\mathrm{T}} \mathbf{D} \mathbf{B} \, dV \tag{7.46}
$$

$$
\mathbf{Q}_{\mathbf{p_g}} = - \int_V \mathbf{B}^{\mathrm{T}} \left[\left(3K\alpha_T \right) \mathbf{m} \mathbf{N} \mathbf{C}_{\mathbf{p_g}}^{\mathbf{T}} + \alpha \ \mathbf{m} \mathbf{N} \right] dV \tag{7.47}
$$

and

$$
\mathbf{Q}_{\mathbf{S_g}} = - \int_V \mathbf{B}^{\mathrm{T}} \left[\left(3K\alpha_T \right) \mathbf{m} \mathbf{N} \mathbf{C}_{\mathbf{S_g}}^{\mathbf{T}} + \alpha \, \mathbf{m} \mathbf{N} \mathbf{C}_{\mathbf{S_g}}^{\mathbf{p}} \right] dV \tag{7.48}
$$

Since the phase-coefficient matrices are constant with respect to the element properties, we can rewrite the coefficient matrices as

$$\mathbf{Q}_{\mathbf{p}_g} = -\left\{\int_V \mathbf{B}^{\mathrm{T}}\left(3K\alpha_T\right)\mathbf{m}\mathbf{N}\,dV\right\}\mathbf{C}^{\mathbf{T}}_{\mathbf{p}_g} - \int_V \mathbf{B}^{\mathrm{T}}\alpha\ \mathbf{m}\,\mathbf{N}\,dV \tag{7.49}$$

and

$$\mathbf{Q}_{\mathbf{S}_g} = -\left\{\int_V \mathbf{B}^{\mathrm{T}}\left(3K\alpha_T\right)\mathbf{m}\mathbf{N}\,dV\right\}\mathbf{C}^{\mathbf{T}}_{\mathbf{S}_g} - \left\{\int_V \mathbf{B}^{\mathrm{T}}\alpha\ \mathbf{m}\mathbf{N}\,dV\right\}\mathbf{C}^{\mathbf{p}}_{\mathbf{S}_g} \tag{7.50}$$

Using the notations applied in single phase for the coefficient matrices it can be written as

$$\mathbf{Q}_{\mathbf{p}_g} = -\mathbf{Q}_{\mathbf{T}}\,\mathbf{C}^{\mathbf{T}}_{\mathbf{p}_g} - \mathbf{Q}_{\mathbf{p}} \tag{7.51}$$

and

$$\mathbf{Q}_{\mathbf{S}_g} = -\mathbf{Q}_{\mathbf{T}}\,\mathbf{C}^{\mathbf{T}}_{\mathbf{S}_g} - \mathbf{Q}_{\mathbf{p}}\,\mathbf{C}^{\mathbf{p}}_{\mathbf{S}_g} \tag{7.52}$$

As can be seen easily, the single phase formulation can be formulated as a special case of the above two equations. In single phase, the independent variables are pressure and temperature hence the phase-coefficient matrices, $\mathbf{C}^{\mathbf{T}}_{\mathbf{p}_g}$ and $\mathbf{C}^{\mathbf{p}}_{\mathbf{S}_g}\left(\text{now}\,\mathbf{C}^{\mathbf{p}}_{\mathbf{T}}\right)$, will be zero. In single phase the variables are pressure and temperature, hence the coefficient $\mathbf{C}^{\mathbf{T}}_{\mathbf{S}_g}$ will be the phase coefficient matrix between temperatures and hence unity, leading to the single phase relations.

7.5 Generalized fully coupled formulation for TOUGH2 Variables

The general formulation, applicable for single phase or two phase condition, can be written as

$$
\begin{aligned}
{}^{t+\Delta t}\begin{pmatrix} (\mathbf{K_e})^{(i-1)}\boldsymbol{\delta\Delta u}^{(i)} \\ +(\mathbf{Q_{V_1}})^{(i-1)}\boldsymbol{\delta\Delta V_1}^{(i)} \\ +(\mathbf{Q_{V_2}})^{(i-1)}\boldsymbol{\delta\Delta V_2}^{(i)} \end{pmatrix} = {}^{t+\Delta t}\left(\int_V \mathbf{N}^{\mathrm{T}}\mathbf{b}\, dV + \int_S \mathbf{N}^{\mathrm{T}}\mathbf{t}\, dS - \left(\int_V \mathbf{B}^{\mathrm{T}}\mathbf{D}\mathbf{B}_u\, dV \right)\boldsymbol{\Delta u}_u \right) \\
- {}^{t+\Delta t}\begin{pmatrix} (\mathbf{K_e})\boldsymbol{\Delta u}_a + (\mathbf{Q_{V_1}})^{(i-1)}\boldsymbol{\Delta V}_1 + (\mathbf{Q_{V_2}})^{(i-1)}\boldsymbol{\Delta V_2} \\ -\left(\int_V \mathbf{B}^{\mathrm{T}}\alpha\ \mathbf{m}\mathbf{N}\mathbf{p_0}\, dV \right) + \int_V \mathbf{B}^{\mathrm{T}}\boldsymbol{\sigma}''_0\, dV \end{pmatrix}^{(i-1)}
\end{aligned}
\tag{7.53}
$$

where $\mathbf{V_1}$ and $\mathbf{V}_2$ represent the primary variables corresponding to the phase condition and matrices $\mathbf{Q}_{\mathbf{V_1}}$ and $\mathbf{Q}_{\mathbf{V_2}}$ are as given in equations (7.51) and (7.52) respectively.

7.6 Other Changes required for implementation in TOUGH2 for Fully Coupled formulation

To solve both these systems as a coupled system we need to find the derivatives of residuals in (6.12) with respect to the displacements $(\mathbf{J_{FS}})$, derivatives of the extra terms in (6.12) with respect to the TOUGH2 primary variables $(\mathbf{J}^{+}_{\mathbf{FF}})$, and derivatives of residuals in (6.45) with respect to the flow primary variables i.e. pressure and temperature $(\mathbf{J_{SF}})$. It can be represented as:

$$
\begin{bmatrix} \mathbf{J_{FF}} & \mathbf{J_{FS}} \\ \mathbf{J_{SF}} & \mathbf{J_{SS}} \end{bmatrix} \begin{Bmatrix} \mathbf{p_F} \\ \mathbf{u_S} \end{Bmatrix} = \begin{Bmatrix} \mathbf{R_F} \\ \mathbf{R_S} \end{Bmatrix} \tag{7.54}
$$

where the unknowns have been divided into the primary variables for the flow solution $\mathbf{p_F}$ and the displacements for the stress solution $\mathbf{u_S}$.

The Jacobian terms $\mathbf{J_{SF}}$ and $\mathbf{J_{SS}}$ can be easily obtained from (7.53).

The residuals of flow equation with respect to flow variables is represented by $(\mathbf{J_{FF}})$, which is already implemented in TOUGH2. They will need modifications to incorporate

the addition due to variable permeability and porosity as function of effective stress. Also, the derivatives of the extra terms in flow equations with respect to the TOUGH2 primary variables will have to be added to $\mathbf{J}_{\mathbf{FF}}$.

The $\mathbf{J}_{\mathbf{FS}}$ represent the partial derivative of flow equations with respect to the displacements and will have to be evaluated newly.

We will discuss all these derivatives required for Jacobian in the next chapter.

7.7 Staggered Coupling for Fractured media

Currently, the implementation involving fractures is carried out only in staggered manner. The staggered approach first solves the fluid flow problem i.e. TOUGH2 simulation is carried out. The TOUGH2 variables pressure, temperature, and/or saturation are provided to the finite element model. The finite element model calculates the displacements and stresses and these are then used for aperture and/or permeability-porosity modification in fracture and rock materials on the fluid flow side. The modified data is used for the next TOUGH2 run and the cycle continues.

7.7.1 Fluid flow equations

Due to the staggered approach, the fluid flow formulation of TOUGH2 remains untouched and the individual time step calculations of the simulation are exactly like original TOUGH2 run.

7.7.2 Newton-Raphson formulation (Modified stress law) for Porous Media

The porous media calculations are now done using single variable formulation similar to the one way coupling, since the pressure and temperature are not varying during the solution of the finite element model. Hence, the Newton-Raphson formulation can be

derived similarly to the one described in one way coupling. The Newton-Raphson equations to be solved are as follows

$$
\begin{aligned}
{}^{t+\Delta t}\left(\left(\mathbf{K}_{\mathbf{e}}\right)^{(i-1)}\boldsymbol{\delta}\Delta\mathbf{u}^{(i)}\right) = {}^{t+\Delta t}\left(\int_V \mathbf{N}^{\mathrm{T}}\mathbf{b}\,dV + \int_S \mathbf{N}^{\mathrm{T}}\mathbf{t}\,dS - \left(\int_V \mathbf{B}^{\mathrm{T}}\mathbf{DB}_u\,dV\right)\Delta\mathbf{u}_u\right) \\
- {}^{t+\Delta t}\begin{pmatrix}\left(\int_V \mathbf{B}^{\mathrm{T}}\mathbf{DB}\,dV\right)\Delta\mathbf{u} - \int_V \mathbf{B}^{\mathrm{T}}\alpha\,\mathbf{mN}\Delta\mathbf{p}\,dV \\ -\left(\int_V \mathbf{B}^{\mathrm{T}}\left(3K\alpha_T\right)\mathbf{mN}\Delta\mathbf{T}\,dV\right) \\ -\left(\int_V \mathbf{B}^{\mathrm{T}}\alpha\;\mathbf{mN}\mathbf{p}_0\,dV\right) + \int_V \mathbf{B}^{\mathrm{T}}\boldsymbol{\sigma}''_0\,dV\end{pmatrix}^{(i-1)}
\end{aligned}
\tag{7.55}
$$

where the coefficient matrix, as before, is as follows,

$$
\mathbf{K}_{\mathbf{e}} = \int_V \mathbf{B}^{\mathrm{T}}\mathbf{DB}\,dV \tag{7.56}
$$

7.7.3 Newton-Raphson formulation for Fracture Behavior

To derive the Newton-Raphson formulation for finite elements with fracture behavior, consider the residual, given earlier,

$$
\mathbf{R} = \left\{\mathbf{F}_{ext} - \left(\int_V \mathbf{B}^{\mathbf{T}}\,\mathbf{m}\,\mathbf{N}\,dV\right)\mathbf{p}\right\} - \left(\int_V \mathbf{B}^{\mathbf{T}}\left(\boldsymbol{\sigma}_{\mathbf{ct}}(\mathbf{a})\right)dV\right) \tag{7.57}
$$

where $\boldsymbol{\sigma}_{\mathbf{ct}}$ is the contact stress vector corresponding to the current aperture vector $\mathbf{a}$.

The Newton-Raphson formulation for single variable is given as

$$
\left(\frac{\partial f}{\partial \Delta u}\right)^{(i-1)}\delta\Delta u^{(i)} = {}^{t+\Delta t}g - {}^{t+\Delta t}f\left(\Delta u\right)^{(i-1)} \tag{7.58}
$$

where the residual at iteration i of time step $t+\Delta t$ is written as

$$ {}^{t+\Delta t}\mathbf{R}^{i} = {}^{t+\Delta t}g - {}^{t+\Delta t}f\left(\Delta u\right)^{i} \tag{7.59} $$

The Newton-Raphson formulation for the joint element then can be written as

$$ \left(\frac{\partial(f)}{\partial \Delta \mathbf{u}}\right)^{(i-1)} \delta \Delta \mathbf{u}^{(i)} = {}^{t+\Delta t}\left\{\mathbf{F}^{\mathbf{e}} - \left(\int_V \mathbf{B}^{\mathbf{T}}\,\mathbf{m}\,\mathbf{N}\,dV\right)\mathbf{p}\right\} - {}^{t+\Delta t}\left(\int_V \mathbf{B}^{\mathbf{T}}\left(\boldsymbol{\sigma}_{\mathbf{ct}}(\mathbf{a})\right)dV\right)^{(i-1)} \tag{7.60} $$

To evaluate the Jacobian, let us first look at the contact stresses. The contact stresses are function of current apertures and in vector form, we can write the Jacobian term as

$$ \begin{aligned} \left(\frac{\partial(f)}{\partial \Delta \mathbf{u}}\right) &= \frac{\partial}{\partial \Delta \mathbf{u}}\left(\int_V \mathbf{B}^{\mathbf{T}}\left(\boldsymbol{\sigma}_{\mathbf{ct}}(\mathbf{a})\right)dV\right) \\ &= \int_V \mathbf{B}^{\mathbf{T}}\left(\frac{\partial \boldsymbol{\sigma}_{\mathbf{ct}}(\mathbf{a})}{\partial \Delta \mathbf{u}}\right)dV \\ &= \int_V \mathbf{B}^{\mathbf{T}}\left(\frac{\partial \boldsymbol{\sigma}_{\mathbf{ct}}(\mathbf{a})}{\partial \mathbf{a}}\frac{\partial \mathbf{a}}{\partial \Delta \mathbf{u}}\right)dV \end{aligned} \tag{7.61} $$

where the vector $\mathbf{a}$ of current apertures is defined as

$$ \mathbf{a} = \begin{bmatrix} a_x \\ a_y \\ a_z \end{bmatrix} \tag{7.62} $$

Since we are neglecting the shear effects due to contact, we can write

$$ \frac{\partial \boldsymbol{\sigma}_{\mathbf{ct}}(\mathbf{a})}{\partial \mathbf{a}} = \begin{bmatrix} kn_x & 0 & 0 \\ 0 & kn_y & 0 \\ 0 & 0 & kn_z \\ 0 & 0 & 0 \\ 0 & 0 & 0 \\ 0 & 0 & 0 \end{bmatrix} \tag{7.63} $$

where the normal stiffness in direction d defined as

$$ kn_d = \frac{\sigma_c}{m\,a_{0d}}\left[1 - \frac{a_d}{a_{0d}}\right]^{\frac{1-m}{m}} \tag{7.64} $$

The expression for normal stiffness is obtained for Gangi's model which gives the contact stress σ_d for given value of aperture a_d as

$$\sigma_d = \sigma_c \left[1 - \frac{a_d}{a_{0d}} \right]^{\frac{1}{m}} \tag{7.65}$$

We can write the aperture vector $\mathbf{a}$ as

$$\mathbf{a} = \begin{bmatrix} a_x \\ a_y \\ a_z \end{bmatrix} = \begin{bmatrix} u_x^{Top} - u_x^{Bottom} + a_{ix} \\ u_y^{Top} - u_y^{Bottom} + a_{iy} \\ u_z^{Top} - u_z^{Bottom} + a_{iz} \end{bmatrix} \tag{7.66}$$

If we define the surface displacement vector $\mathbf{u_s}$ as follows

$$\mathbf{u_s} = \begin{bmatrix} u_x^{Top} \\ u_y^{Top} \\ u_z^{Top} \\ u_x^{Bottom} \\ u_y^{Bottom} \\ u_z^{Bottom} \end{bmatrix} \tag{7.67}$$

then we can write

$$\frac{\partial \mathbf{a}}{\partial \Delta \mathbf{u}} = \frac{\partial \mathbf{a}}{\partial \mathbf{u_s}} \frac{\partial \mathbf{u_s}}{\partial \Delta \mathbf{u}} \tag{7.68}$$

Thus the Jacobian can be written as

$$\begin{aligned} \left(\frac{\partial (f)}{\partial \Delta \mathbf{u}} \right) &= \int_V \mathbf{B}^{\mathbf{T}} \left(\frac{\partial \boldsymbol{\sigma}_{\mathbf{ct}}(\mathbf{a})}{\partial \Delta \mathbf{u}} \right) dV \\ &= \int_V \mathbf{B}^{\mathbf{T}} \left(\frac{\partial \boldsymbol{\sigma}_{\mathbf{ct}}(\mathbf{a})}{\partial \mathbf{a}} \frac{\partial \mathbf{a}}{\partial \mathbf{u_s}} \frac{\partial \mathbf{u_s}}{\partial \Delta \mathbf{u}} \right) dV \end{aligned} \tag{7.69}$$

Differentiating the aperture vector with respect to the surface displacement vector we get

$$\frac{\partial \mathbf{a}}{\partial \mathbf{u_s}} = \begin{bmatrix} 1 & 0 & 0 & -1 & 0 & 0 \\ 0 & 1 & 0 & 0 & -1 & 0 \\ 0 & 0 & 1 & 0 & 0 & -1 \end{bmatrix} \tag{7.70}$$

Then we can write

$$\begin{aligned} \frac{\partial \boldsymbol{\sigma}_{\mathbf{ct}}(\mathbf{a})}{\partial \Delta \mathbf{u}} &= \begin{bmatrix} kn_x & 0 & 0 & -kn_x & 0 & 0 \\ 0 & kn_y & 0 & 0 & -kn_y & 0 \\ 0 & 0 & kn_z & 0 & 0 & -kn_z \\ 0 & 0 & 0 & 0 & 0 & 0 \\ 0 & 0 & 0 & 0 & 0 & 0 \\ 0 & 0 & 0 & 0 & 0 & 0 \end{bmatrix} \frac{\partial \mathbf{u_s}}{\partial \Delta \mathbf{u}} \\ &= \mathbf{T} \frac{\partial \mathbf{u_s}}{\partial \Delta \mathbf{u}} \end{aligned} \tag{7.71}$$

where we have defined the new stiffness matrix $\mathbf{T}$. Now we can write the Jacobian as

$$\begin{aligned} \left(\frac{\partial (f)}{\partial \Delta \mathbf{u}} \right) &= \int_V \mathbf{B}^{\mathbf{T}} \left(\frac{\partial \boldsymbol{\sigma}_{\mathbf{ct}}(\mathbf{a})}{\partial \Delta \mathbf{u}} \right) dV \\ &= \int_V \mathbf{B}^{\mathbf{T}} \left(\mathbf{T} \frac{\partial \mathbf{u_s}}{\partial \Delta \mathbf{u}} \right) dV \end{aligned} \tag{7.72}$$

The surface displacements $\mathbf{u_s}$ are calculated from the nodal displacements as follows

$$\begin{bmatrix} u_x^{Top} \\ u_y^{Top} \\ u_z^{Top} \\ u_x^{Bottom} \\ u_y^{Bottom} \\ u_z^{Bottom} \end{bmatrix} = \begin{bmatrix} 0 & 0 & 0 & \cdots & 0 & 0 & 0 & 0 & 0 & 0 & \cdots & 0 & 0 & 0 \\ 0 & 0 & 0 & \cdots & 0 & N_4 & 0 & 0 & 0 & 0 & \cdots & 0 & N_8 & 0 \\ 0 & 0 & 0 & \cdots & 0 & 0 & 0 & 0 & 0 & N_5 & \cdots & 0 & 0 & N_8 \\ N_1 & 0 & 0 & \cdots & N_4 & 0 & 0 & N_5 & 0 & 0 & \cdots & N_8 & 0 & 0 \\ 0 & N_1 & 0 & \cdots & 0 & 0 & 0 & 0 & N_5 & 0 & \cdots & 0 & 0 & 0 \\ 0 & 0 & N_1 & \cdots & 0 & 0 & N_4 & 0 & 0 & 0 & \cdots & 0 & 0 & 0 \end{bmatrix} \begin{bmatrix} u_x^1 \\ u_y^1 \\ u_z^1 \\ \vdots \\ u_x^4 \\ u_y^4 \\ u_z^4 \\ u_x^5 \\ u_y^5 \\ u_z^5 \\ \vdots \\ u_x^8 \\ u_y^8 \\ u_z^8 \end{bmatrix} \tag{7.73}$$

which in vector form is written as

$$\mathbf{u_S} = \mathbf{N}_C \, \Delta\mathbf{u} \tag{7.74}$$

The complete matrix $\mathbf{N}_C$ is given as

$$\mathbf{N}_C = \begin{bmatrix} 0 & 0 & 0 & N_2 & 0 & 0 & N_3 & 0 & 0 & 0 & 0 & 0 & 0 & 0 & 0 & N_6 & 0 & 0 & N_7 & 0 & 0 & 0 & 0 & 0 \\ 0 & 0 & 0 & 0 & 0 & 0 & 0 & N_3 & 0 & 0 & N_4 & 0 & 0 & 0 & 0 & 0 & 0 & 0 & 0 & N_7 & 0 & 0 & N_8 & 0 \\ 0 & 0 & 0 & 0 & 0 & 0 & 0 & 0 & 0 & 0 & 0 & 0 & 0 & 0 & N_5 & 0 & 0 & N_6 & 0 & 0 & N_7 & 0 & 0 & N_8 \\ N_1 & 0 & 0 & 0 & 0 & 0 & 0 & 0 & 0 & N_4 & 0 & 0 & N_5 & 0 & 0 & 0 & 0 & 0 & 0 & 0 & 0 & N_8 & 0 & 0 \\ 0 & N_1 & 0 & 0 & N_2 & 0 & 0 & 0 & 0 & 0 & 0 & 0 & 0 & N_5 & 0 & 0 & N_6 & 0 & 0 & 0 & 0 & 0 & 0 & 0 \\ 0 & 0 & N_1 & 0 & 0 & N_2 & 0 & 0 & N_3 & 0 & 0 & N_4 & 0 & 0 & 0 & 0 & 0 & 0 & 0 & 0 & 0 & 0 & 0 & 0 \end{bmatrix} \tag{7.75}$$

Also, noting that

$$\frac{\partial \mathbf{u_s}}{\partial \Delta\mathbf{u}} = \mathbf{N}_C \tag{7.76}$$

we can write the expression for Jacobian as

$$\begin{aligned} \left(\frac{\partial (f)}{\partial \Delta\mathbf{u}}\right) &= \int_V \mathbf{B}^{\mathbf{T}} \left(\frac{\partial \boldsymbol{\sigma}_{\mathbf{ct}}(\mathbf{a})}{\partial \Delta\mathbf{u}}\right) dV \\ &= \int_V \mathbf{B}^{\mathbf{T}} \, \mathbf{T} \, \mathbf{N}_C \, dV \end{aligned} \tag{7.77}$$

Define the elemental stiffness $\mathbf{K}^e(\Delta\mathbf{u})$ for the joint element as

$$\begin{aligned} \mathbf{K}^{\mathbf{e}}(\Delta\mathbf{u}) &= \int_V \mathbf{B}^{\mathbf{T}} \, \mathbf{T}(\Delta\mathbf{u}) \mathbf{N}_C \, dV \\ &= \int_V \mathbf{B}^{\mathbf{T}} \, \mathbf{T} \, \mathbf{N}_C \, dV \end{aligned} \tag{7.78}$$

Then the Newton-Raphson formulation for the volume element with fracture behavior can be represented as

$$\left[\mathbf{K}^{\mathbf{e}}(\Delta\mathbf{u})\right]^{(i-1)} \delta\Delta\mathbf{u}^{(i)} = {}^{t+\Delta t}\left\{\mathbf{F}^{\mathbf{ext}} - \left(\int_V \mathbf{B}^{\mathbf{T}} \, \mathbf{m} \, \mathbf{N} \, dV\right)\mathbf{p}\right\} - {}^{t+\Delta t}\left(\int_V \mathbf{B}^{\mathbf{T}} \left(\boldsymbol{\sigma}_{\mathbf{ct}}(\mathbf{a})\right) dV\right)^{(i-1)} \tag{7.79}$$

8 EVALUATION OF JACOBIAN TERMS

8.1 Conservation of Mass

8.1.1 General Method for derivatives

Consider any term in the IFDM equations of conservations of mass and energy. It can be represented as follows

$$I\left(\phi,k,p,T,S_g,u\right)=f_1\left(\phi,k\right)f_2\left(p\right)f_3\left(T,S_g\right)f_4\left(u\right)C \tag{8.1}$$

where I represent terms occurring in both single phase and two phase problems. TOUGH2 uses temperature as the second primary variable for single phase problems and saturation for the two-phase problems. C represents the terms which are constant with respect to variable of differentiation. The functions f_1 represent the terms with porosity and permeability which will be loosely coupled using the data from last time step and hence their derivatives will not be included in the forthcoming analysis.

8.1.2 Derivative with respect to displacements $\left(\mathbf{J}_{\mathbf{FS}}\right)$

Let us consider the derivative of the terms with respect to the displacement as follows

$$\frac{\partial I}{\partial u_n}=f_1f_2f_3C\frac{\partial f_4}{\partial u_n} \tag{8.2}$$

The partials with respect to displacement represent the solid to fluid coupling. They are evaluated while the pore pressure remains constant, (also the other TOUGH2 primary variable). Hence the poroelastic constants used in calculation of these terms, if any, are evaluated at the **drained** condition.

8.1.3 Derivative of additional terms with respect to TOUGH2 variables $(\mathbf{J}_{\mathbf{FF}})$

Now we will consider the derivatives with respect to TOUGH2 primary variables. We will represent the TOUGH2 primary variables $P, T,$ and S_g as X_i where $i = 1...3$. While evaluating these partials we are assuming that other primary variables are constant i.e. if we are finding partial with respect to pressure then temperature, and displacement will be held constant. So in these partials, the derivative with respect to displacement will be zero.

$$\begin{aligned}\frac{\partial I}{\partial X_i} &= f_1 f_3 f_4 C \frac{\partial f_2}{\partial X_i} + f_1 f_2 f_4 C \frac{\partial f_3}{\partial X_i} \\ &= f_1 f_3 f_4 C \frac{\partial f_2}{\partial X_i} + f_1 f_2 f_4 C \frac{\partial f_3}{\partial X_i}\end{aligned} \tag{8.3}$$

These terms represent the fluid-to-solid coupling which is the effect of the changes in fluid pressure or fluid mass on the strain in the solids (Wang, 2000). The poroelastic constants used, if any, while finding the partials of displacement with respect to the TOUGH2 primary variables are evaluated at the **constant stress condition**.

We also have to keep in mind that we are evaluating partial derivatives with respect to the primary variables. Hence in the partial with respect to X_i only one of $\frac{\partial f_2}{\partial X_i}$ or $\frac{\partial f_3}{\partial X_i}$ will exist and the other term will be zero.

8.2 Conservation of Energy

For the terms in energy balance equation, there are no additional terms. Hence we need to calculate only the derivatives of those terms with respect to the displacement. We also need to take into account the additional terms arising due to the derivatives with respect

to the porosity and permeability in the partials with respect to TOUGH2 primary variables. Let us denote the terms in the residual formation of the energy balance equation as

$$I_E\left(\phi,k,p,T,S_g\right)=f_1\left(\phi,k\right)f_2\left(p\right)f_3\left(T,S_g\right)C \tag{8.4}$$

8.2.1 Derivatives with respect to displacements $\left(\mathbf{J}_{\mathbf{FS}}\right)$

The derivative with respect to displacement required for the Jacobian can be expressed as

$$\frac{\partial I_E}{\partial u_n}=0 \tag{8.5}$$

Since there are no additional terms in the energy equation and the effect of displacement through variable porosity and permeability is neglected, with TOUGH2 primary variables held constant, the derivative becomes zero. The effect of variable porosity and permeability is second order effect through change in displacement of the solid. It is neglected with the assumption that the small error in the calculations of the Jacobian term will be compensated by iterative solution procedure to obtain the correct result.

8.2.2 Derivatives with respect to TOUGH2 variables $\left(\mathbf{J}_{\mathbf{FF}}\right)$

The additional terms arising due to variable porosity and permeability do not exist and hence we can see that there is no change in this derivative

$$\frac{\partial I_E}{\partial X_i}=f_1 f_3 C\frac{\partial f_2}{\partial X_i}+f_1 f_2 C\frac{\partial f_3}{\partial X_i} \tag{8.6}$$

One of the above two terms will be zero and the non-zero term is the one which is calculated by TOUGH2 currently.

8.3 Conservation of Momentum

The Jacobian formulation for the conservation of momentum equation was given in (7.53) as

$$
\begin{aligned}
{}^{t+\Delta t}\begin{pmatrix} \left(\mathbf{K_e}\right)^{(i-1)}\boldsymbol{\delta\Delta u}^{(i)} \\ +\left(\mathbf{Q_{V_1}}\right)^{(i-1)}\boldsymbol{\delta\Delta V_1}^{(i)} \\ +\left(\mathbf{Q_{V_2}}\right)^{(i-1)}\boldsymbol{\delta\Delta V_2}^{(i)} \end{pmatrix} &= {}^{t+\Delta t}\left(\int_V \mathbf{N}^{\mathrm{T}}\mathbf{b}\, dV + \int_S \mathbf{N}^{\mathrm{T}}\mathbf{t}\, dS - \left(\int_V \mathbf{B}^{\mathrm{T}}\mathbf{D}\mathbf{B}_u\, dV \right)\boldsymbol{\Delta u}_u \right) \\
&\quad - {}^{t+\Delta t}\begin{pmatrix} \left(\mathbf{K_e}\right)\boldsymbol{\Delta u}_a + \left(\mathbf{Q_{V_1}}\right)^{(i-1)}\boldsymbol{\Delta V}_1 + \left(\mathbf{Q_{V_2}}\right)^{(i-1)}\boldsymbol{\Delta V_2} \\ -\left(\int_V \mathbf{B}^{\mathrm{T}}\alpha\ \mathbf{m}\mathbf{N}\mathbf{p_0}\, dV \right) + \int_V \mathbf{B}^{\mathrm{T}}\boldsymbol{\sigma}''_0\, dV \end{pmatrix}^{(i-1)}
\end{aligned}
\tag{8.7}
$$

Some of the terms required in the coefficient matrices, in particular for two phase condition, are obtained by numerical derivatives as explained before.

8.4 Derivative common to multiple terms

We will look at the individual derivatives which occur in multiple terms and/or are constants throughout the time-step.

Consider the IFDM representation of volumetric strain as (assuming only Cartesian mesh)

$$
\begin{aligned}
\varepsilon_{V_n} &= \sum_m A_{nm}\left(\hat{u}_{nm} - u_n\right) \\
&= \sum_m A_{nm}\, D_{nm}\left(\hat{u}_{nm} - u_n\right)
\end{aligned}
\tag{8.8}
$$

Then we can write

$$\frac{\partial \varepsilon_{V_n}}{\partial u_n} = \frac{\partial\left(\sum_m A_{nm} D_{nm}\left(u_m - u_n\right)\right)}{\partial u_n} = \sum_m \left(-D_{nm} A_{nm}\right) \tag{8.9}$$

and

$$\frac{\partial \varepsilon_{V_n}}{\partial u_m} = \frac{\partial\left(\sum_m A_{nm} D_{nm}\left(u_m - u_n\right)\right)}{\partial u_m} = A_{nm} D_{nm} \tag{8.10}$$

The following relations have not been used in the context of current modifications related to variable porosity and permeability in the implementations. They are listed to relate the physical quantities.

The relation between the mean modified effective stress and volumetric strain for the drained condition (Wang, 2000) is

$$\varepsilon_V = \frac{1}{K}\sigma_m'' \tag{8.11}$$

and for the undrained condition (Wang, 2000) is

$$\varepsilon_V = \frac{1}{K_u}\sigma_m'' \tag{8.12}$$

Hence we can evaluate,

$$\frac{\partial \sigma_m''}{\partial u_n} = \frac{\partial \sigma_m''}{\partial \varepsilon_V}\frac{\partial \varepsilon_V}{\partial u_n} = K\frac{\partial \varepsilon_V}{\partial u_n} = K\sum_m \left(-A_{nm} D_{nm}\right) \tag{8.13}$$

Using the expression for the modified effective stress we can see that

$$\frac{\partial \sigma_m^{''}}{\partial p_n} = 0 \tag{8.14}$$

$$\frac{\partial \sigma_m^{''}}{\partial T} = -3K\alpha_T \tag{8.15}$$

and

$$\frac{\partial \sigma_m^{''}}{\partial S_g} = \frac{\partial \sigma_m^{''}}{\partial T}\frac{\partial T}{\partial S_g} = -3K\alpha_T\left(\left.\frac{\partial T}{\partial S_g}\right|_{\mathbf{T2}}\right) \tag{8.16}$$

8.5 Conservation of Mass (Re-look)

Now, we can re-evaluate the partial derivatives of the terms in conservation of mass equations using these derivatives. The partial with respect to displacement is given as

$$\boxed{\frac{\partial I}{\partial u_n} = f_1 f_2 f_3 C \frac{\partial f_4}{\partial u_n}} \tag{8.17}$$

and with respect to TOUGH2 primary variables as

$$\boxed{\frac{\partial I}{\partial X_i} = f_4\left\{f_1 C\left(f_3 \frac{\partial f_2}{\partial X_i} + f_2 \frac{\partial f_3}{\partial X_i}\right)\Big|_{\mathbf{T2}}\right\}} \tag{8.18}$$

where the term denoted by **T2** is already existing TOUGH2 term.

8.6 Conservation of Energy (Re-look)

The modified partial derivatives in energy balance with respect to displacement is

$$\boxed{\frac{\partial I_E}{\partial u_n} = 0} \tag{8.19}$$

and with respect to TOUGH2 primary variable as

$$\boxed{\frac{\partial I_E}{\partial X_i} = \left\{ f_1 C \left(f_3 \frac{\partial f_2}{\partial X_i} + f_2 \frac{\partial f_3}{\partial X_i} \right) \Big|_{\mathbf{T2}} \right\}} \tag{8.20}$$

8.7 Conservation of Momentum (Re-look)

The partials with respect to the TOUGH2 primary variables added are as shown in (7.53).

8.8 Non-diagonal blocks (Connection Terms)

In conservation of mass and energy equation there will be non-diagonal terms arising due to the connection elements. The partials of the all the above terms with respect to primary the variables of the connection cells also need to be evaluated. These can be evaluated in the similar manner described above using the connection data.

9 VERIFICATION PROBLEM 1 (TERZAGHI'S PROBLEM)

This chapter describes the use of Terzaghi's classical consolidation test, Figure 9.1 In this test, a constant stress is applied suddenly on the surface of a fluid-saturated sample. The piston applying the load is permeable, such that the top boundary is drained. Following an initial step displacement, the sample consolidates gradually as fluid flows out of the top drain. The simulation will be compared to the solution given by Detournay and Cheng (1993).

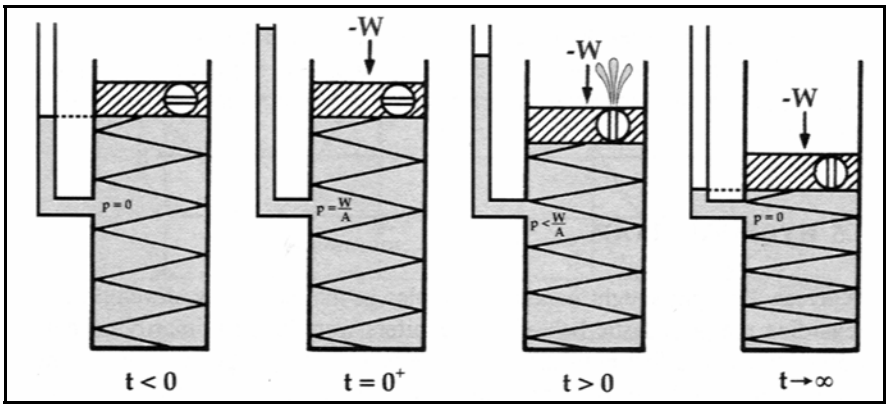

Figure 9.1 Schematic of uniaxially constrained soil consolidation (Wang, 2000).

9.1 Mathematical Model for flow problem

We will derive the mathematical model for the flow in Terzaghi's 1D consolidation test following Terzaghi et al. (1996).

9.1.1 Conservation of Mass

Consider the differential soil element in Figure 2.2. The discharge velocity in the z-direction is denoted by v_z and is defined as the quantity of water that percolates per unit time across a unit area of a section oriented normal to the flow. At the center of element

the rate of flow in the z-direction is $q_z\,dx\,dy$. The net mass of water flowing per unit time into the element of soil element is given by $-\dfrac{\partial(\rho_w q_z)}{\partial z}dx\,dy\,dz$.

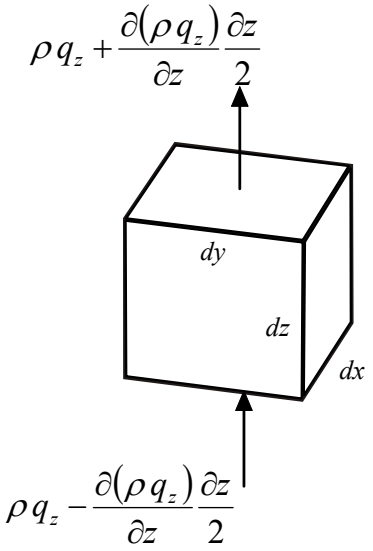

Figure 9.2 Differential Soil Element (Terzaghi's Problem).

Conservation of mass equation states that the net mass inflow of water per unit time is equal to the change per unit time of the mass of water in the element. The volume of water in the element, under fully saturated condition is equal to the pore volume. The pore volume is given as

$$V_p = \phi\,dx\,dy\,dz = \phi V = V_w \tag{9.1}$$

where ϕ is the porosity of the soil and V_w represents the volume of water (assuming that all pores are connected).

Then, the equation of conservation of mass can be written as

$$-\frac{\partial(\rho_w q_z)}{\partial z}dx\,dy\,dz = \frac{\partial}{\partial t}(\phi\,dx\,dy\,dz\,\rho_w) \tag{9.2}$$

In many practical problems $q_z \frac{\partial(\rho_w)}{\partial z} << \phi \frac{\partial}{\partial t}(\rho_w)$ (Bear, 1988), i.e. spatial derivative in ρ are much smaller than the local temporal ones, hence the terms involving the spatial derivative are neglected.

We will look at the some of the parameters to relate the solution obtained from the reference to the poroelastic formulation used in this work.

9.1.2 Darcy's Law and Permeability

Water flow in the soil is in response to a gradient in total or hydraulic head h defined as

$$h = z + \frac{p}{\gamma_w} \tag{9.3}$$

which represents the potential energy per unit weight of fluid. The gradient of hydraulic head will represent force per unit weight.

9.1.2.1 Darcy's Law

Darcy (1856) experimentally deduced the following relationship for the discharge velocity q_z,

$$q_z = \frac{Q}{A} = -K \frac{dh}{dz} \tag{9.4}$$

where, Q is the total volume of the fluid percolating in unit time, K is a constant (coefficient of permeability or hydraulic conductivity) depending on the properties of the fluid and the porous medium. The minus sign indicates that the flow is in the opposite direction of increasing h.

9.1.2.2 Coefficient of permeability

The coefficient of permeability K, as customarily defined in soil mechanics, is a property not only of the soil but also of the fluid. To separate the influence of the porous medium

from that of the liquid, the following relation was suggested by Nutting and popularized by Wyckoff (Bear, 1988). It can be deduced from the analytic derivations of Darcy's law or from dimensional analysis (Bear, 1988).

$$K = \frac{k\gamma}{\mu} \tag{9.5}$$

where, μ, the viscosity and γ, the specific weight are the fluid properties and k is the "intrinsic permeability" of the porous medium.

Darcy's law, in differential form, then is expressed as follows (Scheidegger, 1960)

$$q_z = -K\frac{dh}{dz} = -\frac{k\rho g}{\mu}\frac{\partial\left(z + \frac{p}{\gamma_w}\right)}{\partial z} \tag{9.6}$$

9.1.2.3 Darcy's law in terms of excess pressure

If the fluid is static in the initial reference state, it is useful to decompose the total pressure into the sum of hydrostatic pressure and an excess pressure (Wang, 2000).

$$\begin{aligned} p &= p^{hydro} + p^{ex} \\ &= \rho g(z_0 - z) + p^{ex} \end{aligned} \tag{9.7}$$

where $z_0 - z$ is the height of the overlaying hydrostatic column. Then the total hydrostatic head is obtained by adding the elevation head to the pressure head.

$$\begin{aligned} h &= z + \frac{p}{\gamma_w} \\ &= z + \frac{\rho g(z_0 - z) + p^{ex}}{\rho g} \\ &= z_0 + \frac{p^{ex}}{\rho g} \end{aligned} \tag{9.8}$$

Assuming the height of the static water column is independent of time, we can say that the excess pressure is the same as Darcy's head within an additive constant. Using (9.8) Darcy's law can be written as

$$q_z = -K\frac{dh}{dz} = -\frac{k}{\mu}\frac{\partial p}{\partial z} = -\frac{K}{\gamma}\frac{\partial p}{\partial z} \tag{9.9}$$

where p now denotes the excess pressure and the superscript ex is dropped because the variable p in the constitutive equations is the excess pressure relative to a hydrostatic reference state.

9.1.3 Conservation of Mass using Darcy's law

The conservation of mass, Eq (9.2), now can be written as

$$\rho_w \frac{k}{\mu}\frac{\partial^2 p}{\partial z^2}dx\,dy\,dz = \frac{\partial}{\partial t}\left(\rho_w V_w\right) \tag{9.10}$$

Using the chain rule

$$\rho_w \frac{k}{\mu}\frac{\partial^2 p}{\partial z^2}dx\,dy\,dz = \rho_w \frac{\partial}{\partial t}\left(V_w\right) + V_w \frac{\partial}{\partial t}\left(\rho_w\right) \tag{9.11}$$

which can be written as

$$\frac{k}{\mu}\frac{\partial^2 p}{\partial z^2}dx\,dy\,dz = \frac{\partial}{\partial t}\left(V_w\right) + V_w\left(\frac{1}{\rho_w}\frac{\partial \rho_w}{\partial p}\right)\frac{dp}{dt} \tag{9.12}$$

Introducing the bulk modulus of water (fluid), K_f, and dividing both sides by V, we get

$$\frac{k}{\mu}\frac{\partial^2 p}{\partial z^2} = \frac{1}{V}\frac{\partial}{\partial t}\left(V_w\right) + \left(\frac{\phi}{K_f}\right)\frac{dp}{dt} \tag{9.13}$$

where,

$$\frac{1}{K_f} = \frac{1}{\rho_f}\frac{\partial \rho_f}{\partial p} \tag{9.14}$$

The variation of fluid volume per unit volume of porous material is termed as variation of fluid content and denoted by ς. Then we can write the fluid mass balance as

$$\frac{k}{\mu}\frac{\partial^2 p}{\partial z^2} = \frac{\partial \varsigma}{\partial t} + \left(\frac{\phi}{K_f}\right)\frac{dp}{dt} \tag{9.15}$$

Also, α is the Biot-Willis factor which is the ratio of the fluid volume gained (or lost) in a material element to the volume change of that element (when the pore pressure is allowed to return to its initial state), i.e.

$$\varsigma = \alpha\, \varepsilon_V \tag{9.16}$$

Hence, we can write fluid mass balance as

$$\frac{k}{\mu}\frac{\partial^2 p}{\partial z^2} = \alpha\frac{\partial \varepsilon_V}{\partial t} + \left(\frac{\phi}{K_f}\right)\frac{dp}{dt} \tag{9.17}$$

9.2 Mathematical Model for displacement problem

We will derive the mathematical model for the deformation in Terzaghi's 1D consolidation test following Detournay and Cheng (1993).

9.2.1 Effective Stress Law

The "modified" effective stress law accounting for grain compression is given by

$$\boldsymbol{\sigma} = \boldsymbol{\sigma}'' - \alpha\, \mathbf{m}\, p \tag{9.18}$$

where α is the Biot-Willis factor and the effective stress in this case is given as

$$\Delta\boldsymbol{\sigma}'' = \mathbf{D}\left(\Delta\varepsilon - \Delta\varepsilon_T\right) \tag{9.19}$$

The modified effective stress causes all relevant deformation of the solid skeleton and the constitutive equation relating the modified effective stress to strain, in incremental form, is

$$\boldsymbol{\sigma}'' = \Delta\boldsymbol{\sigma}'' + \boldsymbol{\sigma}''_0 \tag{9.20}$$

$$\boldsymbol{\sigma}'' = \mathbf{D}(\Delta\boldsymbol{\varepsilon} - \Delta\boldsymbol{\varepsilon}_T) + \boldsymbol{\sigma}''_0 \tag{9.21}$$

where: $\mathbf{D}$ is the elastic material matrix, $\Delta\boldsymbol{\varepsilon}$ is the total strain, $\Delta\boldsymbol{\varepsilon}_T$ is the thermal strain, and $\boldsymbol{\sigma}''_0$ is the initial effective stress.

9.2.2 Force Equilibrium Equation

The body forces are neglected in the solution for Terzaghi's problem. Since we are representing the case of uniaxial strain, the mechanical equilibrium equations reduce to a single equation expressed in terms of the total vertical stress σ_z as follows

$$\boxed{\frac{\partial \sigma_z}{\partial z} = 0} \tag{9.22}$$

9.2.3 Constitutive Equations

The constitutive equations for the uniaxial strain are obtained by using the constraints

$$\begin{aligned} \varepsilon_x &= 0 \\ \varepsilon_y &= 0 \end{aligned} \tag{9.23}$$

The stress-strain relationship for an isotropic material with poroelastic effect and neglecting the thermal effects is given as (Lewis and Schrefler, 1998)

$$\varepsilon_i = \frac{1}{E}\left(\sigma_i'' - \nu\left(\sigma_j'' + \sigma_k''\right)\right) \tag{9.24}$$

where $i \neq j \neq k$ and they take values x, y, and z.

The condition $\varepsilon_x = \varepsilon_y$ yields $\sigma_x" = \sigma_y"$. Solving the equations (9.23) with (9.24) gives the expressions for $\sigma_x", \sigma_y"$ and σ_x, σ_y in terms of $\sigma_z"$ and σ_z respectively

$$\begin{aligned} \sigma_x" &= \left(\frac{\nu}{1-\nu}\right)\sigma_z" \\ \sigma_x &= \left(\frac{\nu}{1-\nu}\right)\sigma_z - \left(\frac{1-2\nu}{1-\nu}\right)p \end{aligned} \tag{9.25}$$

The third constitutive equation relating the stress and strain fields in the z-direction yields

$$\varepsilon_z = \frac{(1+\nu)(1-2\nu)}{E(1-\nu)}(\sigma_z + \alpha\, p) \tag{9.26}$$

Hence, we can write the stress in the z-direction as

$$\begin{aligned} \sigma_z &= \frac{E(1-\nu)}{(1-2\nu)(1+\nu)}\varepsilon_z - \alpha p \\ &= K_V \varepsilon_z - \alpha p \end{aligned} \tag{9.27}$$

where K_V represents the drained uniaxial bulk modulus.

The displacement in the z-direction is given by

$$\varepsilon_z = \frac{\partial u_z}{\partial z} \tag{9.28}$$

Substituting the expression for σ_z in (9.22), we get

$$K_V \frac{\partial^2 u_z}{\partial z^2} - \alpha \frac{\partial u_z}{\partial z} = 0 \tag{9.29}$$

or

$$\boxed{\frac{\partial^2 u_z}{\partial z^2} = c_m \frac{\partial u_z}{\partial z}} \tag{9.30}$$

where

$$c_m = \frac{\alpha}{K_V} \tag{9.31}$$

is Geertsma's uniaxial expansion coefficient.

The problem is considered at isothermal conditions and hence does not include thermal strains.

9.3 Mathematical Model for Fluid (re-evaluated)

Differentiating the expression for the stress in z direction, equation (9.27), with respect to time, we get

$$\begin{aligned} \frac{\partial \varepsilon_z}{\partial t} &= \frac{\alpha(1-2\nu)(1+\nu)}{E(1-\nu)} \frac{\partial p}{\partial t} \\ &= \frac{\alpha}{K_V} \frac{\partial p}{\partial t} \end{aligned} \tag{9.32}$$

The fluid mass balance equation (9.17) can be rewritten using the expression for the strain in z direction as

$$\begin{aligned} \frac{k}{\mu} \frac{\partial^2 p}{\partial z^2} &= \alpha \frac{\alpha}{K_V} \frac{\partial p}{\partial t} + \left(\frac{\phi}{K_f} \right) \frac{dp}{dt} \\ &= \left(\frac{\alpha^2}{K_V} + \frac{\phi}{K_f} \right) \frac{dp}{dt} \end{aligned} \tag{9.33}$$

This can be written as

$$\frac{\partial p}{\partial t} - \frac{k}{\mu}\frac{1}{\left(\frac{\alpha^2}{K_V} + \frac{\phi}{K_f}\right)}\frac{\partial^2 p}{\partial z^2} = 0 \tag{9.34}$$

which is in the form of the diffusion equation

$$\frac{\partial p}{\partial t} - c\frac{\partial^2 p}{\partial z^2} = 0 \tag{9.35}$$

where

$$\begin{aligned} c &= \frac{k}{\mu}\frac{1}{\left(\frac{\alpha^2}{K_V} + \frac{\phi}{K_f}\right)} \\ &= \frac{k}{\mu}\frac{1}{\left(\frac{\alpha^2(1-2\nu)(1+\nu)}{E(1-\nu)} + \frac{\phi}{K_f}\right)} \end{aligned} \tag{9.36}$$

9.4 Mathematical Model for Incompressible Fluid and Solid

Differentiating the expression for the stress in z direction, equation with respect to time, and assuming an incompressible solid ($\alpha = 1$), we get

$$\begin{aligned} \frac{\partial \varepsilon_z}{\partial t} &= \frac{(1-2\nu)(1+\nu)}{E(1-\nu)}\frac{\partial p}{\partial t} \\ &= \frac{1}{K_V}\frac{\partial p}{\partial t} \end{aligned} \tag{9.37}$$

The fluid mass balance equation (9.17) can be rewritten using the expression for the strain in z direction and assuming incompressible fluid ($K_f = \infty$) as

$$\frac{k}{\mu}\frac{\partial^2 p}{\partial z^2} = \frac{1}{K_V}\frac{\partial p}{\partial t} = \left(\frac{1}{K_V}\right)\frac{dp}{dt} \tag{9.38}$$

This can be written as

$$\frac{\partial p}{\partial t} - \frac{k}{\mu}\frac{1}{\left(\frac{1}{K_V}\right)}\frac{\partial^2 p}{\partial z^2} = 0 \tag{9.39}$$

which is in the form of the diffusion equation

$$\frac{\partial p}{\partial t} - c\frac{\partial^2 p}{\partial z^2} = 0 \tag{9.40}$$

where

$$c = \frac{kK_V}{\mu} = \frac{kE(1-\nu)}{\mu(1-2\nu)(1+\nu)} \tag{9.41}$$

9.5 Analytical Solution

The solution details for the pressure and displacements are followed from Detournay and Cheng (1993). A constant stress $-\sigma_0$ is applied suddenly on the surface $z = 0$ of a fluid saturated sample of length L. The consolidation test is assumed to satisfy the uniaxial strain condition. As the load is applied, the load produces an instantaneous undrained response, $p(z,0^+) \equiv p^u$, throughout the sample column. The sample consolidates gradually as fluid flows out from the top boundary.

9.5.1 Parameter Definitions

The different parameters and constants used in the analytical solution are explained here (Detournay and Cheng, 1993, Wang, 2000) to be able to relate the analytical solution to the formulation used in this work. These parameters are defined here for invariable porosity i.e. the compressibility of pores K_ϕ is neglected while deriving the parameter formulae where concerned and the analytical solution.

9.5.1.1 Shear modulus

The shear modulus G is given in terms of Young's modulus E and Poisson's ratio ν as follows

$$G = \frac{E}{2(1+\nu)} \tag{9.42}$$

9.5.1.2 Undrained bulk modulus

The undrained bulk modulus K_u defined as follows

$$K_u \equiv \left.\frac{\partial \sigma}{\partial \varepsilon_V}\right|_{\varsigma=0} = K\left[1+\frac{\alpha^2 K_f}{(1-\alpha)(\alpha-\phi)K_f+\phi K}\right] \tag{9.43}$$

9.5.1.3 Undrained Poisson's ratio

The undrained Poisson's ration is given as

$$\nu_u = \frac{3K_u - 2G}{2(3K_u + G)} \tag{9.44}$$

9.5.1.4 Skempton's coefficient

The Skempton's coefficient B defined as the ratio of the induced pore pressure to the change in applied stress for undrained conditions, is given as

$$B \equiv \left.\frac{\partial p}{\partial \sigma}\right|_{\varsigma=0} = \frac{\alpha K_f}{(\alpha-\phi(1-\alpha))K_f+\phi K} \tag{9.45}$$

9.5.1.5 Biot Modulus and Storage Coefficient

M called as Biot modulus and is the inverse of the storage coefficient.

$$\frac{1}{M} \equiv \left.\frac{\partial \varsigma}{\partial p}\right|_{\varepsilon_V} = \frac{\phi}{K_f} + \frac{(\alpha - \phi)}{K_S} \tag{9.46}$$

The constant S called as storage coefficient defined under the conditions of uniaxial strain and constant normal stress in the direction of strain, is related to M as

$$S = \frac{(1-\nu_u)(1-2\nu)}{M(1-\nu)(1-2\nu_u)} \tag{9.47}$$

Note that under the case when $\nu_u = \nu$, $S = 1/M$.

9.5.1.6 Poroelastic stress coefficient

The poroelastic stress coefficient η can be expressed in terms of the fundamental constants as

$$\eta = \frac{\alpha(1-2\nu)}{2(1-\nu)} \tag{9.48}$$

9.5.2 Initial and Boundary conditions

The experimental conditions translate into following initial and boundary conditions.

$$\begin{aligned} \sigma_{zz}(0,t) &= -\sigma_0 \\ w(L,t) &= 0 \\ p(0,t) &= 0 \\ \left.\frac{\partial p}{\partial z}\right|_{z=L} &= 0 \end{aligned} \tag{9.49}$$

9.5.3 Pore Pressure

The initial pore pressure is the undrained response, $p^u = \frac{\eta \sigma_0}{GS}$. The initial and boundary conditions are the same as for a classical heat-conduction problem (Wang, 2000). The

solution is given in terms of dimensionless coordinate $\chi = z/L$ and dimensionless time $\tau = ct/4L^2$ as follows

$$p(z,t) = \frac{\eta\sigma_0}{GS}\left[1 - F_1(\chi,\tau)\right] \tag{9.50}$$

where

$$F_1(\chi,\tau) = 1 - \sum_{m=1,3,\ldots}^{\infty} \frac{4}{(m\pi)} \sin\left[\frac{m\pi\chi}{2}\right] \exp\left[-m^2\pi^2\tau\right] \tag{9.51}$$

such that $F_1(\chi,0^+) = 0$ and $F_1(\chi,\infty) = 1$.

9.5.4 Displacement

A finite column length means that the initial instantaneous displacement, on application of load, is finite. The total displacement at any time is the sum of the instantaneous undrained response and the time dependent response during the pore pressure diffusion phase. The initial displacement is obtained as

$$u_0(z) = \frac{\sigma_0 L(1-2\nu_u)}{2G(1-\nu_u)}(1-\chi) \tag{9.52}$$

The additional displacement during drainage is given as

$$\Delta u(z,t) = \frac{\sigma_0 L(\nu_u - \nu)}{2G(1-\nu)(1-\nu_u)} F_2(\chi,\tau) \tag{9.53}$$

where

$$F_2(\chi,\tau) = \sum_{m=1,3,\ldots}^{\infty} \frac{8}{m^2\pi^2} \cos\left[\frac{m\pi\chi}{2}\right]\left(1 - \exp\left[-m^2\pi^2\tau\right]\right) \tag{9.54}$$

Note again that $F_2(\chi,0^+) = 0$ and $F_2(\chi,\infty) = 1-\chi$.

9.6 Simulations

To simulate the uniaxial strain problem, a long column of size 50m x 1m x 1m is created with the grid of size 78 x 3 x 3 in TOUGH2. The dual mesh in G3D represents a single long column. To keep the domain size as close as possible, the top and bottom most layers as well as the side layers in TOUGH2 were kept thin. Gravity was neglected for the simulation. TOUGH2 needs to have some finite value for the atmospheric pressure. The analytical solution developed is based on zero atmospheric pressure. To have an effective atmospheric pressure to be zero, at the start of the simulation, the correct initial stress was used to compensate for non-zero initial pressure.

9.7 Results and Comparison (Set 1 [$\alpha = 1$])

The simulation run assumed the matrix to be incompressible. The simulation parameters are listed in Table 9.1. The pressures and the additional displacements at three different times are compared in the following sections.

9.7.1 Pressure

The plot of the comparison of the analytically obtained pore pressure and the simulated result are as shown in Figure 9.3. The plots are shown at three different times, close to the start, intermediate and at steady state. Initially, the pressure in the fluid is zero. When the load is applied, the pressure instantly increases by a value (1.4058E6 Pa) which is the portion of the load carried by the fluid. Then, as time increases, the fluid is drained and the pressure is reduced. At long times, the pressure will approach zero and all the load is carried by the porous media and not the fluid. As can be seen, the comparison between the analytic and calculated pressures is very good.

Table 9.1 Simulation Parameters (Terzaghi's Problem Set 1).

Parameter	Value
Rock Density	2600 kg/m^3
Porosity	0.2
Permeability (x, y, z)	1e-14
Heat Conductivity	2 W/m C
Specific Heat	1000 J/kg C
Poisson's ratio	0.2
Young's Modulus	1.44e10 Pa
Biot-Willis Factor	1.0
Gravity	0
Initial Stress	-2.00e6 Pa

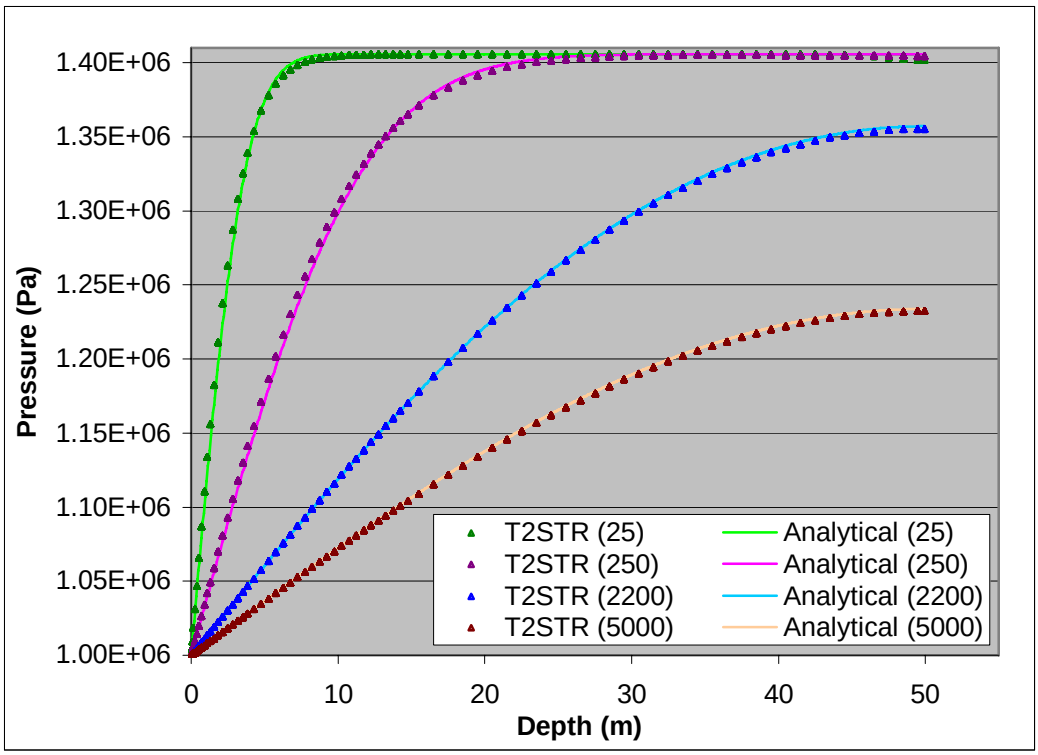

Figure 9.3 Comparison of pressures in column for times following the step load (Set 1).

9.7.2 Displacements

The additional displacement during drainage is shown in Figure 9.4. As can be seen, initially the drainage displacement is only near the top. However, as more fluid is drained, this displacement becomes larger. Again, the comparison between the analytic and calculated displacements is very good.

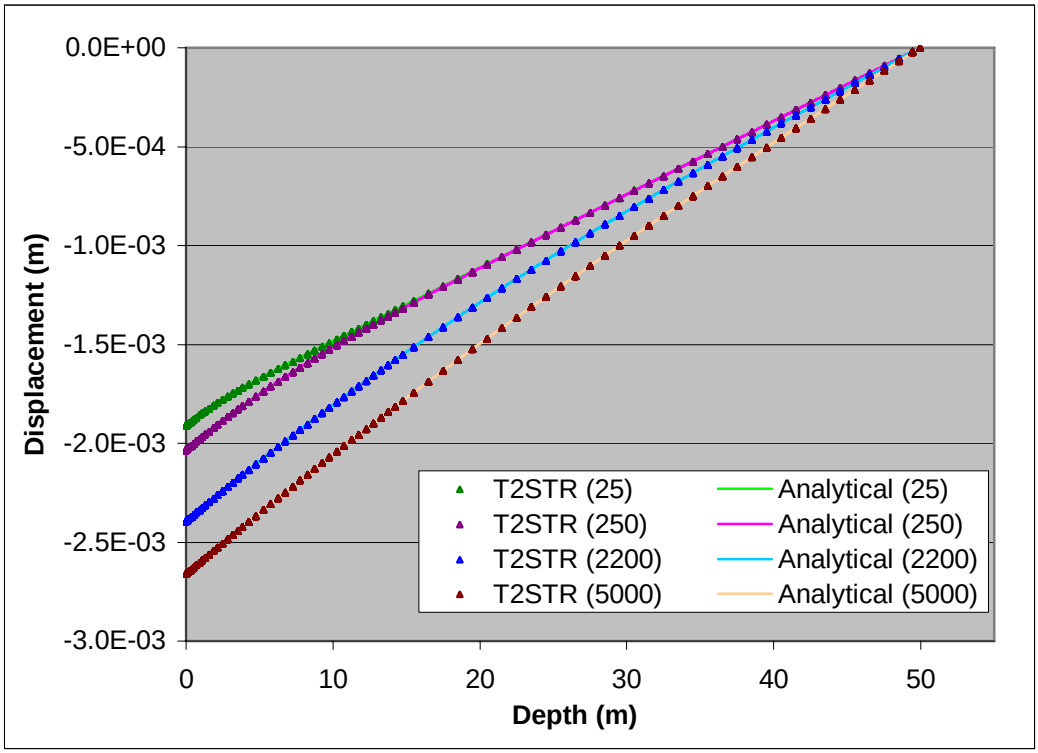

Figure 9.4 Comparison of drainage displacements (Set 1).

9.8 Results and Comparison (Set 2 [$\alpha = 0.778$])

This simulation assumes the matrix and fluid, both to be compressible. The simulation parameters are listed in Table 9.2. As seen in the parameters, the initial external load applied is not same as in the case of $\alpha = 1$. The external load for the analysis is assumed as 1e6. To cancel the effect of non-zero initial pressure in the reservoir, the external load

need to be increased with the factor of αp. Hence the external applied load is 1.778e6 Pa and not 2e6 Pa as in the case of $\alpha = 1$. Similar to the earlier set, the pressures and the additional displacements at three different times are compared in the following sections.

9.8.1 Pressure

The plot of the comparison of the analytically obtained pore pressure and the simulated is shown in Figure 9.5. The plots are shown at three different times, close to the start, intermediate and at steady state. Initially, the pressure in the fluid is zero. When the load is applied, the pressure instantly reaches value of 1.334E6 Pa. This is the portion of the load carried by the fluid. Then, as time increases, the fluid is drained and the pressure is reduced. At long times, the pressure will approach zero and all the load is carried by the porous media and not the fluid.

Table 9.2 Simulation Parameters (Terzaghi's Problem - Set 2).

Parameter	**Value**
Rock Density	2600 kg/m^3
Porosity	0.20
Permeability (x, y, z)	1e-14
Heat Conductivity	2 W/m C
Specific Heat	1000 J/kg C
Poisson's ratio	0.2
Young's Modulus	1.44e10 Pa
Biot-Willis Factor	0.778
Gravity	0
Initial Stress	-1.778e6Pa

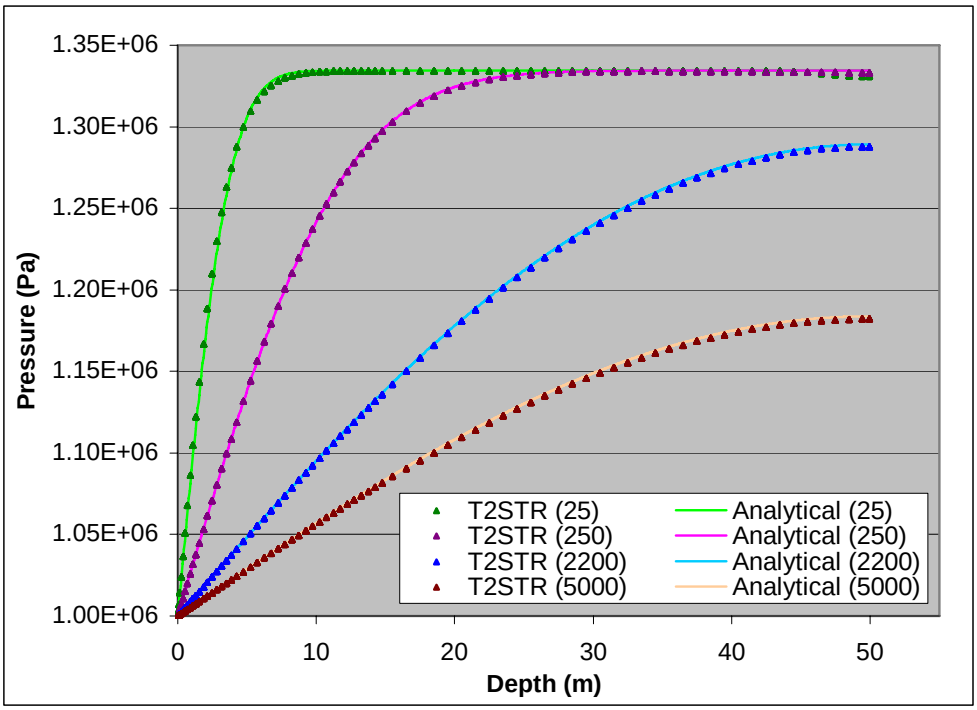

Figure 9.5 Comparison of pressured in column for times following the step load (Set 2).

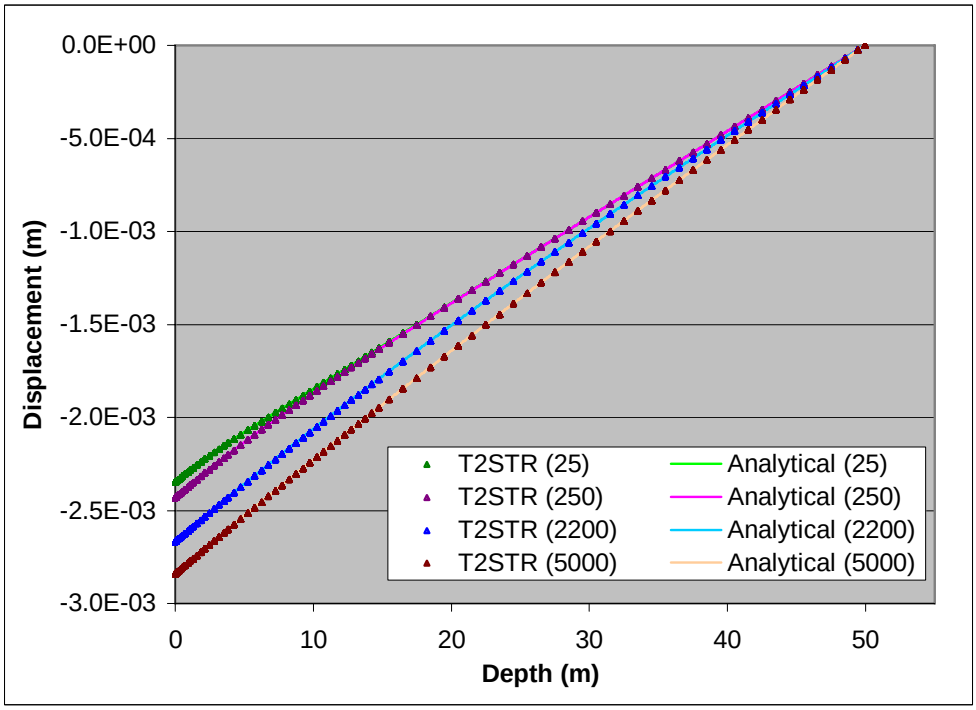

Figure 9.6 Comparison of drainage displacements (Set 2).

9.8.2 Displacements

The additional displacement during drainage is shown in Figure 9.6. As can be seen, initially the drainage displacement is only near the top. However, as more fluid is drained, this displacement becomes larger. Again, the comparison between the analytic and calculated displacements is very good.

9.9 Results and Comparison (Set 3 [$\alpha = 1$, $Kf = \infty$])

The simulation parameters and model is same as in Set 1 but the fluid is made incompressible by invoking the incompressibility option (modification in COWAT). The analytical solution is obtained using the coefficient derived in (9.41).

9.9.1 Pressure

The plot of the comparison of the analytically obtained pore pressure and the simulated is shown in Figure 9.7. When the load is applied, the pressure instantly reaches a value (2.0E6 Pa) that is equal to the applied load. Since the fluid as well as solid is incompressible the fluid, the applied load has to be carried by the fluid initially. Then, as time increases, the fluid is drained and the pressure is reduced to the initial pressure and load is carried by the porous media. The comparison is very good.

9.9.2 Displacements

The additional displacement during drainage is shown in Figure 9.8. As can be seen, initially the drainage displacement is only near the top. However, as more fluid is drained, this displacement becomes larger. Again, the comparison between the analytic and calculated displacements is very good.

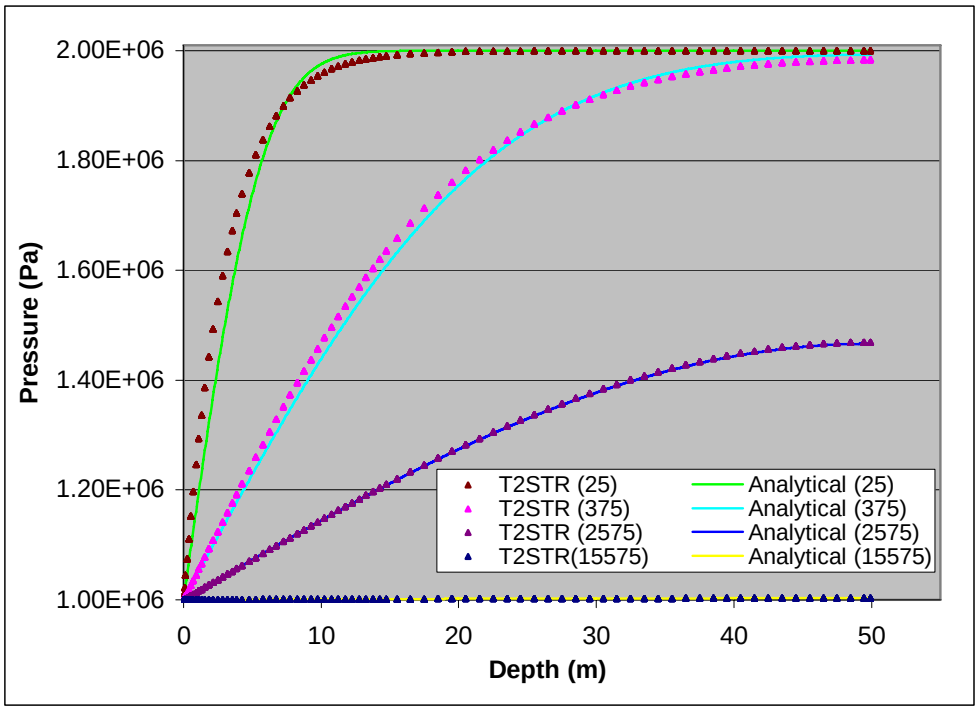

Figure 9.7 Comparison of pressured in column for times following the step load (Set 3).

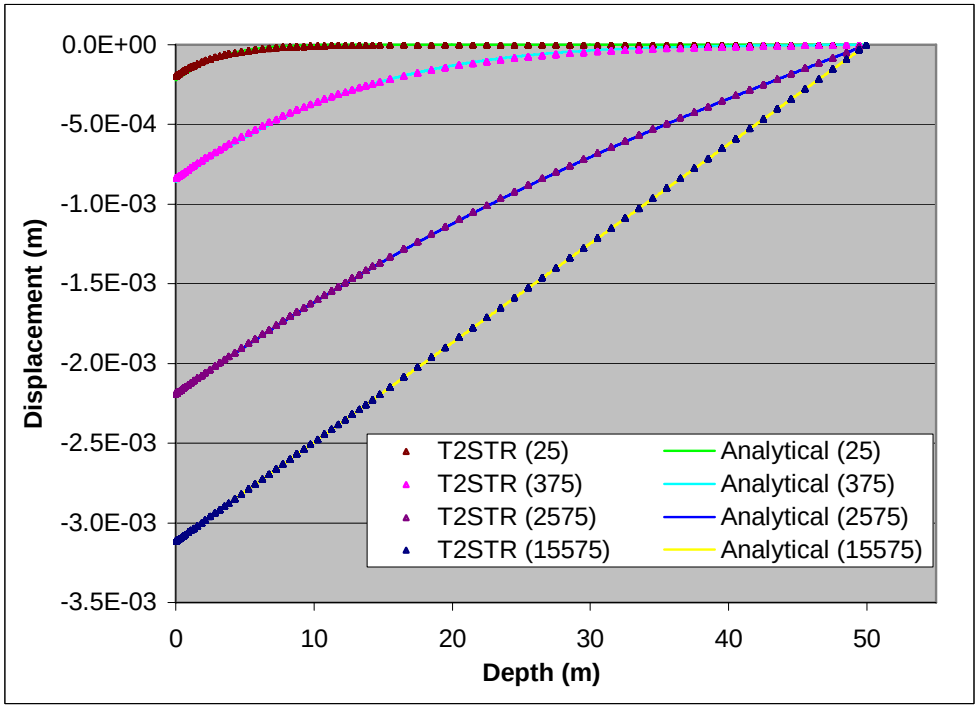

Figure 9.8 Comparison of drainage displacements (Set 3).

9.10 Conclusion

The full coupling established is verified using the uniaxial strain problem of Terzaghi's classical 1D consolidation test. The fluid compressibility as well as the solid compressibility are taken into account while doing the analysis. The fully coupled T2STR code and the analytically obtained results are found to be in good agreement and validate the code.

10 VERIFICATION PROBLEM 2 (GIBSON'S 2D PROBLEM)

This chapter discusses a two dimensional plain strain consolidation problem studied by Gibson et al. (1970) is used for verification purpose. Gibson et al. (1970) provided the exact analytical solution to the problem. The solution is expressed using the dimensionless parameters and obtained using two displacement functions.

We consider a finite strip loaded over the center as shown in Figure 10.1. Due to symmetry only half of the reservoir is modeled.

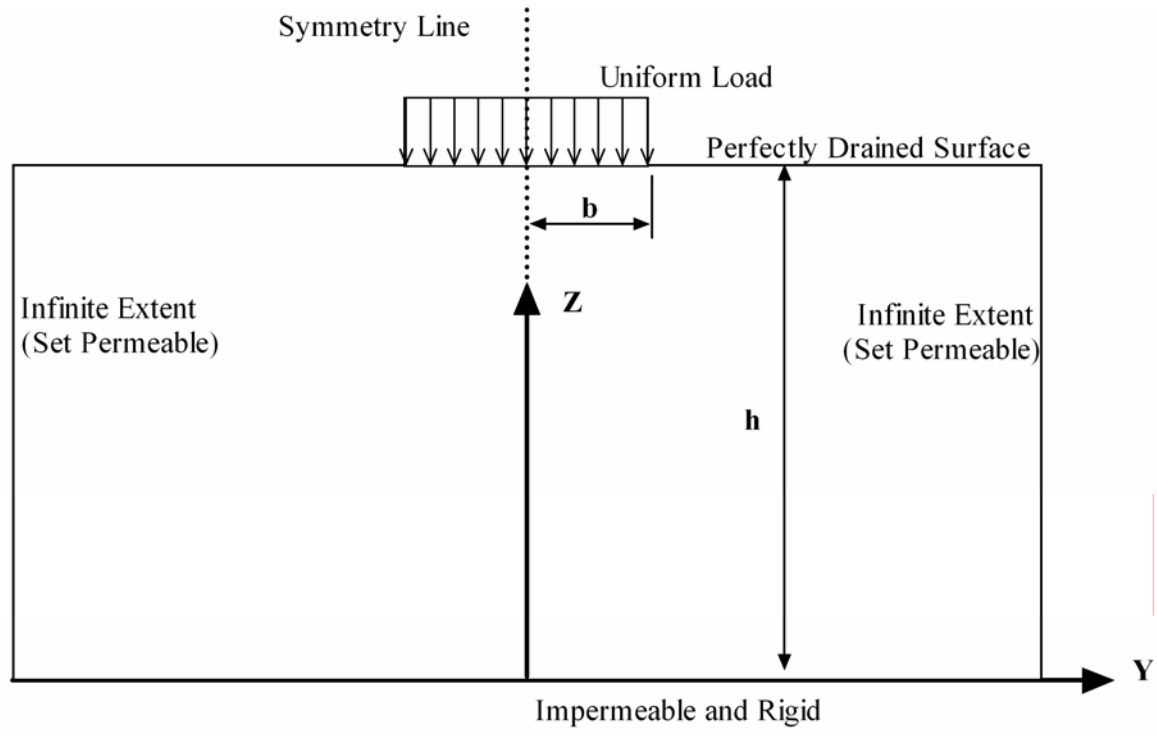

Figure 10.1 Schematic of plain strain consolidation on a smooth impervious boundary.

10.1 Mathematical Model for flow problem

The fluid flow equation, neglecting the diffusive flux, is written as

$$\boxed{\begin{aligned}&\left[\frac{\partial\left(\phi\, S_\psi\, \rho_\psi^\kappa\right)}{\partial t}-\nabla\bullet\left\{\rho_\psi^\kappa\frac{\mathbf{k}k_{r\psi}}{\mu_\psi}\left(\nabla p_\psi+\rho_\psi g\nabla z\right)\right\}+Q_\psi^{\kappa e}-Q^\kappa\right]+\\&\left[S_\psi\,\rho_\psi^\kappa\left(\frac{(\alpha-\phi)}{K_S}\frac{\partial\left(\sum S_\psi p_\psi\right)}{\partial t}-(\alpha-\phi)\alpha_T\frac{\partial T}{\partial t}+\alpha\frac{\partial\varepsilon_V}{\partial t}-\frac{\partial\phi}{\partial t}\right)\right]=0\end{aligned}} \tag{10.1}$$

The plain strain problem is solved by Gibson et al. (1970) by neglecting gravity, without any source, under isothermal and single phase conditions, with invariant porosity and assuming incompressible solid and incompressible fluid. The fluid flow equation, then reduces to

$$\boxed{\frac{k}{\mu}\nabla^2 p=\frac{\partial\varepsilon_V}{\partial t}} \tag{10.2}$$

10.2 Mathematical Model for displacement problem

The plain strain problem is characterized so that the displacement components are independent of x. The static equilibrium equation, in absence of body forces and considering the plain strain conditions, can be written as follows

$$\frac{\partial\sigma_{ij}}{\partial x_j}=0 \qquad i,j=\{y,z\} \tag{10.3}$$

where the stresses are given as

$$\boldsymbol{\sigma}=\mathbf{D}\,\Delta\boldsymbol{\varepsilon}-\mathbf{m}\left(p+p_0\right) \tag{10.4}$$

under isothermal conditions and without any initial stresses, assuming incompressible solid.

10.3 Analytical Solution

The solution details are followed from Gibson et al. (1970). A constant stress $-\sigma_0$ is applied suddenly on the surface $z = 0$ over the width b ($2b$ for the entire model) of a fluid saturated sample of height h. The consolidation test is assumed to satisfy the plain strain condition.

10.3.1 Initial and Boundary conditions

The experimental conditions translate into following initial and boundary conditions.

$$\sigma_{zz}(0,t) = -\sigma_0 \qquad \forall\, |x| \le b, t > 0 \tag{10.5}$$

In addition to the applied load on the surface, the other boundary conditions are an impermeable surface at the bottom of the reservoir, and a permeable boundary at the top.

$$\begin{aligned} p(z=0,t) &= p_0 \\ \left.\frac{\partial p}{\partial z}\right|_{z=-h} &= 0 \end{aligned} \tag{10.6}$$

The displacements at the symmetry line are set to zero due to symmetry condition. Under plain strain conditions, the strain in x direction is zero and the surface at the bottom of the reservoir is assumed to be rigid.

$$\begin{aligned} w(z=-h,t) &= 0 \\ v(y=0,t) &= 0 \\ u(x,t) &= 0 \end{aligned} \tag{10.7}$$

10.3.2 Displacement

The solution is obtained using two displacement functions E and Ψ, each being function of two space variables and time and satisfying the following equations (Gibson et al., 1970)

$$c\nabla^4 \mathrm{E} = \nabla^2\left(\partial \mathrm{E}/\partial t\right), \quad \nabla^2 \Psi = 0 \tag{10.8}$$

where c, the coefficient of consolidation is given as

$$c = \frac{2G\kappa\eta}{\gamma_w} \tag{10.9}$$

Also, the coefficient used for plotting c` is given as

$$c` = \frac{c}{\eta} = \frac{2G\kappa}{\gamma_w} \tag{10.10}$$

The permeability coefficient κ is calculated using the permeability relation

$$\kappa = \frac{k\gamma_w}{\mu} \tag{10.11}$$

where γ_w denotes the specific weight of water, k the permeability of the medium and μ denotes the fluid viscosity.

The solution at the corner ($y = 0, z = 0$) is given for different conditions. The final settlement is given by

$$w_0(\infty) = \frac{\eta\sigma_0 h}{2(2\eta - 1)G'} \tag{10.12}$$

where η is an auxiliary elastic constant given by

$$\eta = \frac{1-\nu}{(1-2\nu)} \tag{10.13}$$

The "immediate" settlement is given by

$$w_0(0) = \frac{\sigma_0 h}{4G} \tag{10.14}$$

The time evolution of the surface displacement for different h/b ratios and for different values of Poisson's ratio is given in the paper.

10.4 Simulations

To simulate the plain strain problem, a domain of size 2m x 150m x 10m is created with the grid of size 2 x 125 x 23 in TOUGH2. The load is applied over 10m. Gravity effects were neglected for the simulation to be consistent with the assumption in the solution obtained by Gibson et al. (1970).

TOUGH2 needs to have some finite value for the atmospheric pressure. The analytical solution developed is based on the assumption of zero atmospheric pressure. To have an effective atmospheric pressure to be zero, the correct initial stress was used to cancel the effect of non-zero initial pressure at the start of the simulation.

Also, TOUGH2 includes the fluid compressibility by default. An option was introduced in the Record "T2STR" where the fluid can be simulated as incompressible with user-defined value of fluid compressibility.

10.5 Results and Comparison (Set 1 [h/b = 1,v = 0])

The simulation parameters are listed in Table 10.1. Figure 10.2 and Figure 10.3 show the comparative results of the fully coupled code with the analytical solution provided by Gibson et al. (1970).

The results compare very well except for a small deviation at the start of the simulation. The deviation can be attributed to coarser mesh and comparatively smaller time step.

Table 10.1 Simulation Parameters (Gibson's Problem - Set 1).

Parameter	**Value**
Rock Density	2600 kg/m^3
Porosity	0.1
Permeability (x, y, z)	1e-14
Poisson's ratio	0.0
Young's Modulus	1.8e9 Pa
Biot-Willis Factor	1.0
Gravity	0
Initial Stress (+y & z s/c)	-1.00e6 Pa

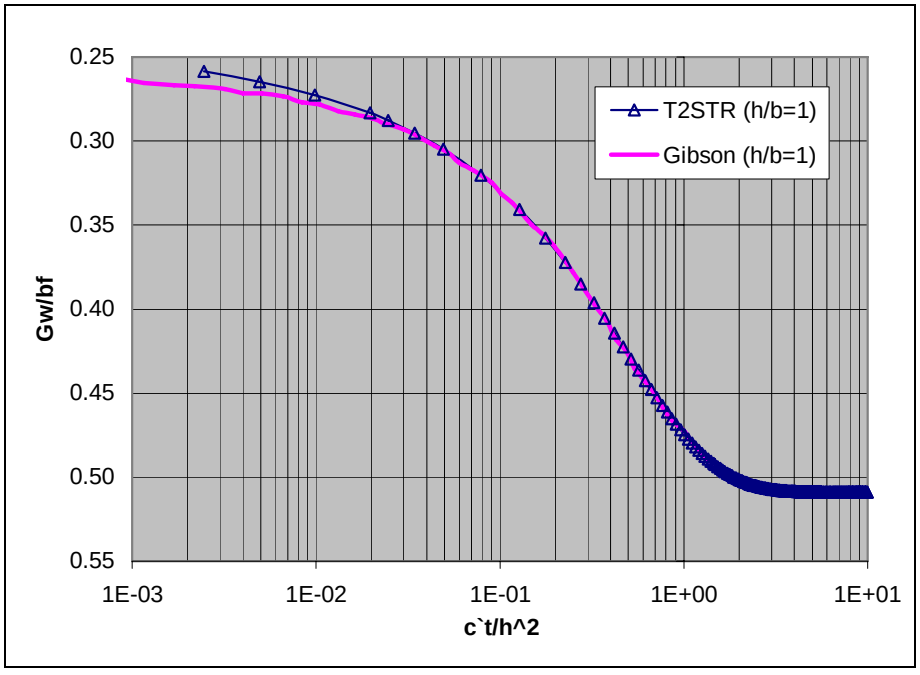

Figure 10.2 Comparison of Corner Node displacement (dimensionless) for $\nu = 0$.

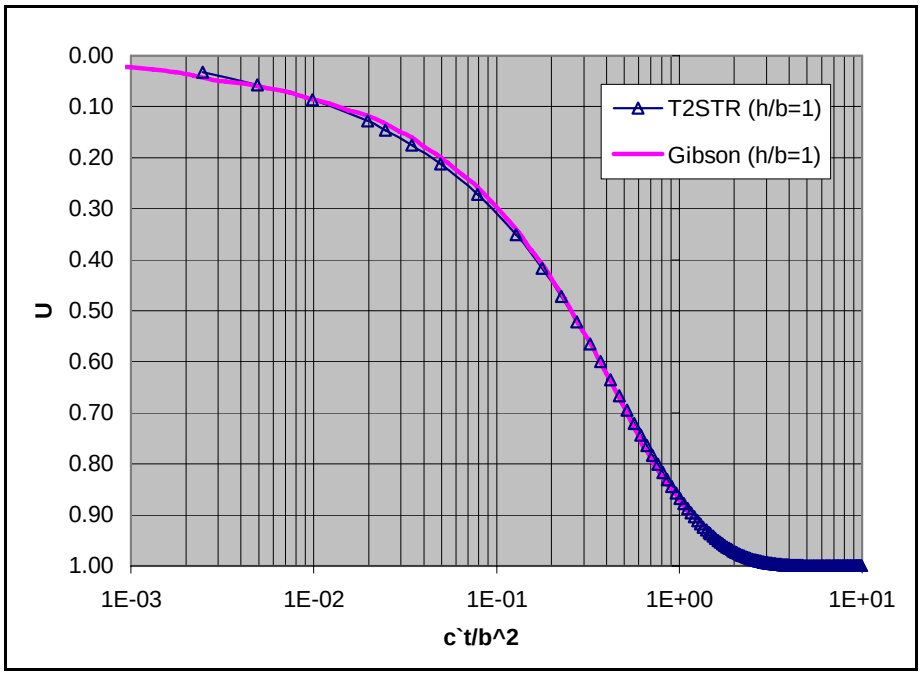

Figure 10.3 Comparison of $U[(w-w_0)/(w_\infty - w_0)]$ at corner node for $\nu = 0$.

10.6 Results and Comparison (Set 2 [h/b = 1,v = 0.2])

The Poisson's effect due to non-zero ν can be seen in reduced final settlement.

Table 10.2 Simulation Parameters (Gibson's Problem - Set 2).

Parameter	**Value**
Rock Density	2600 kg/m^3
Porosity	0.10
Permeability (x, y, z)	1e-14 m^2
Poisson's ratio	0.2
Young's Modulus	1.8e9 Pa
Biot-Willis Factor	1.0
Gravity	0
Initial Stress (+y & z s/c)	-1 e6Pa

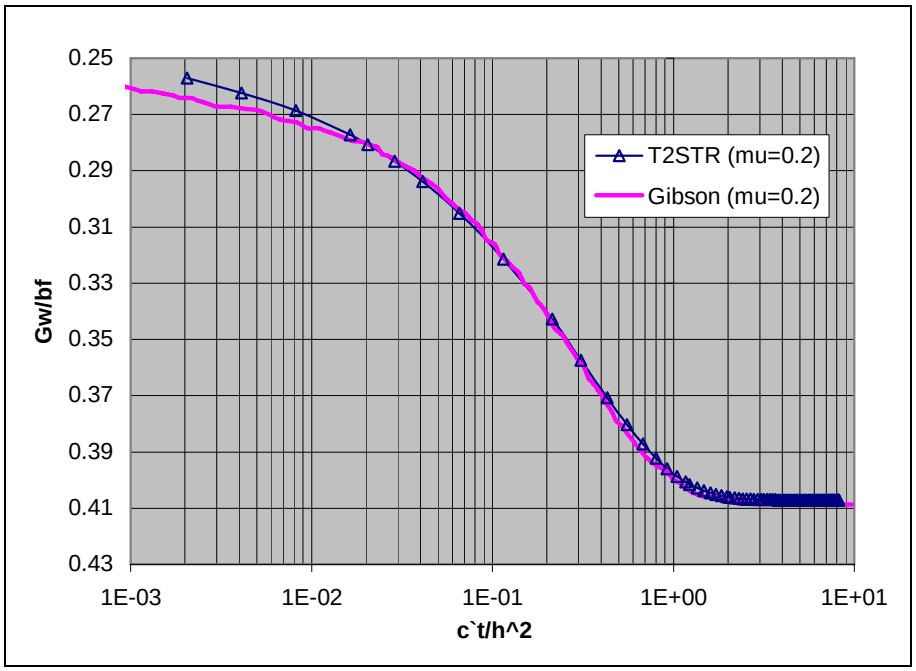

Figure 10.4 Comparison of Corner Node displacement (dimensionless) for $\nu = 0.2$.

The dimensionless displacements compare very well as seen in Figure 10.4. The difference at the initial stages of the simulation can be attributed to the coarser mesh and comparatively smaller time steps.

10.7 Conclusion

The full coupling established between in T2STR is verified using the 2D plain strain problem solved analytically using displacement functions by Gibson et al. (1970). The fully coupled T2STR code and the analytically obtained results are found to be in excellent agreement and validate the correctness of code.

11 VERIFICATION PROBLEM 3 (1D THM PROBLEM, LEWIS-SCHREFLER)

Aboustit et al. (1982, 1985) have given the coupled finite element formulation of quasi-static, linear thermoelastic consolidation assuming infinitesimal strain. Lewis and Schrefler (1998) have solved the same problem studying the isothermal consolidation, thermo-elastic deformation, and non-isothermal consolidation as well. Gatmiri and DeLage (1997) also have studied the problem using a new concept of thermal void ratio state surface. An analysis, similar to that of Lewis and Schrefler (1998), is carried out using T2STR.

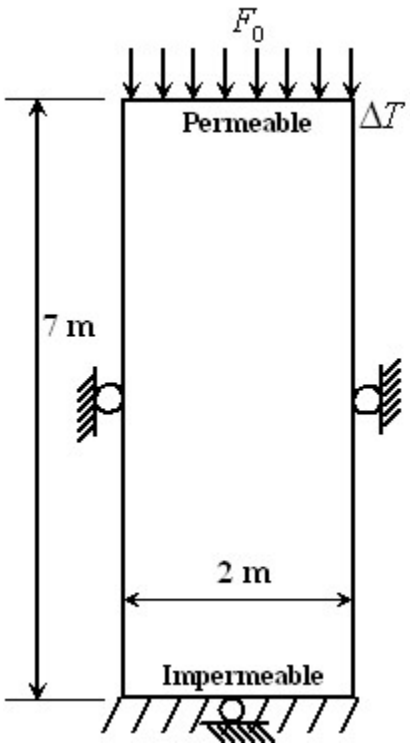

Figure 11.1 One dimensional model of thermo-elastic consolidation problem.

The problem consists of a column subjected to surface load F_0 and a constant surface temperature T, differing by ΔT from the reservoir initial temperature of T_0. The fluid

and solid are considered incompressible and the thermal expansion of fluid is neglected. In the heat transfer problem the convective heat transfer is also neglected by Lewis & Schrefler (1998). The variation in viscosity with temperature and pressure is neglected in the problem, as well. The top surface is permeable and the sides and bottom are supported on rollers. The analysis is done in three steps, initially only the isothermal consolidation is compared, then only surface temperature is applied and the deformation due to only thermal effects are studied and finally a couple thermo-hydro-mechanical problem i.e. non-isothermal consolidation problem is solved.

11.1 Governing Equations

Considering the above assumptions, the equation of conversation of mass reduces to

$$\boxed{\left(\phi \frac{\partial\left(S_\psi \rho_\psi^\kappa\right)}{\partial t} + \nabla \bullet \mathbf{q}_{r\psi}^\kappa\right) + S_\psi \rho_\psi^\kappa \frac{\partial \varepsilon_V}{\partial t} = 0} \tag{11.1}$$

where the terms due to solid and fluid compressibility are neglected and no external source is present.

In the case of non-isothermal analysis, the conservation of energy equation is given as

$$\frac{\partial\left(\phi \sum S_\psi \rho_\psi^\kappa u_\psi^E + (1-\phi)\rho_S u_S^E\right)}{\partial t} = -\nabla \bullet \left(\sum \mathbf{q}_{r\psi}^\kappa h_\psi\right) - \nabla \bullet \mathbf{J}_C^H \tag{11.2}$$

where

$$\begin{aligned} \mathbf{J}_C^H &= \sum\nolimits_\psi \mathbf{J}_{C\psi}^H + \mathbf{J}_S^H \\ &= \left(\phi \sum\nolimits_\psi \lambda_\psi + (1-\phi)\lambda_S\right)\Delta T \end{aligned} \tag{11.3}$$

The λs represent the thermal conductivities of the solid and fluids. Neglecting the convective heat transfer term and considering heat transfer only in one dimension, the energy equation becomes

$$\boxed{\frac{\partial\left(\phi\sum S_\psi \rho_\psi^\kappa u_\psi^E + (1-\phi)\rho_S u_S^E\right)}{\partial t} = -\left(\phi\sum\nolimits_\psi \lambda_\psi + (1-\phi)\lambda_S\right)\frac{\partial T}{\partial z}} \tag{11.4}$$

where the thermal conductivities have been assumed constant with respect to time.

TOUGH2 calculates the internal energy term of fluid using the enthalpy relation

$$u = h - \frac{p}{\rho} \tag{11.5}$$

such that

$$\frac{\partial\left(\phi\sum S_\psi \rho_\psi^\kappa\left(h_\psi - \frac{p_\psi}{\rho_\psi}\right) + (1-\phi)\rho_S c_S \Delta T\right)}{\partial t} = -\left(\phi\sum\nolimits_\psi \lambda_\psi + (1-\phi)\lambda_S\right)\frac{\partial T}{\partial z} \tag{11.6}$$

and Lewis et al. express the internal energy using the specific heat capacity as

$$\frac{\partial\left(\phi\sum S_\psi \rho_\psi^\kappa c_\psi + (1-\phi)\rho_S c_S\right)\Delta T}{\partial t} = -\left(\phi\sum\nolimits_\psi \lambda_\psi + (1-\phi)\lambda_S\right)\frac{\partial T}{\partial z} \tag{11.7}$$

or using the average heat capacity can be written as

$$\frac{\partial(\rho c)_a \Delta T}{\partial t} = -(\lambda)_a \frac{\partial T}{\partial z} \tag{11.8}$$

In the implementation using T2STR, to match the average heat capacity and avoid its variation with temperature and pressure, the fluid internal energy term is zeroed and equivalent constant value is added to obtain the correct average heat capacity.

11.2 Simulation

The parameters required for the simulation were obtained from the relevant references. The values and/or units of some of the parameters are inconsistent in all of the references. Hence the parameter value selection (from the different sets) was done using the simulation results. The parameters used were as listed in Table 11.1.

Table 11.1 Simulation Parameters (Thermo-elastic consolidation).

Parameter	**Value**
Size	2m x 2m x 7m
Mesh	3 x 3 x 49
Young's Modulus, E	5.886e7 Pa
Poisson's ratio, ν	0.4
Permeability, k	7.3e-13 m^2
Avg. Thermal Conductivity, λ	836.8 W/mC
Avg. heat capacity, $(\rho c)_a$	40 kCal/ m^3C
Specific Heat (derived from heat cap.), c	104.67 J/ kg C
Thermal Expansion Coefficient, α_T	0.3e-6 1/C
Biot-Willis Coefficient, α	1.0
Density of rock, ρ_S	2200 kg /m^3
Density of water, ρ_w	1000 kg/m^3
External Load, F_0	1e4 Pa
Initial reservoir pressure, p_0	1e5 Pa
Initial reservoir temperature, T_0	5 C
Applied surface temperature, T_S	55 C

While determining the simulation parameters, the already established hydro-mechanical coupling was taken as reference and comparing the results for it, some parameter values were confirmed.

11.3 Results and Comparison

The results were compared with the plots given by Lewis et al. (1998) and are shown in Figure 11.2.

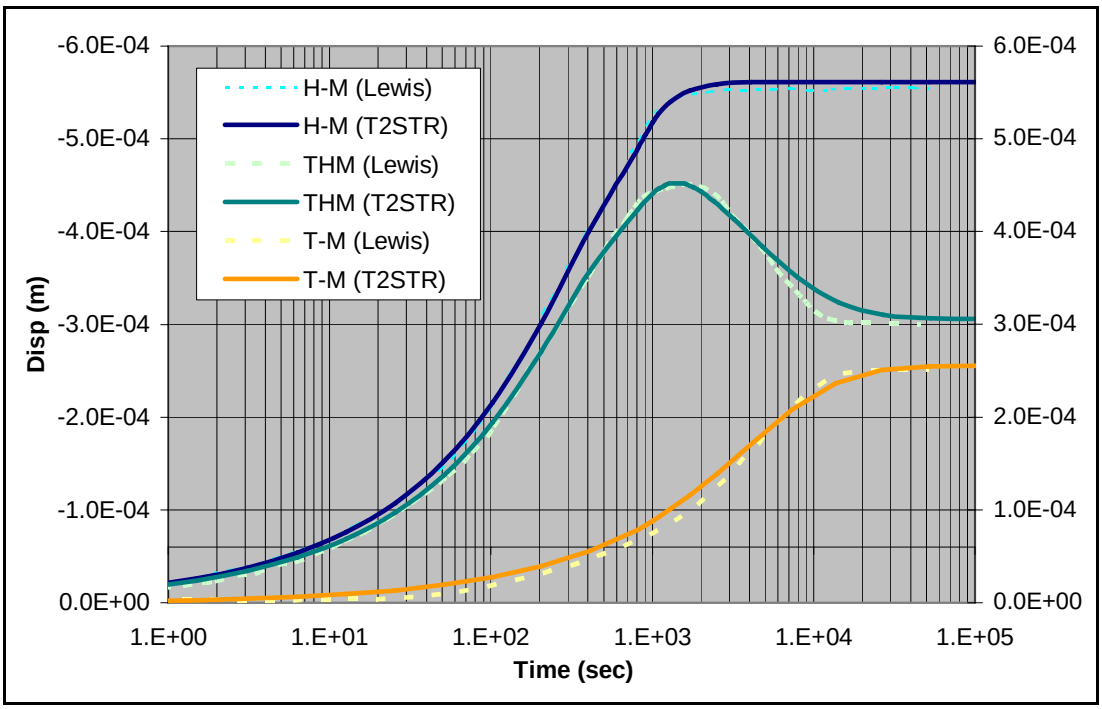

Figure 11.2 Comparison of displacements at the top.

The slight variations in the plots can be attributed to the adjusted parameter values to obtain similar effect, assumptions regarding constant parameters (values not available) and differences in the implementation. Considering that, the results compare very well.

This verifies the accuracy of the coupled thermo-hydro-mechanical T2STR code.

12 VERIFICATION PROBLEM 4 (WELL TEST ANALYSIS)

The following verification problem is well test analysis compared with analytical solution. The analytic solution for an infinite reservoir derived by Horner (1967) is given below. The analytic solutions used to check the implementation in T2STR.

12.1 Analytic Solution

The governing equation of flow by Horner (1967) is given as

$$\frac{\partial^2 p}{\partial r^2} + \frac{1}{r}\frac{\partial p}{\partial r} = \left(\frac{c_t \phi \mu}{k}\right)\frac{\partial p}{\partial t} \tag{12.1}$$

The analytic solution for the case of a well at the center of an infinite circular reservoir is then given as:

$$p = p_0 + \frac{q\mu}{4\pi kh}\left\{Ei\left(-\frac{r^2 \phi \mu c_t}{4kt}\right)\right\} \tag{12.2}$$

where, Ei is the exponential integral function, c_t is the total compressibility.

12.2 Simulation

A T2STR model, with parameters specified in Table 12.1, was used to simulate the infinite reservoir model. The reservoir boundary was assumed to be at 700 m and hence the far-field effects are negligible prompting the comparison with the infinite reservoir model. A quarter model of the reservoir was modeled using the symmetry conditions. The corner well cells were of the size, 0.025m, obtained approximately equivalent to same cross sectional area using the well radius of 0.035m. The height of TOUGH2 model was 13.65 m. The flow rate condition was specified at the well cells.

Table 12.1 Simulation Parameters (Well test analysis).

Parameters	Values
Initial reservoir pressure, p_0	530 KPa
Constant Flow rate, q_1	3.5e-2 kg/s
Viscosity, μ	0.00105 Ns/m^2
Formation thickness(withdrawal height), h	13.65 m
Porosity, ϕ	0.05
Well radius, r_w	0.035 m
Radius of the boundary, r_b	700 m
Young's Modulus, E	1e9 Pa
Poisson's ratio, ν	0.1
Biot-Willis Coefficient, α	0.7091

The total compressibility, c_t, is the combined compressibility of the solid and fluid and the value used in the analytic solution is 4.83e-10 1/Pa. The fluid compressibility is calculated by TOUGH2 as function of pressure and temperature. Since the temperature is constant, the variation in fluid compressibility is going to be negligible and we can assume it to be constant. The solid compressibility in T2STR is decided through the Biot-Willis coefficient α. The reservoir model in the analysis is subjected to boundary conditions of roller support on all sides. Hence the volumetric strain is going to be zero. The governing equation of fluid flow without the source term, then becomes

$$\left[\phi\frac{\partial\left(\rho_\psi\right)}{\partial t}+\nabla\bullet\mathbf{q}_\psi\right]+\left[\rho_w\left(\frac{\left(\alpha-\phi\right)}{K_S}\frac{\partial p_\psi}{\partial t}\right)\right]=0 \tag{12.3}$$

Using Darcy's Law and comparing the coefficients of the term with pressure variation with time, we can find the relation between compressibilities as follows

$$c_t = \frac{\phi}{K_f} + \frac{(\alpha - \phi)}{K_S} \tag{12.4}$$

Using the relation (3.14) we can obtain the Biot-Willis coefficient by solving for compressibility.

12.3 Results and Conclusion

The comparison of the analytical solution and the simulation results using T2STR are shown in Figure 12.1. As seen the pressures at the well compare very well. The negligible variation can be attributed to the varying viscosity (the variation is also negligible) in T2STR with pressure and assumption of constant viscosity in the analytical model.

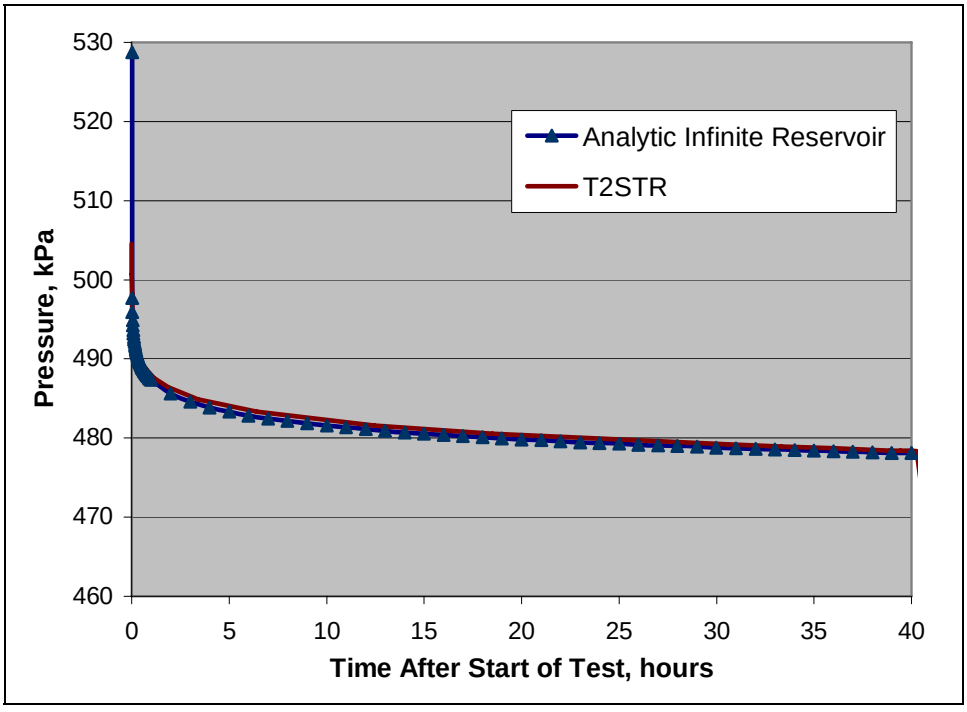

Figure 12.1 Comparison of pressures at the well during withdrawal test.

The well test analysis confirms the accuracy of implementation of the effects of the solid grain compressibility in the fluid flow equation.

13 DEMONSTRATION PROBLEM 1 (1D THM PROBLEM, TWO-PHASE)

The same 1D thermo-elastic consolidation problem was solved with two phase condition. Lewis and Schrefler (1998) have done it for lower temperature and taking into account the air as a third phase.

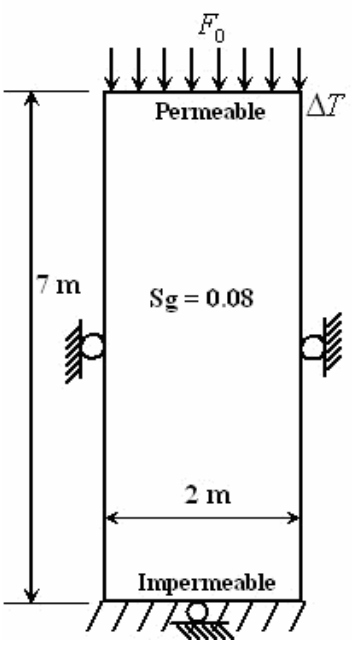

Figure 13.1 One dimensional thermo-elastic consolidation problem (Two-phase).

Currently T2STR can simulate using EOS1 module (water) of TOUGH2. Hence the problem was done only for two phase analysis. But the temperature was kept high enough to see the phase change effects prominently in the simulation.

The problem consists of a column subjected to surface load F_0 and a constant surface temperature T, differing by ΔT from the reservoir initial temperature of T_0. The fluid is considered compressible but the solid is incompressible. The variation in viscosity with temperature and pressure is not neglected in this problem. The top surface is permeable

and the sides and bottom are supported on rollers. The analysis is done as a thermo-hydro-mechanical problem i.e. non-isothermal consolidation problem is solved.

13.1 Governing Equations

The governing equations are same as stated in single phase problem since it is general formulation. In the implementation using T2STR, no changes were made in TOUGH2 code and hence the analysis carried out is general.

13.2 Simulation

The parameters required for the simulation was mostly similar to the single-phase consolidation problem. The initial conditions were changed to demonstrate the implementation for a two phase problem. The parameters used were as listed in Table 13.1.

13.3 Results and Comparison

There is no analytical solution available for this problem and hence the results are shown and are discussed with the physical understanding of the problem.

The variation in pressure, temperature and saturation is seen in Figure 13.2, Figure 13.3, and Figure 13.4 at time 10, 1e4 and 1e7 seconds respectively. The displacement plots under different simulation runs are also shown in Figure 13.5.

Table 13.1 Simulation Parameters (Two Phase).

Parameter	Value
Size	2m x 2m x 7m
Mesh	3 x 3 x 49
Young's Modulus, E	5.886e7 Pa
Poisson's ratio, ν	0.4
Permeability, k	7.3e-13 m^2
Avg. Thermal Conductivity, λ	836.8 W/mC
Specific Heat (derived from heat cap.), c	100 J/ kg C
Thermal Expansion Coefficient, α_T	0.31e-6 1/C
Biot-Willis Coefficient, α	1.0
Density of rock, ρ_S	2200 kg /m^3
Density of water, ρ_w	1000 kg/m^3
External Load, F_0	1e4 Pa
Initial reservoir pressure, p_0	1e5 Pa
Initial gas saturation, S_g	0.08
Applied surface temperature, T_S	150 C
Initial reservoir temperature, T_0 (corresponding to given p_0 and S_g)	99.6 C

As is evident, since there is small amount of gas, initially the load is taken by the solid and hence we see the downward displacement corresponding to the load. This displacement can be easily calculated using the simple elasticity calculations and is verified. In the case of a single phase isothermal problem, the load would shift to the liquid and the pressure would increase. But since there is highly compressible gas existing in the reservoir, we should not expect significant rise in pressure. However, this

problem includes heating at the top of the reservoir. This causes vaporization and increased pressure in the heated cells. Due to the relatively low permeability of the reservoir, the drainage is not rapid.

As the pressure increases in the reservoir with increase in temperature, the reservoir expands and we see positive displacement at the surface. As seen from the displacement plots, Figure 13.5, major part of the expansion of the reservoir is due to the increase in pressure and the thermal expansion contributes to a smaller part. In the later times, the reservoir is full of gas and it starts draining through the surface. Thus we can see the pressure dropping rapidly.

Eventually pressure reaches the atmospheric pressure value of 1e5 Pa with temperature of 150C and the column is fully saturated with gas. Due to the drop in pressure the surface falls down and the final displacement of the surface is, as expected, equal to the resultant of the displacements due to the thermal expansion of the column and due to the external load applied.

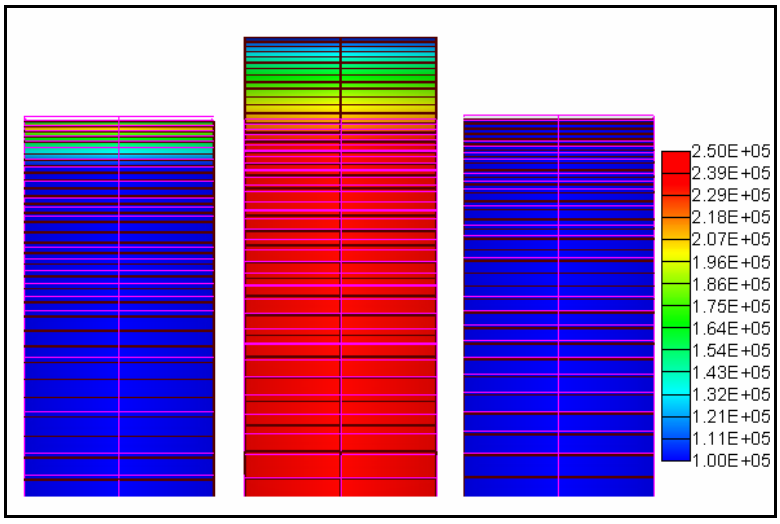

Figure 13.2 Comparison of pressures and deformation of the column (Two Phase).

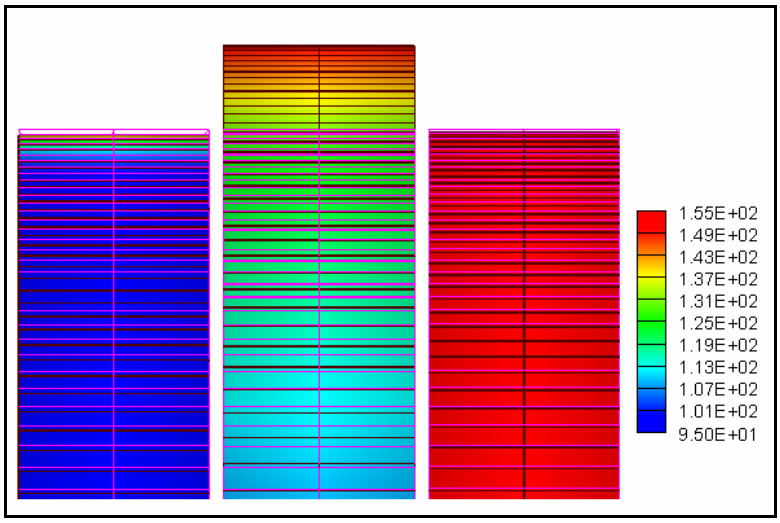

Figure 13.3 Comparison of temperature and deformation of the column (Two Phase).

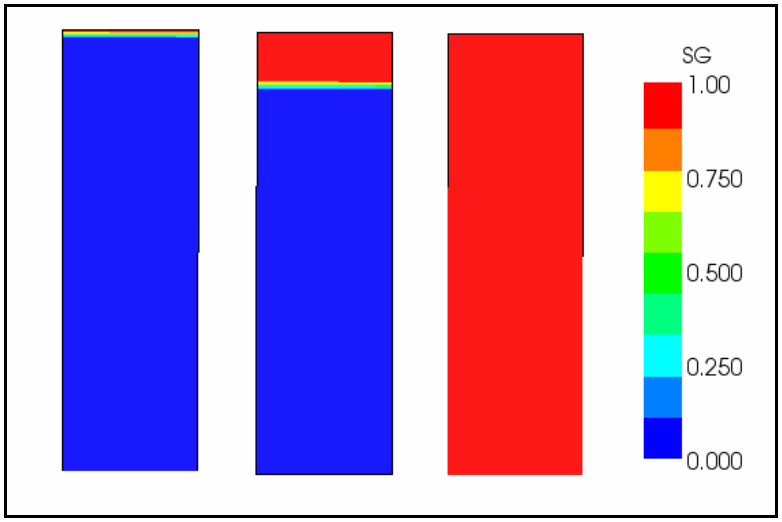

Figure 13.4 Comparison of saturation of gas in the column (Two Phase).

In the displacement plots, Figure 13.5, the simulations other than the complete THM is carried out using one way coupling. This helps to see the individual effects of pressure and temperature on the column.

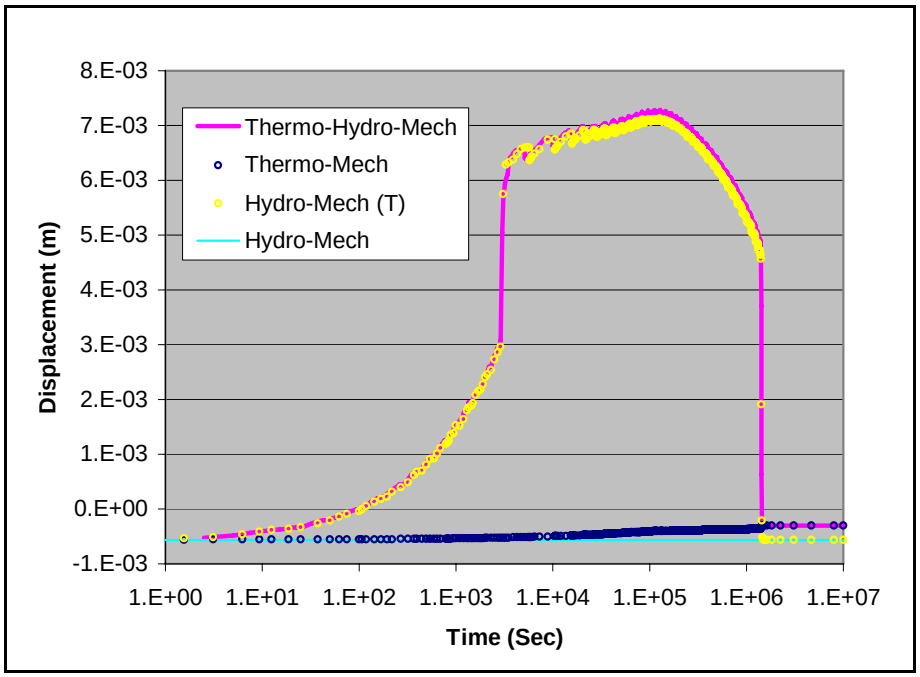

Figure 13.5 Comparison of displacements for analysis of two phase problem.

The "Hydro-Mech" plot indicates the one way coupling simulation under isothermal conditions. Hence it shows the deformation mainly due to the externally applied load only, since there is negligible pressure change in the column as the small quantity of the compressible gas is already present in the column.

The "Thermo-Mech" displacement plot shows the combined effect of the externally applied load and the thermal effects. This was achieved by turning off the poroelastic effects using the respective flag in the T2STR record in the TOUGH2 input file.

The "Hydro-Mech (T)" indicates the simulation, where in, TOUGH2 run was done using non-isothermal conditions, thus capturing the pressure variation due to the phase changes and increase in pressure due to undrained condition as explained above. But the thermal effects on displacement were neglected by setting the flag in T2STR record of the TOUGH2 input file to zero. Hence in "Hydro-Mech (T)" displacement plot, we see the

final deformation exactly equal to the initial deformation, which is solely due to externally applied load.

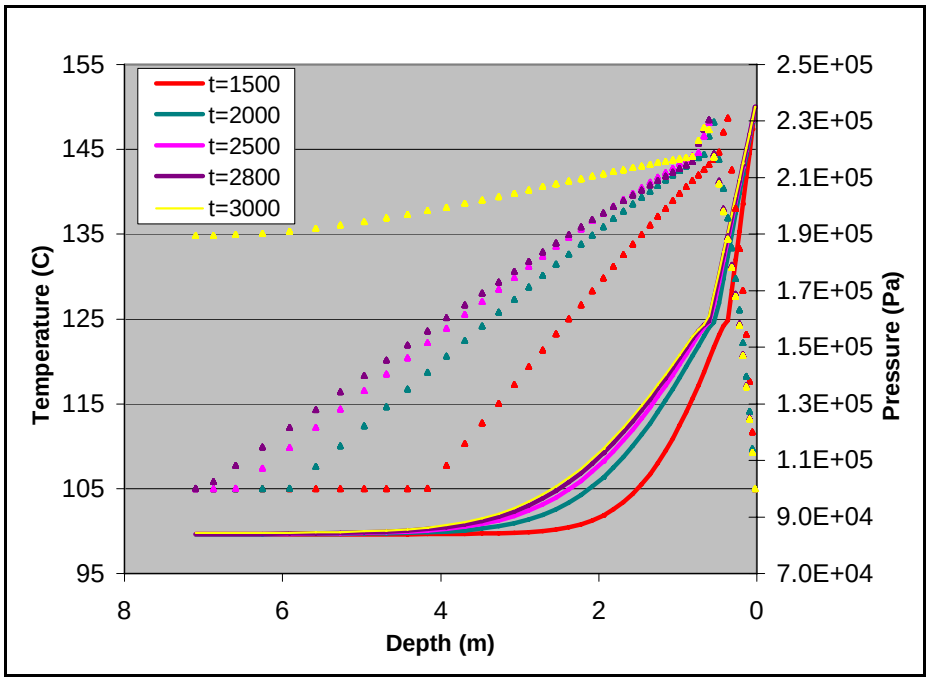

Figure 13.6 Pressure and Temperature comparisons between 1500 to 3000 secs.

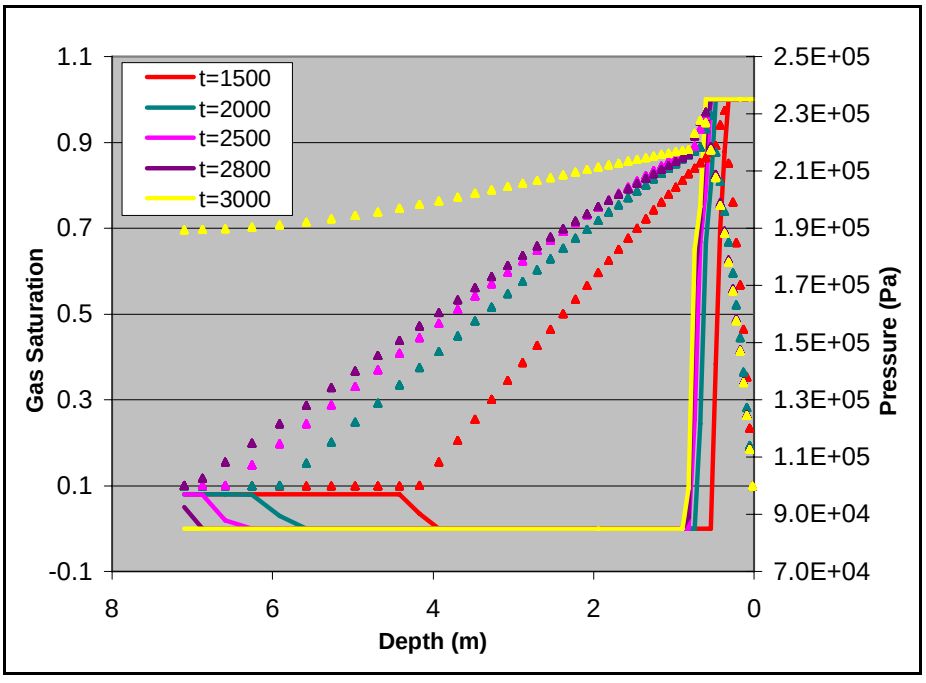

Figure 13.7 Pressure and Gas Saturation comparisons between 1500 to 3000 secs.

In the “THM” simulation, there is a clear jump in the displacements between time 2500 sec to 3000 sec and later at time 1.4e6 seconds. Consider Figure 13.6, Figure 13.7, and Figure 13.8, which show the comparison of pressure, temperature and saturation between different time steps. Note that in Figure 13.8, the saturation legend is between 0.1 and 0.0 and not 1.0 and 0.0.

As the phase change from liquid to gas due to heating from the top of the column happens, the phase change travels from the top of the reservoir to the bottom. Since we have not included gravity in the analysis, presence of gas below the liquid phase can be explained in line with the initial conditions. Also the movement of the fluid phases is controlled by the extent of the heating due to conduction from the top to the bottom in the reservoir. The transitional phase-line, i.e. the depth at which the phase change is occurring at the instance in time, moves down as the heating progresses. As the transitional phase-line moves, the location of the maximum pressure in the column moves with it. The top of the column is fixed at lower pressure and the bottom of the reservoir is at lower pressure due to gaseous phase and absence of gravitational load. With the fluid movement to equilibrate the pressure in the column inducing the increase in pressure in the bottom of the transitional phase-line, the phase change from gas to fluid occurs. Due to phase change then, there is sudden change in the pressure resulting in the sudden jump in displacement.

In the later part of the simulation, due to heating there is complete phase change from liquid to gas, which also is accompanied by the drainage from the top resulting in sudden pressure drop inducing the compaction of the column.

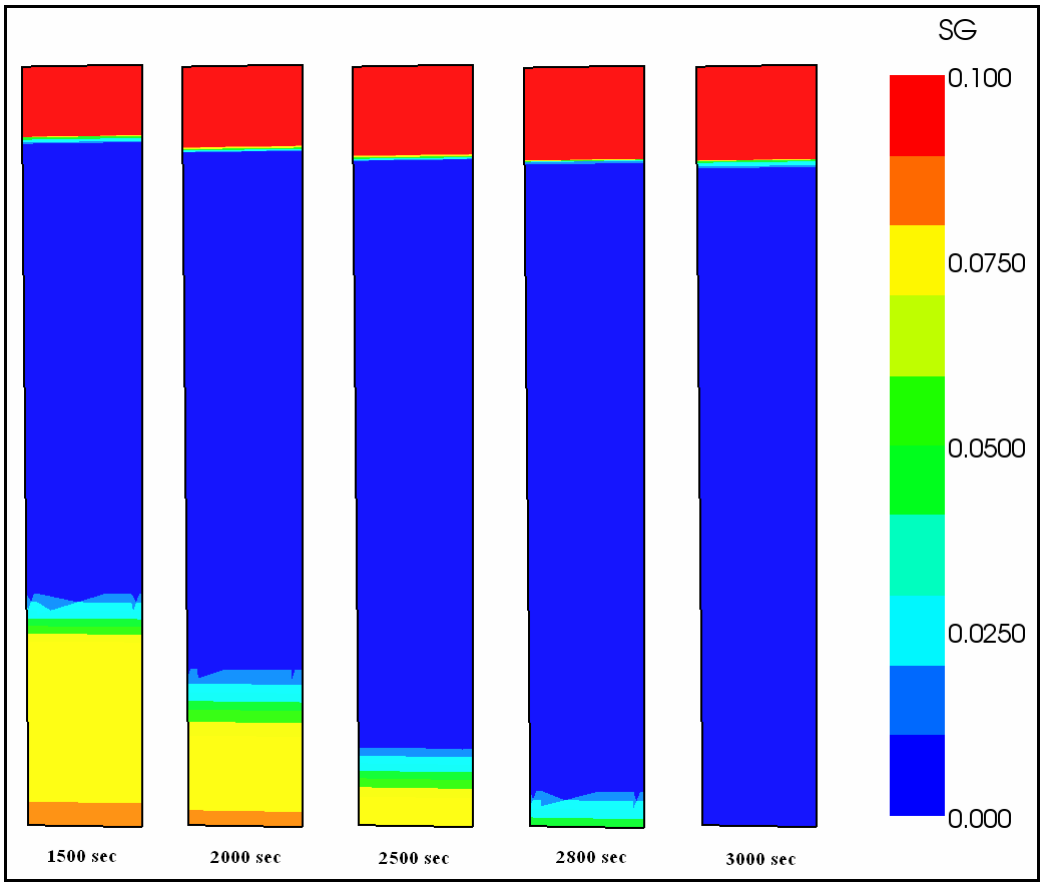

Figure 13.8 Saturation comparison between 1500 and 3000 seconds.

The simulation results are consistent with the physical understanding of the problem and show the ability of T2STR code to simulate two-phase problems. It also shows how the different options of the code allow us to gain deeper understanding into the physical phenomena and study the individual effects into the coupled process.

14 VERIFICATION PROBLEM 6 (FRACTURE BEHAVIOR)

To verify the fracture element implementation two different problems were solved testing the two aspects, pressure forces and contact stresses, of the fracture behavior.

14.1 Verification Problem A (Contact Stresses)

This problem verifies the correct implementation of the effects of contact stresses in the fracture behavior. The pressure forces between the rock and the fracture are in equilibrium. The insitu stresses are set to zero. The initial aperture of the fracture is induces contact stresses according to Gangi's model and are responsible for the deformation which will establish equilibrium condition.

14.1.1 Simulation

A 2 x 2 x 4 TOUGH2 mesh was used to generate a three element (1m x 1m x 1m) finite element model as shown in Figure 5.1. In TOUGH2, the inner two layers in Z-direction represent the fracture, constituting the center (finite) element as the element with fracture behavior. The problem parameters are listed in Table 14.1. The displacement obtained from the simulation is 5.5398e-6 m.

14.1.2 Analytical Solution

The analytical solution is obtained by solving the problem shown in the schematic in Figure 14.1. Due to the symmetry, as seen in Figure 14.1 (a), we can solve the problem in Figure 14.1 (b) with the aperture modified using twice the displacement of the node.

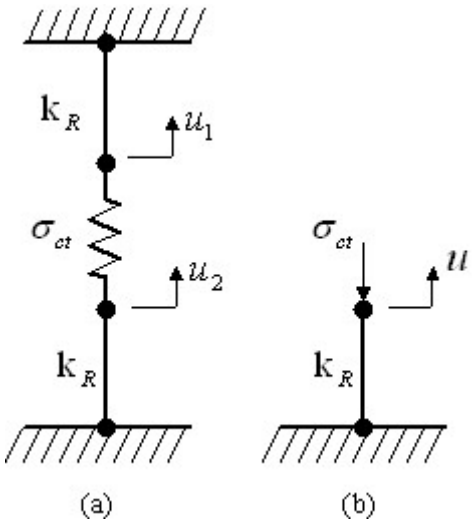

Figure 14.1 Schematic representation to obtain analytical solution.

Table 14.1 Simulation Parameters (Fracture).

Parameter	**Value**
Young's Modulus, E	8.512e10 Pa
Poisson's ratio, ν	0.0
Fracture- Initial Aperture, a_i	8.62e-5 m
Fracture- Zero Stress Aperture, a_0	1.85e-4 m
Fracture- Closing contact stress, σ_c	5e7 Pa
Fracture- Gangi's model index, m	0.16

Writing the force balance, we get

$$
\begin{aligned}
&-\mathrm{k}_R\, u + \sigma_{ct}(u).A = 0 \\
&-\mathrm{k}_R\, u + \sigma_c \left[1 - \frac{a_i + 2u}{a_0}\right]^{\frac{1}{m}}.A = 0
\end{aligned}
\tag{14.1}
$$

Considering the problem parameters i.e. zero Poisson's ratio, the non-linear equation to be solved for the displacement becomes

$$-\left(\frac{AE}{L}\right)u+\sigma_c\left[1-\frac{a_i+2u}{a_0}\right]^{\frac{1}{m}}.A=0 \qquad (14.2)$$

Solving the non-linear equation in MATLAB using "fsolve", we obtain the displacement to be 5.5398e-6 m.

The results match exactly and hence the contact stress implementation is verified.

14.2 Verification Problem B (Pressure Forces)

The same problem is solved without any contact stresses and adding source to the fracture element in TOUGH2.

The pressure in the fracture element increases exerting the force on the rock elements. The pressure variation in the rock element is linear due to the linear volume element, varying between initial pressure in the rock and the increased pressure in the fracture. Thus the pressure difference exerting the force on the rock is equivalent to half of the actual pressure rise in the fracture element. The simulated results and analytical calculations give the exact same result of 1.0468e-5 m for the displacement of the fracture walls or the rock elements. This verifies the pressure force implementation.

It can be seen from both the verification problems that the fracture behavior implementation is correct and is verified.

14.3 Demonstration examples

Two problems demonstrating the fracture implementation are described here.

The first problem is an axisymmetric 3D problem with a single planar fracture. Cold water is injected into the fracture and the thermal effects on the fracture aperture are

emphasized. The fracture opening is shown in the Figure 14.2 in middle of the simulation run.

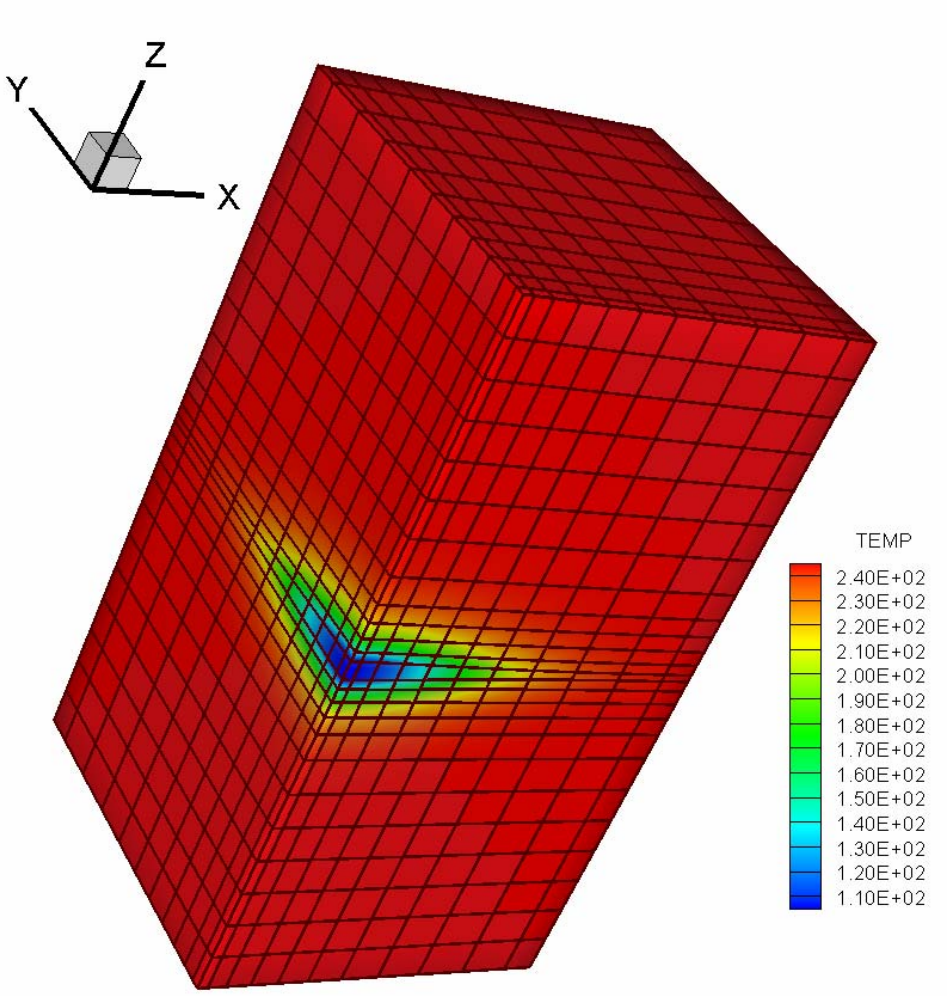

Figure 14.2 3D fracture implementation demonstration problem with planar fracture.

The second problem demonstrates the ability to handle multiple fracture networks. A set of fractures in both directions are introduced in the domain for this 2D problem. Cold water is injected and the effect of thermal stresses on the aperture and flow is visualized. The multiple material assignments are shown in Figure 14.3. The deformed meshes with thermal contours at different times are also shown in Figure 14.4.

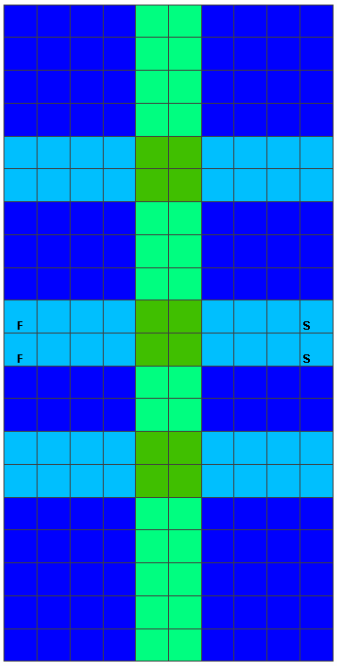

Figure 14.3 Material assignment for multiple fracture problem.

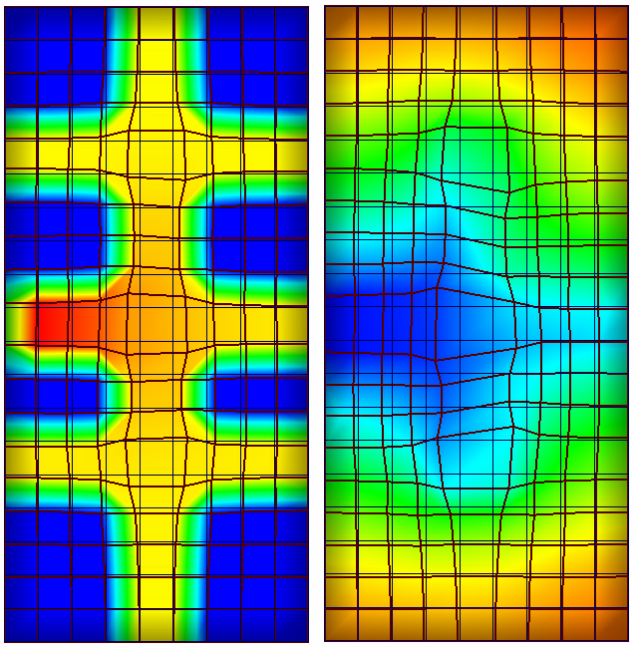

Figure 14.4 Deformed mesh with pressure contours at 10secs and temperature contours at 5e5 secs.

15 DEMONSTRATION PROBLEM 2 (5 SPOT EXAMPLE – ONE WAY)

The following problem considers a large field with wells arranged in a "five-spot" geometric pattern as shown in Figure 15.1. This is an example problem 4 in TOUGH2 user's manual (Pruess et al., 1999). Only half of the domain is modeled due to symmetry.

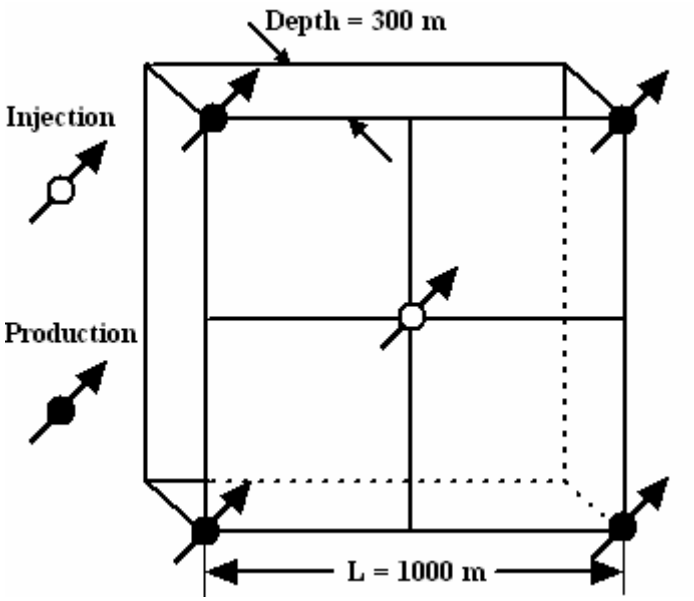

Figure 15.1 Five-spot geothermal well pattern model.

The problem is solved using one way coupling and only porous media assumption. The boundary conditions for the displacement problem are roller support on all the sides and bottom of the reservoir, and the top surface is free.

15.1 Simulation

A 21 x 11 x 6 TOUGH2 mesh was used to generate a finite element model for the five-spot problem. The problem parameters are listed in Table 15.1. The simulation was carried in two stages. Initially, a steady state run was carried out to obtain the equilibrium condition and then a transient run to model the five-spot problem.

Table 15.1 Simulation Parameters (Five-Spot Example).

Parameter	Value
Young's Modulus, E	1.44e10 Pa
Poisson's ratio, ν	0.2
Permeability, k	6.0e-15 m^2
Thermal Conductivity, λ	2.1 W/m C
Specific Heat, c	1000 J/ kg C
Thermal Expansion Coefficient, α_T	7.5e-7 1/C
Biot-Willis Coefficient, α	1.0
Density of rock, ρ_S	2650 kg /m^3
Initial reservoir temperature, p_0	300 C
Initial gas saturation, S_g	0.01
Injection rate (full well basis)	30 kg/s
Injection enthalpy	500 kJ/ kg
Production rate (full well basis)	30 kg/s

15.2 Results and conclusion

During this initial run, the liquid phase in the reservoir settles down due to gravity as seen in Figure 15.2 and hence the pressure will increase in the lower part of the reservoir. Due to this pressure increase the reservoir expands as shown in Figure 15.3.

Then the transient one way simulation is carried out with the injection and production rates as specified in the parameter table.

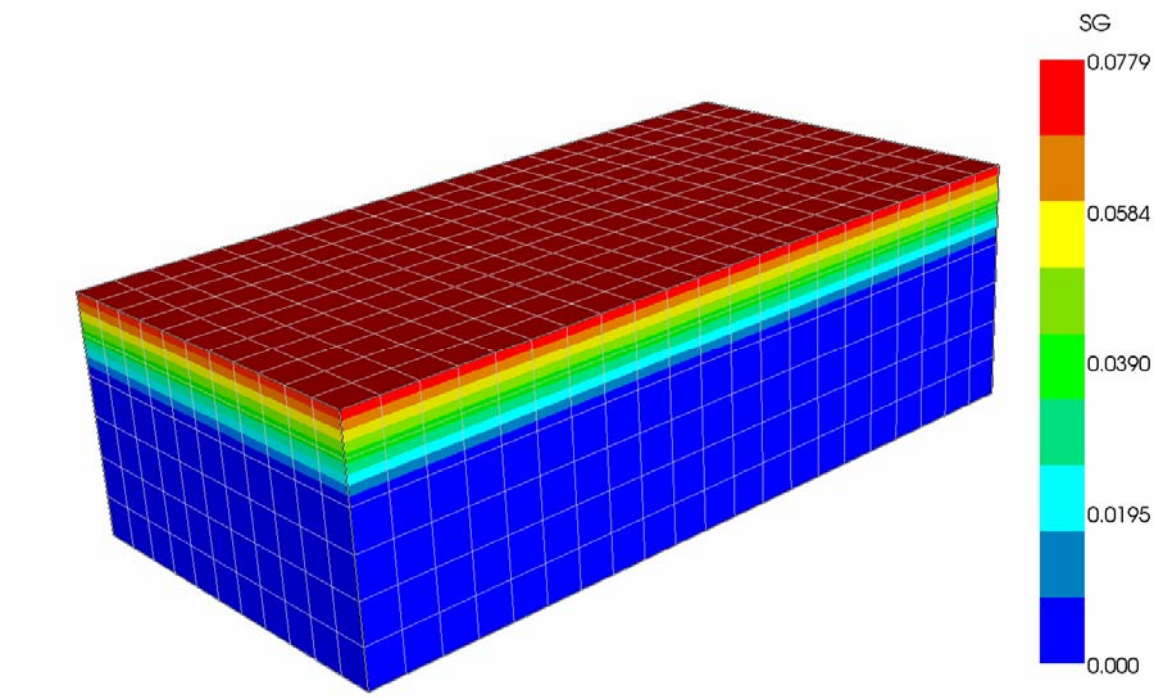

Figure 15.2 Gas phase saturation at the end of steady state simulation run.

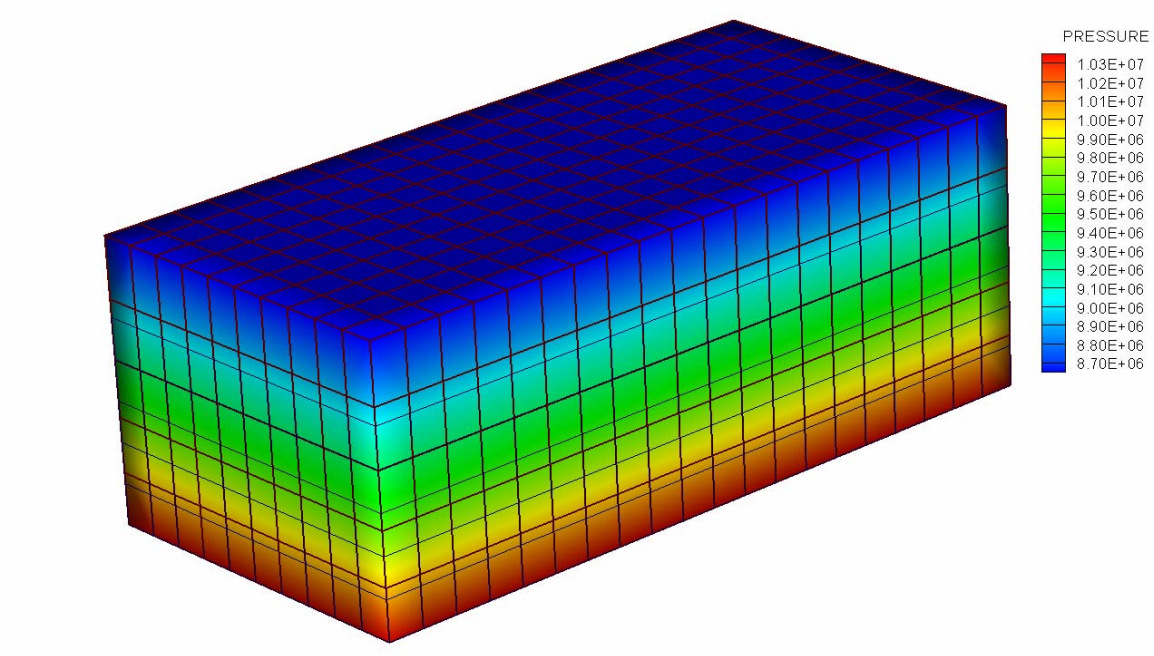

Figure 15.3 Pressure and deformation at equilibrium condition.

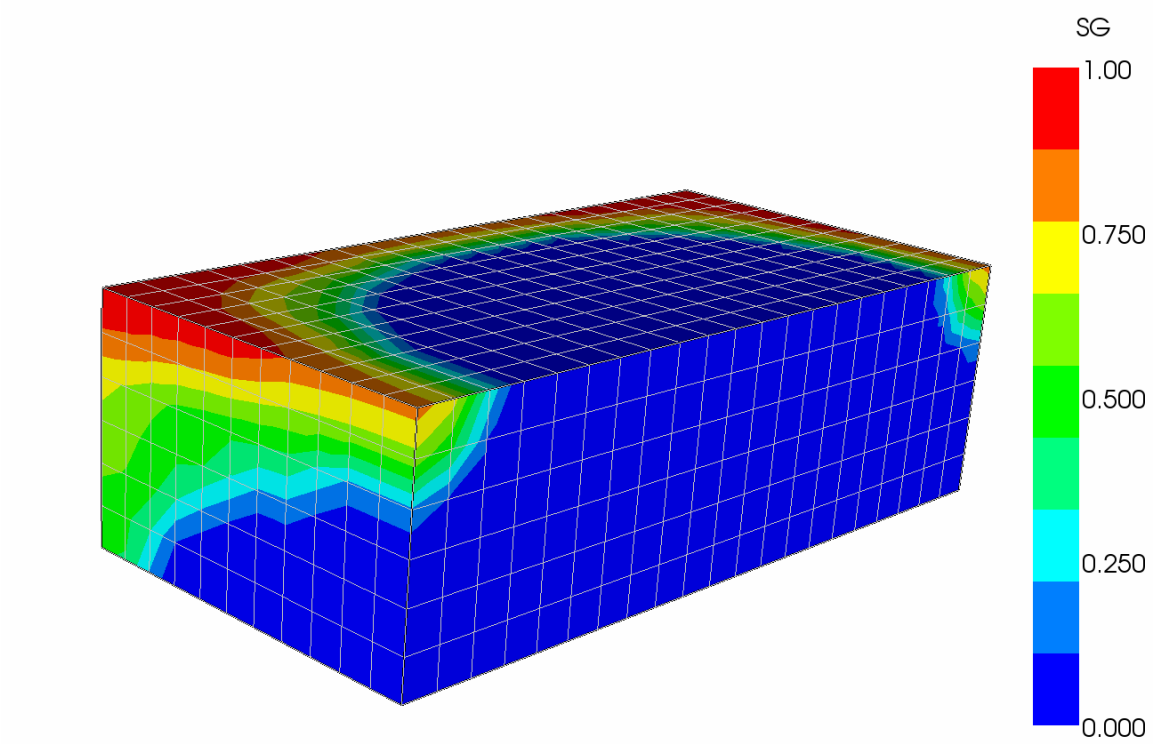

Figure 15.4 Gas phase saturation at the end of 36.5 years.

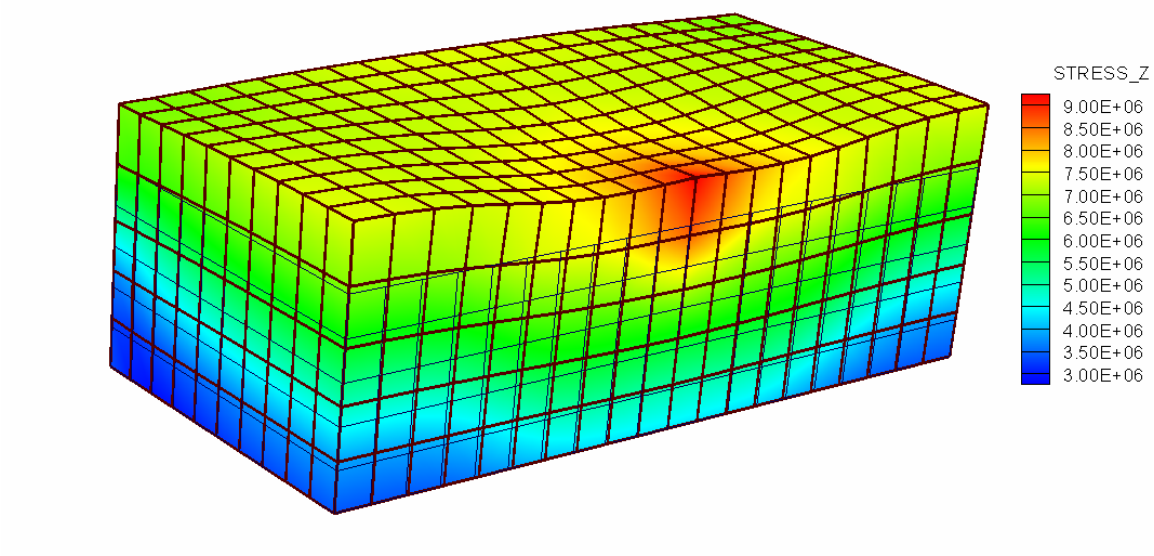

Figure 15.5 Stress in Z direction and deformation of the reservoir after 36.5 years.

The injection is done at lower temperature than the reservoir temperature. The profiles of gas phase saturations and stresses in Z direction at the end of 36.5 years are shown in

Figure 15.4 and Figure 15.5 respectively. Due to cooling, the rock near the injection well contracts and a trench like formation is seen in the cooled region. But near the injection well there is an expansion due to increase pressure due to injection. Also, we can see the increased gas phase saturation near the production well areas due to the lowered pressure due to production.

The simulation shows the ability of T2STR to model field case problems. It also shows the restart capability of T2STR allowing the user to obtain the equilibrium condition and then carry out the transient simulation. This also would enable user to carry out the history matching simulation and use the end result for a predictive model.

16 CONCLUSIONS AND RECOMMENDATIONS

This work developed a fully coupled geomechanics and fluid flow simulator, T2STR, for multiphase flow in porous media combining two different discretization techniques viz. finite element method to solve the momentum equation and integrated finite difference method (IFDM) to solve the mass balance and energy balance equations. The simulator is also capable of simulating the coupled THM processes in fractured porous media in a staggered manner.

16.1 Summary and Conclusions

- A general set of fully coupled equations is derived for multiphase, multi-component fluid flow, heat transfer and deformation in porous media.
- A novel, simple but effective approach is developed to combine any cell based method and node based method. A cell based representation for volumetric strain, "the volumetric strain is approximated as summation of displacements of confining areas", is proposed and used effectively to communicate with the node based method.
- A generalized formulation is obtained to tackle the switching variable implementation used in multiphase flow analysis for the finite element code. A set of phase coefficient matrices is defined which automatically compensate for switching of variables to evaluate accurate Jacobian matrices in either condition.
- A discrete fracture behavior is implemented to model fractures using a re-derived fracture joint model exhibiting the fluid pressure and contact stress effects. Hence, T2STR can simulate discrete fracture networks (DFN) in the reservoir model.

- The fractured porous media formulation is implemented using staggered approach in which the flow simulator calculations are finished and the results are used for the deformation calculations. The effect of deformation on fluid flow is then implemented through varying permeability and porosity as function of deformation.
- Several options are made available in T2STR for user to study one way, staggered or fully coupled approach. Also, T2STR is capable to switch on/off the thermal or poroelastic effects. This provides ability to study individual effects and gain deeper understanding into the physics of the problem.
- A set of verification problems is used to validate the code. The data is provided with the results to allow exact duplication of the problems.
- The T2STR is limited to EOS1 module of TOUGH2 i.e. only water components can be modeled.

16.2 Recommendations

- Extend the current work to other EOS modules in TOUGH2.
- Extend the model for Brick20 volume element to be consistent with fluid flow model.
- Implement a fully coupled THM model for fractured porous media.
- Study the convergence and stability issues related to the geomechanics problem in comparison to other fully coupled approaches as well as in comparison to one way and iteratively coupled approaches.
- Realistic field scale problems should be used to test the stability and full capability of T2STR code.

REFERENCES

1. Aboustit, B.L., Advani, S.H., Lee, J.K., 1985, "Variational principles and finite element simulations for thermoelastic consolidation", Int. J. for Numerical and Analytical Methods in Geomechanics, Vol. 9, pp. 49-69.

2. Aboustit, B.L., Advani, S.H., Lee, J.K., and Sidhu, R.S., 1982, "Finite element evaluations of thermoelastic consolidation", Issues on Rock Mechanics, 23rd Symposium on Rock Mechanics, ASME, University of California-Berkley, pp. 587-595.

3. Amadei, B., Goodman, R.E., 1981, A 3D constitutive relation for fractured rock masses, Proceedings of International Symposium on Mechanical Behavior of Structured Media, Ottawa, pp. 249-268.

4. Avatsmark A., Barkve. T., Boe, O., and Mannseth, T., 1998a, "Discretization on Unstructured Grids for Inhomogeneous, Anisotropic Media. Part I: Derivation of the Methods", *SIAM J Sci Comput.*, Vol. 19(5), pp. 1700-1736.

5. Bathe, Klaus-Jurgen, 1997, "Finite Element Procedures", Prentice Hall, ISBN 81-203-1075-6.

6. Bear, J., 1972, "Dynamics of Fluids in Porous Media", American Elsevier, New York, ISBN 0-486-65675-6.

7. Bear, J., Buchlin, J-M., 1991, "Modelling and Applications of Transport Phenomena in Porous Media", Vol. 5, Kluwer Academic Publishers, The Netherlands, ISBN 0-7923-1443-3.

8. Bear, J., and Corapcioglu, M.Y., 1982, "Fundamentals of Transport Phenomena in Porous Media", Proceedings of NATO Advanced Study Institute on Mechanics of Fluids in Porous Media, Newark, Delaware, 18-27 July, ISBN 90-247-2982-3

9. Bear, J., Bachmat, Y., 1991, "Introduction to modeling of transport phenomena in porous media", Kluwer Academic Pub., The Netherlands, ISBN 0-792-30557-4.

10. Bemer, E., Bouteca, M., Vincke, O., Hoteit, N., and Ozanam, O., 2001, "Poromechanics: From Linear to Nonlinear Poroelasticity and Poroviscoelasticity", *Oil & Gas Science and Technology- Rev. IFP*, Vol. 56(6), pp. 531-544.

11. Berryman, J.G., 1992, "Exact effective-stress rules in rock mechanics", *Physical Review A*, Vol. 46 (6), pp. 3307-3311.

12. Biot MA., 1941, "General theory of three dimensional consolidation", *J Appl. Phys.*, Vol. 12, pp. 155-164.

13. Bird, R.B., Stewart, W.E., Lightfoot, E.N., 2002, "Transport Phenomena", John Wiley & Sons, New York, ISBN 9-971-51420-6.

14. Bodvarsson, G.S., Birkholzer, J.T., Finsterle, S., Liu, H.H., Rutqvist, J., and Wu, Y.S., 2003, "The Use of TOUGH2/iTOUGH2 in Support of the Yucca Mountain Project: Successes and Limitations", TOUGH2 Symposium LBNL, Berkley, California, May 12-14.

15. Bogdanov, I.I., Mourzenko, V.V., Thovert, J-F., Adler, P.M., 2003, "Two-phase flow through fractured porous media", Physical Review E, Vol. 68.

16. Boley, B.A., Weiner, J.H., 1997, "Theory of Thermal Stresses", Dover Publications, ISBN 0-486-69579-4.

17. Borgesson, L., 1996, “ABAQUS”, In: Stephansson, O., Jing, L., Tsang, C-F, editors, *Coupled Thermo-hydro-mechanical processes of fractured media*, Elsevier: Developments in Geotechnical Engineering, Vol. 79, pp. 565-570.

18. Bouteca, M., and Gueguen, Y., 1999, “Mechanical Properties of Rocks: Pore Pressure and Scale Effects”, *Oil & Gas Science and Technology- Rev. IFP*, Vol. 54(6), pp. 703-714.

19. Carroll, M.M., 1979, “An Effective Stress Law for Anisotropic Elastic Deformation”, *Journal of Geophysical Research*, Vol. 84, pp. 7510-7512.

20. Chen Q., Kinzelbach W., Ye C.,Yue Y., 2002, “Variations of Permeability and Pore Size Distribution of Porous Media with Pressure”, *J.Environ.Qual.*, Vol. 31, pp. 500-505.

21. Chen Z., Qin G., Ewing R., 2000, “Analysis of a Compositional Model for Fluid Flow in Porous Media”, *Society for Industrial and Applied Mathematics,* Vol. 60(3), pp. 747-777.

22. Chen, H.Y. and Teufel, L.W., 1997, "Coupling Fluid-Flow and geomechanics in dual-porosity modeling of naturally fractured reservoirs", paper SPE 38884 presented at the SPE Annual Technical Conference and Exhibition held in San Antonio, Texas, 5-8 October.

23. Chin, L.Y., Thomas, L.K., Sylte, J.E., Pierson, R.G., 2002, “Iterative Coupled Analysis of Geomechanics and Fluid Flow for Rock Compaction in Reservoir Simulation”, *Oil & Gas Science and Technology*, Vol. 57 (5), pp. 485-497.

24. Christian, J.T., 1977, “Two- and three-dimensional consolidation”, In: C.S. Desai and J.T. Christian, eds., Numerical Methods in Geotechnical Engineering, McGraw-Hill, San Francisco, CA, pp. 399-426.

25. Corapcioglu, M.Y. and Bear, J., 1982, “Land Subsidence”, In: Bear,J., Corapcioglu, M.Y. , editors. Fundamentals of Transport Phenomena in Porous Media. NATO Advanced Study Institute on Mechanics of Fluid in Porous Media, Newark, July 18-27.

26. Cosmi, F., Di Marino, F., 2000, “A New Approach to Sintered Alloys Mechanical Behaviour Modeling”, *Proc. Of 17*th *Danubia Adria Symposium on Experimental Methods in Solid Mechanics,* Prague, Czech Republic.

27. Coussy, O., 2004, “Poromechanics”, John Wiley & Sons Inc., ISBN 0-470-84920-7.

28. Daim, F., Eymard, R., Hilhorst D., Mainguy M., Masson R., 2002, “A Preconditioned Conjugate Gradient Based Algorithm for Coupling Geomechanical-Reservoir Simulations”, *Oil & Gas Science and Technology- Rev. IFP,* Vol. 57(5), pp. 515-523.

29. Davies, J.P., Davies, D.K., 1999, “Stress-Dependent Permeability: Characterization and Modeling”, *Society of Petroleum Engineers*, SPE 56813.

30. De Vries, D.A., 1987, “The theory of heat and moisture transfer in porous media revisited”, *Int. J. Heat Mass Transfer*, Vol. 30(7), pp.1343-1350.

31. Dean, R.H., Gai, X., Stone, C.M., and Minkoff, S.E., 2003, “A Comparison of Techniques for Coupling Porous Flow and Geomechanics”, paper SPE 79709 presented at the SPE Reservoir Simulation Symposium held in Houston, Taxes, Feb. 3-5.

32. Detournay, E., and Cheng, A.H.D., 1993, "Fundamental of poroelasticity", Chapter 5 in Comprehensive Rock Engineering: Principles, Practice and Projects, (2), Analysis and Design Methods, ed. C. Fairhurst, Pergamon Press, pp. 113-171.

33. Diersch, H.-J.G., Kolditz, O., 2002, "Variable-density Flow and Transport in Porous Media: Approach and Challenges", *Advances in Water Resources*, Vol. 25, pp. 899-944.

34. Durlofsky, L.J., 1994, "Accuracy of mixed and control volume finite element approximations to Darcy velocity and related quantities", *Water Resources Research*, Vol. 30, pp. 965-973.

35. Eymard, R., and Sonier, F., 1994, "Mathematical and Numerical Properties of Control-Volume, Finite-Element Scheme for Reservoir Simulation", *SPE Reservoir Engineering*, pp. 283-289, November.

36. Faust, C.R., and Mercer, J.W., 1979, "Geothermal Reservoir Simulation 1. Mathematical Models for Liquid- and Vapor-Dominated Hydrothermal Systems", *Water Resources Research*, Vol. 15(1), pp. 23-30.

37. Garg, S.K., and Pritchett, J.W., 1977, "On Pressure-Work, Viscous Dissipation and the Energy Balance Relation for Geothermal Reservoirs", *Advances in Water Resources*, Vol.1(1),pp.41-47.

38. Gatmiri, B., Delage, P., 1997, "A formulation of fully coupled thermal-hydraulic-mechanical behaviour of saturated porous media- Numerical Approach", Int. J. for Numerical and Anlytical methods in Geomechanics, Vol. 21, pp. 199-255.

39. Geertsma, J., 1957, "The effect of fluid pressure decline on volumetric changes of porous rocks", *Trans. AIME*, Vol. 210, pp. 331-340.

40. Geiger, S., Roberts, S., Matthai, S.K., and Zoppou, C., 2003. "Combining finite volume and finite element methods to simulate fluid flow in geologic media", *Australian and New Zealand Industrial and Applied Mathematics Journal*, Vol. 44, pp. C180-C201.

41. Ghabbousi, J. and Wilson, E.L., 1973, "Flow of compressible fluid in porous elastic media*", I.J. of Num. Meth. Eng.*, Vol. 5, pp. 419-442.

42. Goodman, R.E., 1976, "Methods of geological engineering", West Publishing Co.

43. Gosavi, S., Swenson, D., 2005, "Architecture for a coupled code for Multiphase fluid flow, heat transfer, and deformation in porous rock", Proceedings of Thirtieth Workshop on Geothermal Reservoir Engineering, Stanford University, Stanford, California.

44. Gosavi, S., Swenson, D., 2006, "Implementation and verification of the fully coupled T-H-M code, T2STR, for multiphase flow in porous media", Proceedings of Thirty-first Workshop on Geothermal Reservoir Engineering, Stanford University, Stanford, California.

45. Gray, W.G., 1982, "Comparison of Finite Difference and Finite Element Methods", In: Bear,J., Corapcioglu, M.Y. , editors. *Fundamentals of Transport Phenomena in Porous Media*. NATO Advanced Study Institute on Mechanics of Fluid in Porous Media, Newark, pp. 899-952, July 18-27.

46. Gresho, P.M., and Sani RL., 1999, “Incompressible flow and the finite element method”, Chichester, J Wiley.

47. Gutierrez, M. and Hansteen, H., 1994, “Fully coupled analysis of reservoir compaction and subsidence”, paper SPE 28900 presented at the European Petroleum Conference held in London, U.K., 25-27 October.

48. Gutierrez, M. and Lewis, R.W., 1998, “The role of geomechanics in reservoir simulation”, paper SPE/ISRM 47392 presented at SPE/ISRM Eurock'98 held in Trondhelm, Norway, 8-10 July.

49. Horne, R. N., 1995, *Modern Well Test Analysis, A Computer-Aided Approach,* Petroway, Inc..

50. Horner, D.R., 1967, “Pressure Build-up in Wells”, Society of Petroleum Engineers of AIME, Petroleum Transactions reprint Series. Vol. (9), pp. 25-43.

51. Hughes, T.J.R., 1987, “The Finite Element Method”, Prentice-Hall Inc., New Jersey, ISBN 0-486-41181-8.

52. Jing L., Hudson, J.A., 2002, “Numerical methods in rock mechanics”, *International Journal of Rock Mechanics & Mining Sciences,* Vol. 39, pp. 409-427.

53. Jonge, J. de, Xie, M., and O. Kolditz., 2003, “Numerical implementation of thermally and hydraulically coupled processes in non-isothermal porous media”, In Stephansson et al., editor, GeoProc.

54. Juanes, R., Patzek, T.W., 2003, “Multiscale Numerical Modeling of Three Phase Flow”, paper SPE 84369 presented at the SPE Annual Technical Conference and Exhibition held in Denver, Colorado, Oct 5-8.

55. Kim, J.G., and Finsterle, S., 2003, "Application of Automatic Differentiation in TOUGH2", *TOUGH2 Symposium*, LBNL, Berkley, California, May 12-14.

56. Kohl, T., Evans, K.F., Hopkirk, Jung R., Rybach L., 1997, "Observation and simulation of non-Darcian flow transients in fractured rock", *Water Resources Research,* Vol. 33(3), pp. 407-418, March.

57. Kohl, T., Evans, K.F., Hopkirk, R.J., Rybach, L., 1995, "Coupled Hydraulic, Thermal, and Mechanical Considerations for the Simulation of Hot Dry Rock Reservoirs", *Geothermics*, Vol. 24(3), pp. 345-359.

58. Kohl, T., Hopkirk, R.J., 1995, "FRACTure- A Simulation Code for Forced Fluid Flow and transport in Fractured, Porous Rock", *Geothermics*, Vol. 24(3), pp. 333-343.

59. Kohlmeier, M., Kaiser, R., Kolditz, O., and Zielke W., 2002, "Finite element simulation of consolidation processes and bentonite swelling in the framework of unsaturated porous media", In Hassanizadeh et al, editor, *Developments in Water Science*, Vol. 1 of XIV International Conference on Computational Methods in Water Resources, Delft , pp. 57-64.

60. Laloui, L., Klubertanz, G., Vulliet, L., 2003, "Solid-liquid-air coupling in multiphase porous media", *Int. J. Numer. Anal. Meth. Geomech.*, Vol. 27, pp. 183-206.

61. Lewis, R. and Schrefler, B., 1987, "The Finite Element Method in the Deformation and Consolidation of Porous Media", John Wiley & Sons, ISBN 0-471-91210-7.

62. Lewis, R.W. and Sukirman, Y., 1993, "Finite Element Modeling of Three-Phase Flow in Deforming Saturated Oil Reservoirs", *Intl. J. for Num. and Anal. Methods in Geomech.*, Vol. 17, pp. 577-598.

63. Lewis, R.W., and Schrefler, B.A., 1998, "The Finite Element Method in the Deformation and Consolidation of Porous Media", John Wiley & Sons, ISBN 0-471-92809-7.

64. Lewis, R.W., Makurat, A., Pao, W.K.S., 2003, "Fully Coupled Modeling of Seabed Subsidence and Reservoir Compaction of North Sea Oil Fields", *Hydrogeology Journal*, Vol. 11, pp. 142-161.

65. Lewis, R.W., Roberts, G.K. and Zienkiewicz, O.C., 1976, "A non-linear flow and deformation analysis of consolidation problems", *Numerical Methods in Geomechanics*, ASCE, New York, Vol. 2, pp. 1106-1118.

66. Mainguy M., Longuemare P., 2002, "Coupling Fluid Flow and Rock Mechanics: Formulations of the Partial Coupling between Reservior and Geomechanical Simulators", *Oil & Gas Science and Technology- Rev. IFP,* Vol. 57(4), pp. 355-367.

67. Masters, I., Pao, W.K.S., and Lewis, R.W., 2003, "Coupling temperature to a double-porosity model of deformable porous media", *Int. J. Numer. Meth. Engng*, Vol. 49, pp. 421-438.

68. Minkoff, S., Stone, C., Bryant, S., and Peszynska, M., 2004, "Coupled Geomechanics and Flow Simulation for Time-lapse Seismic Modeling", *Geophysics*, Vol. 69(1), pp. 200-211.

69. Minkoff, S., Stone, C., Bryant, S., Peszynska, M., and Wheeler, M., 2003, "Coupled fluid flow and geomechanical deformation modeling", *Journal of Petroleum Science and Engineering*, Vol. 38, pp. 37-56.

70. Minkoff, S., Stone, C.M., Arguello, J.G., Bryant, S., Eaton, J., Peszynska, M., Wheeler, M., 1999, "Staggered in Time Coupling of Reservoir Flow Simulation and Geomechanical Deformation: Step 1- One-Way Coupling", paper SPE 51920 in Proceedings of the Reservoir Simulation Symposium, Houston, TX, Feb. 14-17.

71. Moridis G.J., Pruess K., 1998, "T2SOLV: An Enhanced Package of Solvers for the TOUGH2 Family of Reservior Simulation Codes", *Geothermics,* Vol. 27(4), pp. 415-444.

72. Narasimhan, T.N., and Witherspoon, P.A., 1976, "An Integrated Finite Difference Method for Analyzing Fluid Flow in Porous Media", *Water Resources Research*, Vol. 12(1), pp. 57-64.

73. Narasimhan, T.N., and Witherspoon, P.A., 1977, "Numerical Model for Saturated - unsaturated Flow in Deformable Porous Media, 1, Theory", *Water Resources Research*, Vol. 13(3), pp. 657-664.

74. Narasimhan, T.N., Witherspoon, P.A., and Edwards, A.L., 1978, "Numerical Model for Saturated-unsaturated Flow in Deformable Porous Media, 2, The Algorithm", *Water Resources Research*, Vol. 14(2), pp. 255-261.

75. Nguyen, T.S., 1996, "Description of the computer code FRACON", In: Stephansson, O., Jing, L., Tsang, C-F, editors. *Coupled Thermo-hydro-mechanical processes of*

fractured media, Elsevier: Developments in Geotechnical Engineering, Vol. 79, pp. 539-544.

76. Noorishad, J., Tsang, C-F., 1996, "ROCMAS-simulator: a thermo-hydro-mechanical computer code", In: Stephansson, O., Jing, L., Tsang, C-F, editors. *Coupled Thermo-hydro-mechanical processes of fractured media*, Elsevier: Developments in Geotechnical Engineering, Vol. 79, pp. 551-558.

77. Nur, A., and Byerlee, J.D., 1971, "An Exact Effective Stress Law for Elastic Deformation of Rock with Fluids", *Journal of Geophysical Research*, Vol. 76, pp. 6414-6419.

78. Ohnishi, Y., Kobayashi, A., 1996, "THAMES", In: Stephansson, O., Jing, L., Tsang, C-F, editors. *Coupled Thermo-hydro-mechanical processes of fractured media*, Elsevier: Developments in Geotechnical Engineering, Vol. 79, pp. 545-549.

79. Pruess, K., Oldenburg, C., and Moridis, G., 1999, "TOUGH2 User's Guide, Version 2.0", Report LBNL-43134, Lawrence Berkeley National Laboratory, Berkeley, Calif.

80. Pyrah, I.C., 1991, "Elasto-Plastic Analysis in Geotechnical Engineering Using Finite Differences", Computational Plasticity: Models, Software and Applications, edited by D.R.J. Owen, E. Hinton, and E. Onate, Elsevier, pp. 1607-1620.

81. Rice, J.R., and Cleary, M.P., 1976, "Some Basic Stress Diffusion Solutions for Fluid-Saturated Elastic Porous Media with Compressible Constituents", *Reviews of Geophysics and Space Physics*, Vol. 14 (2), pp. 227-241.

82. Rutqvist, J., Borgesson, L., Chijimatsu, M., Nguyen, TS., Jing, L., Noorishad, J., Tsang, C-F, 2001a, "Thermohydromechanics of partially saturated geological media:

governing equations and formulation of four finite element models", *I.J. of Rock Mechanics and Mining Sciences,* Vol. 38, pp. 105-127.

83. Rutqvist, J., Borgesson, L., Chijimatsu, M., Nguyen, TS., Jing, L., Noorishad, J., Tsang, C-F., 2001b, "Coupled thermo-hydro-mechanical analysis of a heater test in a fractured rock and bentonite at Kamashi – comparison of field results to predictions of four finite element codes", *Int J Rock Mech Min Sci*, Vol. 38, pp. 129-142.

84. Rutqvist, J., Stephansson, O., 2003a, " The role of hydromechanical coupling in fractures rock engineering", *Hydrogeology Journal*, Vol. 11(1), pp. 7-40.

85. Rutqvist, J., Tsang, C-F., 2003b, "TOUGH-FLAC: A Numerical Simulator for Analysis of Coupled Thermal-Hydrologic-Mechanical Processes in Fractured and Porous Geological Media Under Multi-phase Flow Conditions", *TOUGH2 Symposium*, LBNL, Berkley, California, May 12-14.

86. Rutqvist, J., Wu, Y-S. , Tsang C-F. , and Bodvarsson, G., 2002, "A modeling approach for analysis of coupled multiphase fluid flow, heat transfer, and deformation in fractured porous rock", *I.J. of Rock Mechanics and Mining Sciences,* Vol. 39, pp. 429-442.

87. Sandhu, R.S. and Wilson, E.L., 1995, "Finite Element Analysis of flow in saturated porous media", *J. Eng. Mech. Div.*, ASCE, (EM3), pp. 641-652.

88. Scheidegger, A.E., 1960, "The Physics of Flow Through Porous Media", University of Toronto Press.

89. Settari, A. and Mourits, F.M., 1998, "A coupled reservoir and geomechanical modeling system", *SPE J.*, pp.219-226, September.

90. Settari, A. and Walters, D.A., 1999, "Advances in coupled geomechanical and reservoir modeling with applications to reservoir compaction", paper SPE 51927 presented at the 1999 SPE Reservoir Simulation Symposium held in Houston, Texas, February 14-17.

91. Sheng, D., and Sloan, S.W., 2003, "Time stepping schemes for coupled displacement and pore pressure analysis", Computational Mechanics, Vol. 31, pp. 122-134.

92. Small. J.C., Booker, J.R., and Davis, E.H., 1976, "Elastoplastic Consolidation of Soil", *I.J. Solids and Struct,* Vol. 12, pp. 431-448.

93. Stephansson, O., Jing, L., Tsang, C.F., 1996, "Coupled Thermo-Hydro-Mechanical Processes of Fractured Media", Elsevier, Amsterdam.

94. Stone, T., Bowen, G., Papanastasiou, P. and Fuller, J., 2000, "Fully coupled Geomechanics in a commercial reservoir simulator", paper SPE 65107 presented at the 2000 SPE European petroleum conference held in Paris, France, 24-25 October.

95. Swenson, D., 2001, "Well Test Analysis: Comparison of Fracture and Porous Models", Report prepared for GERD Co. Ltd., Japan.

96. Swenson, D., Gosavi, S., Hardman, B., 2004, "Integration of Stress Analysis in TOUGH2", Proceedings of Twenty-Ninth Workshop on Geothermal Reservoir Engineering, Stanford University, Stanford, California.

97. Terzaghi, K., 1943, "Theoretical Soil Mechanics", Wiley, New York.

98. Terzaghi, K., Peck, R.B., Mesri, G., 1996, "Soil Mechanics in Engineering Practice", John Wiley & Sons, Inc., ISBN 0-471-08658-4.

99. Thompson, M., Willis, J.R., 1991, "A Reformation of the Equations of Anisotropic Poroelasticity", *Transactions of the ASME*, Vol. 58, pp. 612-616.

100. Timoshenko, S. and Goodier, J.N., 1969, "Theory of Elasticity" (3rd ed.), McGraw-Hill, New York.

101. Todesco, M., Rutqvist, J., Chiodini, G., Pruess, K., Oldenburg, C.M., 2003, "Modeling of Recent Volcanic Episodes at Phlegrean Fields (Italy): Geomechanical Variations and Ground Deformation", *TOUGH2 Symposium* LBNL, Berkley, California, 12-14 May.

102. Tonti, Enzo, 2001, "A Direct Discrete Formulation of Field Laws: The Cell Method", *Computer Modeling in Engineering & Sciences*, Vol. 2(2).

103. Tsang, C-F., 1999, "Linking thermal, hydrological, and mechanical processes in fractured rocks", *Annu Rev Earth Planet Sci,* Vol. 27, pp. 359-384.

104. Verma, S., and Aziz, K, 1997, "A control volume scheme for flexible grids in reservoir simulation", paper SPE 37999 in Proc. SPE Reservoir Simulation Symposium held at Dallas, Texas, 8-11 June.

105. Wan, J., 2002, "Stabilized Finite Element Methods for Coupled Geomechanics and Multiphase Flow", Ph.D. Thesis, Stanford University.

106. Wang, H., 1993, "Quasi-static Poroelastic Parameters in Rock and Their Geophysical Applications", *Pure Appl. Geophys.*, Vol 141, 269-286.

107. Wang, H., 2000, "Theory of Linear Poroelasticity with Applications to Geomechanics and Hydrogeology", Princeton University Press, ISBN 0-691-03746-9.

APPENDIX A MATERIAL DERIVATIVE

The material derivative of a variable G with respect to a particle is the (temporal) rate of change of that variable for the considered particle. It is denoted and expressed as (Bear and Bachmat, 1991)

$$\frac{DG}{Dt} = \left.\frac{\partial G(\xi, t)}{\partial t}\right|_{\xi=const}$$

where ξ is the initial position vector. Is also can be interpreted as the rate of change of variable G of a fixed particle to an observer situated on that particle. It can be expressed in terms of the spatial or Eulerian description as follows

$$\begin{aligned}\frac{DG}{Dt} &= \frac{\partial G}{\partial t} + \frac{\partial G}{\partial x_k} v_k \\ &= \frac{\partial G}{\partial t} + \mathbf{v} \bullet \nabla G\end{aligned}$$

where v denotes the instantaneous velocity of the particle at the given point. The first term represents the local rate of change of G at the specified point and second term represents the convective rate of change of the quantity G. The convective rate of change is due to the variation of G along the path of the particle.

APPENDIX B SOLID VELOCITY AND VOLUMETRIC STRAIN

Consider the Lagrangian derivative of the volume of a differential element as follows

$$\begin{aligned}\left(\dot{dV}\right) &= \left(dx\dot{dy}dz\right) \\ &= \dot{dx}\,dydz + \dot{dy}\,dxdz + \dot{dz}\,dxdy\end{aligned}$$

As the volume dV is being displaced and deformed, the material derivative of the length dx_i is related to the velocities at the end points $x_i + dx_i$ and x_i, by

$$\begin{aligned}\left(\dot{dx_i}\right) &= \left(x_i + \dot{dx_i}\right) - \left(\dot{x_i}\right) \\ &= \mathbf{v}_{Si}\big|_{x_i+dx_i} - \mathbf{v}_{Si}\big|_{x_i}\end{aligned}$$

Hence, for $i = 1,2,3$, we can write

$$\left(\dot{dx_i}\right) = \frac{\partial \mathbf{v}_{Si}}{\partial x_i}\,dx_i$$

Substituting in the expression for the $\left(\dot{dV}\right)$,

$$\left(\dot{dV}\right) = \frac{\partial \mathbf{v}_{Sx}}{\partial x}\,dxdydz + \frac{\partial \mathbf{v}_{Sy}}{\partial y}\,dxdydz + \frac{\partial \mathbf{v}_{Sz}}{\partial z}\,dxdydz$$

Hence using the definition of volumetric strain ε_V,

$$\begin{aligned}\dot{\varepsilon}_V &= \frac{\left(\dot{dV}\right)}{dV} = \frac{\partial \mathbf{v}_{Sx}}{\partial x} + \frac{\partial \mathbf{v}_{Sy}}{\partial y} + \frac{\partial \mathbf{v}_{Sz}}{\partial z} \\ &= \nabla \bullet \mathbf{v}_S\end{aligned}$$

Now using the definition of material derivative

$$\nabla \bullet \mathbf{v}_S = \dot{\varepsilon}_V$$
$$= \frac{\partial \varepsilon_V}{\partial t} + \mathbf{v}_S \bullet \nabla \varepsilon_V$$

and since $\nabla \varepsilon_V << \frac{\partial \varepsilon_V}{\partial t}$, we have

$$\boxed{\nabla \bullet \mathbf{v}_S \approx \frac{\partial \varepsilon_V}{\partial t}}$$

APPENDIX C PRE-PROCESSOR AND POST-PROCESSORS

C.1 Java based GUI for Pre-processor

In T2STR, a dual mesh concept is used for coupling the poroelasticity with the flow simulation. The finite element mesh is derived from the TOUGH2 finite difference mesh. TOUGH2 creates a MESH file which stores all the information related to its mesh. A translator, a GUI using JAVA, was created to generate the finite element mesh, the dual of the finite difference mesh, by reading the respective TOUGH2 MESH file. This translator generates the Tough2Geo.g3d file which holds the finite element mesh and the constants related to the stress analysis. Figure shows the example menu of the Java based GUI pre-processor.

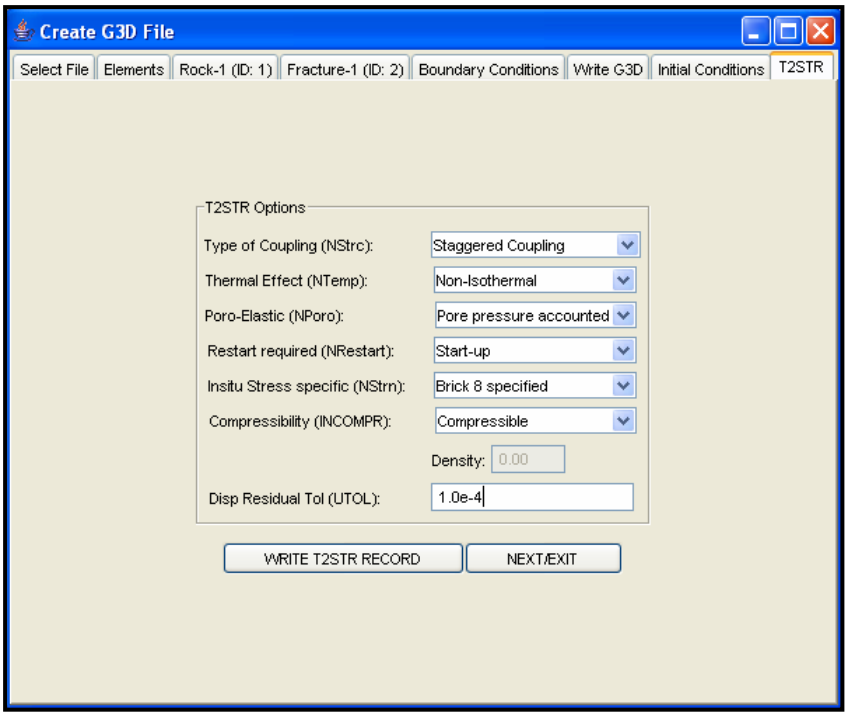

Figure: C.1 Example GUI of the Java based pre-processor.

The pre-processor also allows the specification of the displacement and load boundary conditions at the surfaces of the analysis domain. Boundary conditions at other locations in the domain can be inserted manually into the Tough2Geo.g3d file.

It also allows the user to select the number of materials, rock and/or fractures, depending on the material assignments in the MESH file. The user can also specify the rock and fracture properties for multiple materials and related modification lines are generated which can be cut-pasted in the TOUGH2 input file.

The T2STR record required to be added at the end of the TOUGH2 input file is generated based on the information provided by the user. INSITU file to specify the insitu stresses is generated according to the user input.

C.2 Post-processor

The results in T2STR are written in output files so that they are compatible with PetraSim as well as Tecplot and Excel. A set of macros are written to post-process the data. These will be publicly available with the information on how to run these macros to generate specific kind of visualization for the results of the T2STR simulation.

APPENDIX D JACOBIAN ANALYSIS

D.1 Conservation of Mass (Term by term)

D.1.1 Derivative with respect to displacements

$$T^1 = M_n^{\kappa,i+1} - M_n^{\kappa,i} = \left(\phi_n \sum_{\psi} S_\psi \rho_\psi^\kappa X_\psi^\kappa \right)_n^{\kappa,i+1} - \left(\phi_n \sum_{\psi} S_\psi \rho_\psi^\kappa X_\psi^\kappa \right)_n^{\kappa,i}$$

$$\boxed{\frac{\partial(T^1)}{\partial u_n} = 0}$$

$$T^2 = -\frac{\Delta t}{V_n}\left[\sum_m A_{nm} q_{nm}^{\kappa,i+1} - V_n Q_{nm}^\kappa \right]$$

$$\frac{\partial(T^2)}{\partial u_n} = \frac{\partial\left(-\frac{\Delta t}{V_n}\left[\sum_m A_{nm} q_{nm}^{\kappa,i+1} - V_n Q_{nm}^\kappa \right] \right)}{\partial u_n}$$

which can be written as

$$\boxed{\frac{\partial(T^2)}{\partial u_n} = 0}$$

$$T^3 = \theta_n^{\kappa,i+1} \frac{\left(\alpha - \phi_n^{i+1}\right)}{K_S} \left(\sum_{\psi} S_n^\psi \left\{ p_n^{\psi,i+1} - p_n^{\psi,i} \right\} \right)$$

$$\boxed{\frac{\partial(T^3)}{\partial u_n} = 0}$$

$$T^4 = -\theta_n^{\kappa,i+1}\left(\alpha - \phi_n^{i+1}\right)\alpha_T\left(T_n^{i+1} - T_n^{i}\right)$$

$$\boxed{\frac{\partial(T^4)}{\partial u_n} = 0}$$

$$T^5 = -\theta_n^{\kappa,i+1}\left(\phi_n^{i+1} - \phi_n^{i}\right)$$

$$\boxed{\frac{\partial\left(T^5\right)}{\partial u_n} = 0}$$

$$T^6 = \theta_n^{\kappa,i+1}\frac{\alpha}{V_n}\left(\sum_m A_{nm}\left\{u_{nm}^{i+1} - u_{nm}^{i}\right\}\right)$$

$$\boxed{\frac{\partial\left(T^6\right)}{\partial u_n} = \theta_n^{\kappa,i+1}\frac{\alpha}{V_n}\left(\sum_m\left(-A_{nm}D_{nm}\right)\right)}$$

D.1.2 Derivative with respect to TOUGH2 primary variables

We will represent the partials already calculated in TOUGH2 by "T2 term". For new terms, we will use $-\Big|_{\mathbf{T2}}^{\mathbf{ND}}$ to indicate derivatives calculated using the incremental values.

$$T^1 = M_n^{\kappa,i+1} - M_n^{\kappa,i} = \left(\phi_n\sum_\psi S_\psi\rho_\psi^\kappa X_\psi^\kappa\right)_n^{\kappa,i+1} - \left(\phi_n\sum_\psi S_\psi\rho_\psi^\kappa X_\psi^\kappa\right)_n^{\kappa,i}$$

$$\boxed{\frac{\partial\left(T^1\right)}{\partial X_i} = \mathbf{T2}\text{ - term}}$$

$$T^2 = -\frac{\Delta t}{V_n}\left[\sum_m A_{nm}q_{nm}^{\kappa,i+1} - V_n Q_{nm}^{\kappa}\right]$$

$$\boxed{\frac{\partial\left(T^2\right)}{\partial X_i} = \mathbf{T2}\text{ - term}}$$

$$T^3 = \theta_n^{\kappa,i+1}\frac{\left(\alpha - \phi_n^{i+1}\right)}{K_S}\left(\sum_\psi S_n^\psi\left\{p_n^{\psi,i+1} - p_n^{\psi,i}\right\}\right)$$

$$\frac{\partial\left(T^3\right)}{\partial X_i}=\left(\frac{\partial\left(T^3\right)}{\partial X_i}\bigg|_{\mathbf{T2}}^{\mathbf{ND}}\right)$$

$$T^4=-\theta_n^{\kappa,i+1}\left(\alpha-\phi_n^{i+1}\right)\alpha_T\left(T_n^{i+1}-T_n^{i}\right)$$

$$\frac{\partial\left(T^4\right)}{\partial X_i}=\left(\frac{\partial\left(T^4\right)}{\partial X_i}\bigg|_{\mathbf{T2}}^{\mathbf{ND}}\right)$$

$$T^5=-\theta_n^{\kappa,i+1}\left(\phi_n^{i+1}-\phi_n^{i}\right)$$

$$\frac{\partial\left(T^5\right)}{\partial X_i}=\left(\frac{\partial\left(T^5\right)}{\partial X_i}\bigg|_{\mathbf{T2}}^{\mathbf{ND}}\right)$$

Even if the porosity is not varying and the displacements are assumed to constant while varying the TOUGH2 primary variables, the term θ_n^{κ} could vary hence

$$T^6=\theta_n^{\kappa,i+1}\frac{\alpha}{V_n}\left(\sum_m A_{nm}\left\{u_{nm}^{i+1}-u_{nm}^{i}\right\}\right)$$

$$\frac{\partial\left(T^6\right)}{\partial X_i}=\left(\frac{\partial\left(T^6\right)}{\partial X_i}\bigg|_{\mathbf{T2}}^{\mathbf{ND}}\right)$$

D.1.3 Non-diagonal derivatives

The non-diagonal terms will arise from connection relations.

D.1.3.1 Derivative with respect to displacements

$$T^6=\theta_n^{\kappa,i+1}\frac{\alpha}{V_n}\left(\sum_m A_{nm}\left\{u_{nm}^{i+1}-u_{nm}^{i}\right\}\right)$$

$$\boxed{\frac{\partial\left(T^6\right)}{\partial u_m}=\theta_n^{\kappa,i+1}\frac{\alpha}{V_n}\left(\sum_m A_{nm}D_{nm}\right)}$$

D.1.3.2 Derivative with respect to primary variables

The original terms' partials do not change from currently implemented values and there are no cross-terms in the newly added terms to the mass equation, there are no additions in the non-diagonal terms.

D.2 Conservation of Energy (Term by term)

D.2.1 Derivative with respect to displacements

$$T^1=M_n^{\kappa,i+1}-M_n^{\kappa,i}$$
$$=\left(\left(1-\phi_n\right)\rho_S C_S T+\phi_n\sum_\psi S_\psi\rho_\psi u_\psi^E\right)\Bigg|_n^{\kappa,i+1}-\left(\left(1-\phi_n\right)\rho_S C_S T+\phi_n\sum_\psi S_\psi\rho_\psi u_\psi^E\right)\Bigg|_n^{\kappa,i}$$

$$\boxed{\frac{\partial\left(T^1\right)}{\partial u_n}=0}$$

$$T^2=-\frac{\Delta t}{V_n}\left[\sum_m A_{nm}q_{nm}^{\kappa,i+1}-V_n Q_{nm}^{\kappa}\right]$$
$$=\frac{\Delta t}{V_n}\left[\sum_m A_{nm}\left(\lambda\left(\frac{T_n-T_m}{D_{nm}}\right)+\sum_\psi h_\psi k_{nm}\left[\frac{k_{r\psi}\rho_\psi}{\mu_\psi}\right]_{nm}\left[\frac{P_{\psi,n}-P_{\psi,m}}{D_{nm}}-\rho_{\psi,nm}g_{nm}\right]\right)+V_n Q_{nm}^{\kappa}\right]$$

$$\boxed{\frac{\partial\left(T^2\right)}{\partial u_n}=0}$$

D.2.2 Derivative with respect to TOUGH2 primary variables

Since there are no new terms in the Energy equation, there is no change in any terms in energy equations. The current TOUGH2 terms will be all.

D.2.3 Non-diagonal derivatives

There will not be any additional non-diagonal Jacobian terms in the energy equation.

D.2.3.1 Derivative with respect to displacements

There are no displacement effects in the old term if we assume constant porosity and permeability during individual time step.

D.2.3.2 Derivative with respect to primary variables

The non-diagonal terms in Jacobian due to original equation are already implemented. There are no cross effect terms in the newly added terms and hence there are no non-diagonal additions due to them.

This concludes the analysis and evaluation of Jacobian terms.